Gene regulation in skeletal muscle function; exercise and atrophy

Yukino Hatazawa

2018

Contents

Chapter 1

General introduction

A well-balanced body energy budget controlled by limiting the intake of calories and/or increasing energy expenditure, which is typically achieved by appropriate physical exercise, is very effective at preventing the development of obesity and diabetes mellitus. Skeletal muscle is the largest organ in the human body, accounting for approximately 40% of the total body weight, and plays important roles in exercise, energy expenditure, and glucose/amino acid metabolism. Skeletal muscle plastically adapts to its environment, and appropriate exercise with sufficient nutrition increases muscle mass. Various life conditions, such as bedrest, aging, cancer, and other diseases, are associated with muscle atrophy, which decreases energy expenditure (leading to obesity), reduces glucose uptake/increases blood glucose (causing diabetes), and has a negative impact on the quality of life. In aging societies, which are becoming more prevalent among developed countries, including the US and Japan, the prevention/treatment of muscle atrophy is of particular importance. In the US, muscle atrophy has been reported in more than 20% of 60-year-old and 50% of 80-year-old individuals, and the medical cost of sarcopenia is exorbitant ($18.5 billion in 2000).

Exercise is beneficial not only for skeletal muscle, but also for other organs. A deeper understanding of the molecular mechanisms underlying muscle metabolism during exercise and muscle hypertrophy/atrophy is important for developing strategies to prevent muscle atrophy/dysfunction, which seriously impairs human health and the quality of life.

The present study aims to clarify the molecular mechanisms underlying exercise performance as well as muscle atrophy associated with aging. This is important in the fields of nutrition, exercise physiology, and metabolic disease. The results obtained will potentially lead to the development of novel functional foods and drugs.

Chapters 2 and 3 focused on PGC1α, a transcriptional regulator, the expression of which

is increased in skeletal muscle by exercise, and exercise-related metabolism pathways regulated by PGC1α were investigated.

Chapter 4 focused on DNA methylation, an epigenetic mode of regulation, and the mechanisms responsible for a decreased muscle regeneration capacity during muscle atrophy, such as aging, were examined.

Chapter 2-1

PGC-1α-Mediated Branched-Chain Amino Acid Metabolism in the Skeletal Muscle

Introduction

Peroxisome proliferator-activated receptor (PPAR) γ coactivator 1 α (PGC-1α) was identified as a nuclear receptor coactivator of PPARγ in brown adipose tissue and found to be upregulated in brown adipose tissue and skeletal muscle in response to cold exposure [1]. PGC-1α is now known to be involved not only in the regulation of thermogenesis but also in energy metabolism and other biological processes that are critical in controlling phenotypic characteristics of various organ systems [1-5]. PGC-1α coactivates a broad range of transcription factors, including PPARs, glucocorticoid receptor (GR), nuclear respiratory factors, myocyte enhancing factors, estrogen-related receptor, and forkhead box O1 [6-9]. PGC-1α acts through the recruitment of coactivators with histone acetyl transferase activity as well as interaction with proteins involved in transcriptional initiation and RNA processing [10].

It has recently been shown that there are several isoforms of PGC-1α mRNA [11-14]. We previously reported that among the PGC-1α isoforms, PGC-1α-b expression was markedly increased in response to exercise [15]. PGC-1α-b, considered to be similar in function to PGC-1α1 (originally found full-length PGC-1α [1]), structurally differs by 16 amino acids at its amino terminal [12]. We demonstrated that overexpression of PGC-1α-b in skeletal muscle but not in heart increases mitochondrial biogenesis and capillary density, contributing to improved exercise capacity [4]. Moreover, animal and cellular genetic models with altered expression of the PGC-1α gene have much evidence for the role of PGC-1α in fiber type specificity [16, 17], mitochondrial biogenesis [17-19], angiogenesis [20], and improved exercise performance [21].

Mammalian cells have a high capacity system for oxidative disposal of branched-chain amino acids (BCAA). In contrast to other essential amino acids, which are primarily oxidized in the liver, the most active system for the oxidation of BCAA is located in skeletal muscle cells [22]. The degradation of BCAA mainly occurs in the mitochondria via reversible transamination by branched-chain aminotransferase (BCAT) to produce the corresponding branched-chain α-keto acids (BCKA), which in turn are subjected to oxidative decarboxylation by branched-chain α-keto acid dehydrogenase (BCKDH) to produce CoA esters. The enzymes that catalyze these two reactions are common to the

three BCAA (Val, Leu, and Ile). The second step enzyme, BCKDH, catalyzes an irreversible reaction that commits individual BCKA to their respective degradation pathways [23] and is considered to be the most important regulatory enzyme in the catabolism of the three BCAA [24]. BCKDH activity is regulated by BCKDH kinase (BCKDK); BCKDH phosphorylation attenuates its enzyme activity [23]. In this study, microarray analysis revealed that the BCAA catabolic pathway was coordinately activated in skeletal muscle of transgenic mice overexpressing PGC-1α. Thus, we investigated whether PGC-1α stimulates BCAA metabolism with an increase in the expression of enzymes involved in BCAA metabolism, such as BCAT, BCKDH and BCKDK, using cultured cells and murine skeletal muscle overexpressing PGC-1α.

Materials and Methods

Transgenic (Tg) mice

Tg mice overexpressing PGC-1α-b in skeletal muscle (hereafter, PGC-1α Tg mice or just Tg mice) were generated as described [12]. In brief, the human α-skeletal actin promoter was used to express PGC-1α-b in skeletal muscle (C57BL6 background). We used the B line of Tg mice in this study; Two independent lines of Tg mice showed similar phenotypes in our previous study [4]. Mice were killed by rapid neck disarticulation. A total of 32 mice were used.

Ethics Statement

Mice were cared for in accordance with the National Institutes of Health (NIH) Guide for the Care and Use of Laboratory Animals and our institutional guidelines. All animal experiments were performed with the approval of the National Institute of Health and Nutrition Ethics Committee on Animal Research (approval ID: No 908, 1008, and 1111) and Institutional Animal Care and Use Committee of University of Shizuoka.

cDNA microarray analysis

RNA was isolated from skeletal muscle (gastrocnemius) of Tg mice (age, 12 weeks) and age-matched WT control mice. Samples from WT and Tg mice (N=5) were pooled and used. Each sample was labeled with a cyanine 3-CTP using the Low Input Quick Amp Labeling Kit (Agilent Technologies, Inc., Santa Clara, CA) and hybridized to the Agilent

whole mouse genome microarray (4× 44K), which contains 41,534 genes including expressed sequence tags. Signal detection and data analysis were performed according to the manufacturer's instructions [25].

Functional annotation analysis in genes up-regulated by PGC-1α overexpression

We conducted pathway analysis using the Kyoto Encyclopedia of Genes and Genomes (KEGG) database resource with DAVID v6.7 [26], which is a web application providing a comprehensive set of functional annotation tools to understand the biological meaning of a large list of genes. A list of gene symbols that showed increased expression in skeletal muscle of PGC-1α Tg mice was submitted, and a significant overrepresentation of the KEGG pathway was detected.

Bioinformatics analysis of transcription factors enriched in the BCAA metabolic pathway genes up-regulated in PGC-1α Tg mice

We employed ChIP Enrichment analysis (ChEA) software [27] to explore the transcription factors involved in the regulation of genes whose expression was induced by PGC-1α overexpression classified as BCAA metabolic pathway by DAVID v6.7 [26]. ChEA is a tool that computes over-representation of transcription factor targets from the database of ChIP-seq and ChIP-chip experiments [27]. The database as of Dec 23, 2013 contains 471,284 extracted entries, from 228 publications, describing the binding of 203 transcription factors to 47,119 target genes (http://amp.pham.mssm.edu/lib/chea.jsp).

Quantitative real-time RT-PCR analysis

Total RNA was prepared usnig TRIzol (Life Technologies Japan, Tokyo, Japan). cDNA was synthesized from 1 μg of total RNA using the QuantiTect Rev. Transcription Kit (QIAGEN K.K, Tokyo, Japan). Gene expression levels were measured as described [25]. The following primers were used:

BCAT2 Fw, 5'-CGGACCCTTCATTCGTCAGA -3'; BCAT2 Rv, 5'-CCATAGTTCCCCCCCAACTT-3'; BCKDHa Fw, 5'-CCAGGGTTGGTGGGATGAG-3'; BCKDHa Rv, 5'-GGCTTCCATGACCTTCTTTCG-3'; BCKDK Fw, 5'-GATCCGAATGCTGGCTACTCA-3'; BCKDK Rv, 5'-GCCAACAAAATCAGGCTTGTC-3'; PGC-1α Fw, 5'-CGGAAATCATATCCAACCAG-3'; PGC-1α Rv, 5'-

TGAGGACCGCTAGCAAGTTTG-3’; 36B4 Fw, 5’-GGCCCTGCACTCTCGCTTTC-3’; 36B4 Rv, 5’-TGCCAGGACGCGCTTGT -3’;

Stable cell lines

PlatE cells were cultured in 90-mm dishes and transfected at 70% confluence using Lipofectamine 2000 (Life Technologies Japan, Tokyo, Japan) according to the manufacturer’s instructions using 2 μg pMX-derived expression plasmid [28] containing PGC-1α cDNA or vector alone. Virus-containing supernatants were harvested 48 h after transfection and added to dishes of C2C12 cells, which were selected using 5 μg/ml puromycin to eliminate uninfected cells. After drug selection, virally infected stable cells were cultured to confluence in Dulbecco’s Modified Eagle Medium (DMEM) containing 10% fetal calf serum, and the medium was changed every 2 days. On 3 day after confluence, cells were used for RNA preparation.

Western blotting analysis

Frozen skeletal muscle (gastrocnemius) was homogenized in RIPA Lysis Buffer (25 mM Tris-HCl pH 7.6, 150 mM NaCl, 1% NP-40, 1% sodium deoxycholate, 0.1% SDS) containing 0.2 mM sodium orthovanadate, 2 mM phenylmethylsulfonyl fluoride, and protease inhibitor cocktail (1/100 volume) (Sigma Aldrich Japan, K.K. Tokyo, Japan). The supernatant was separated by centrifugation at 20,400 g for 15 min at 4°C. Protein from the supernatant (20 μg) was applied onto an SDS-PAGE gel. A commercially available precast ready-made gel (10% acrylamide, e-PAGEL, ATTO Co. Tokyo, Japan) was used. The following primary antibodies were used for Western blotting: anti-PGC-1α (Rabbit polyclonal IgG) against the carboxyl terminus 777–797 (Millipore, Billerica, MA), and anti-BCKDH (rabbit polyclonal, [29]).

Amino acid analysis

Skeletal muscle (gastrocnemius) and blood from PGC-1α Tg mice (in the feeding condition) were used for amino acid analysis. In addition, C2C12 cells overexpressing PGC-1α were examined for the amino acid content. Skeletal muscle and C2C12 cells were extracted with methanol/chloroform/water (5/5/2 in volume), and centrifuged. The supernatant was dried with nitrogen gas and dissolved in water. Amino acid levels were

measured by HPLC assays (SRL, Tokyo, Japan).

Statistical analysis

Statistical analysis was performed using Student’s t test. Data were expressed as the mean ± SE. P value <0.05 was considered statistically significant. Standard P-values (Fisher’s exact test) and Benjamini P-values were evaluated for functional annotation analysis. The Fisher exact test with the Bonferroni's correction P-values were evaluated for transcription factor search analysis.

Results and Discussion

Increased BCAA metabolism in skeletal muscle of PGC-1α Tg mice

To characterize the phenotype of the skeletal muscle of Tg mice, we performed microarray analysis of gene expression. Microarray analysis revealed that the expression of many genes was changed in Tg mice as compared with that in WT mice. Among these, 315 genes (Table S1) were up-regulated (more than 2.5-hold) and used to conduct pathway analysis, which detected 7 categories (Table 1), including oxidative phosphorylation, TCA cycle, and fatty acid metabolism, which were related to mitochondrial function. These results were consistent with previous reports that PGC-1α increases the mitochondrial number and enhances their function [3, 5]. We observed pathway categories of Parkinson's disease, Huntington's disease and Alzheimer's disease (Table 1), and individual genes increased in the categories were all related to mitochondrial functions (data not shown). In addition, we found that BCAA metabolic pathway (i.e., Val, Leu, Ile degradation, Table 1). As shown in Figure 1, gene expression of many enzymes involved in BCAA catabolism was increased, suggesting that PGC-1α stimulates BCAA metabolism in skeletal muscle. Thus, we examined whether PGC-1α stimulates BCAA metabolism.

Levels of BCAA and its catabolic enzymes in skeletal muscle of PGC-1α Tg mice

We examined the gene expression of BCAA metabolic enzymes (BCAT2, BCKDH, BCKDK). RNA was obtained from the skeletal muscle of Tg and WT mice. The expression of BCAT2 (2.0-fold) and BCKDH (3.5-fold) was significantly increased in Tg mice compared with that in WT mice (Fig. 2A, B). Meanwhile, the expression of BCKDK was decreased (Fig. 2C). Subsequently, we examined protein expression of BCAA metabolic enzymes by Western blot analysis. PGC-1α protein (100 kDa) increased 4-fold in Tg mice compared with WT mice (Fig. 3A). In this experiment, we also observed increased 45 kDa and 25 kDa bands, whose physiological significance in currently unclear. Using a BCKDH antibody, we observed the strongest band at 55 kDa (arrowhead), which corresponded to the E2 subunit, and was slightly (1.3-fold) increased in Tg mice. The faint band in WT mice at approximately 45 kDa (arrowhead, long exposure), which probably represents E1α subunits [29], increased in Tg mice significantly (1.5-fold). The band at approximately 35 kDa (arrowhead), which probably represents E1β subunits [29], increased markedly (11-fold). Thus, we observed an

increased protein level of BCKDH (Fig. 3B), which is consistent with the increased mRNA level. Next we examined BCAA levels from skeletal muscle in Tg mice and WT mice. Val and Leu levels were significantly decreased in Tg mice compared with that in WT mice (Fig. 4A). Ile was detected in WT mice but observed only at trace levels in Tg mice (Fig. 4A). The level of Glu, a metabolite of BCAA catabolism, was increased, in contrast to the decreased BCAA level. Levels of other amino acids are shown in Table 2. We also measured BCAA levels in blood (plasma). BCAA levels tended to be decreased in blood as observed in skeletal muscle (although not significant, $P = 0.067$ for Val, $P = 0.072$ for Leu and $P = 0.063$ for Ile; Fig. 4B and Table 3). These findings indicate that changes in the expression of BCAA metabolic enzymes are functional, and accompanied by enzyme activation.

BCAA metabolism gene expression in C2C12 cells overexpressing PGC-1α

Next, to examine whether the effect of PGC-1α on increased BCAA metabolism was cell autonomous, we used C2C12 cells, which are ectopically overexpressed PGC-1α by retrovirus, and examined BCAA metabolism gene expression. Gene expression of BCAT2 (1.5-fold) and BCKDH (2-fold) was increased but that of BCKDK was not (Fig. 5), as observed in Tg mice. These data suggest that PGC-1α regulates BCAA catabolic gene expression in a cell autonomous manner. Then, we examined the amino acid levels in the cells. Ile was observed only at a trace level. Val was slightly lower in mock cells than in cells overexpressing PGC-1α ($P = 0.162$). Leu levels were detectable in mock cells; however, it was detected only at a trace level in cells overexpressing PGC-1α (Table 4). In summary, BCAA levels appeared to be decreased in C2C12 cells overexpressing PGC-1α, suggesting that BCAA catabolism is regulated by PGC-1α in muscle cells.

Changed level of other amino acids caused by PGC-1α overexpression

In addition to BCAA, the levels of other amino acids were also changed. For example, in skeletal muscle of Tg mice, Glu levels were significantly increased (Table 2). During BCAA degradation by BCAT, α-keto glutarate is catabolized to Glu. Thus, increasing Glu levels are consistent with the stimulation of BCAA degradation in muscle. Alternatively, in cells overexpressing PGC-1α, Glu was not increased, but Ala was increased (Table 4). The reason for this may be that BCAT catalyzes amino base transfer from BCAA to

pyruvate, thereby producing Ala. However, in Tg mice, the expression of genes involved in glycolysis is markedly decreased [4], resulting in inadequate pyruvate, a product of the glycolysis pathway, for Ala production, or Ala may be moved and used in other tissues in animals.

How did PGC-1α increase expression of BCAA metabolism enzyme?

PGC-1α Tg mice have muscle, which has a much higher oxidative capacity [4]. BCAT2 and BCKDH are mitochondrial enzymes [30]. Therefore, the increased expression of BCAT2 and BCKDH could be due to an increased number of mitochondria in the muscles of the Tg mice. Alternatively, PGC-1α may activate BCAA metabolism via the coactivation of glucocorticoid receptor (GR) and PPARα. PGC-1α is a transcriptional coactivator of nuclear receptor and other transcriptional factors, some of which have been reported to activate the transcription of the BCAT2 gene. For example, the expression of BCAT2 was decreased in KLF15-KO mice [31], and the rat BCAT2 promoter was activated by KLF15 and GR [32]. Moreover, PPARα activated the BCKDH complex in the liver [22]. In addition, bioinformatics analysis revealed that several nuclear receptors, including PPAR and estrogen receptor-related receptor (ERR), are significantly frequently recruited to the BCAA metabolic pathway genes up-regulated in skeletal muscle of PGC-1α Tg mice (Table 5). These data suggest that PGC-1α activates BCAA metabolism through multiple nuclear receptors.

Conclusion

In this study, we investigated whether PGC-1α stimulates BCAA metabolism by increasing the expression of involved enzymes, such as BCAT and BCKDH, using cultured cells and murine skeletal muscle overexpressing PGC-1α. Our data suggest that BCAA degradation is mediated by increased expression of PGC-1α, and the physiological relevance, such as condition of induced expression in PGC-1α i.e., exercise, remain to be analyzed by further experiments.

References

1. Puigserver P, Wu Z, Park CW, Graves R, Wright M, et al. (1998) A cold-inducible coactivator of nuclear receptors linked to adaptive thermogenesis. Cell 92: 829-839.
2. Liang H, Balas B, Tantiwong P, Dube J, Goodpaster BH, et al. (2009) Whole body overexpression of PGC-1alpha has opposite effects on hepatic and muscle insulin sensitivity. Am J Physiol Endocrinol Metab 296: E945-954.
3. Puigserver P and Spiegelman BM (2003) Peroxisome proliferator-activated receptor-gamma coactivator 1 alpha (PGC-1 alpha): transcriptional coactivator and metabolic regulator. Endocr Rev 24: 78-90.
4. Tadaishi M, Miura S, Kai Y, Kano Y, Oishi Y, et al. (2011) Skeletal muscle-specific expression of PGC-1alpha-b, an exercise-responsive isoform, increases exercise capacity and peak oxygen uptake. PLoS One 6: 8.
5. Wareski P, Vaarmann A, Choubey V, Safiulina D, Liiv J, et al. (2009) PGC-1alpha and PGC-1beta regulate mitochondrial density in neurons. J Biol Chem 284: 21379-21385.
6. Kamei Y, Ohizumi H, Fujitani Y, Nemoto T, Tanaka T, et al. (2003) PPARgamma coactivator 1beta/ERR ligand 1 is an ERR protein ligand, whose expression induces a high-energy expenditure and antagonizes obesity. Proc Natl Acad Sci U S A 100: 12378-12383.
7. Kelly DP and Scarpulla RC (2004) Transcriptional regulatory circuits controlling mitochondrial biogenesis and function. Genes Dev 18: 357-368.
8. Lin J, Handschin C, and Spiegelman BM (2005) Metabolic control through the PGC-1 family of transcription coactivators. Cell Metab 1: 361-370.
9. Rodgers JT, Lerin C, Gerhart-Hines Z, and Puigserver P (2008) Metabolic adaptations through the PGC-1 alpha and SIRT1 pathways. FEBS Lett 582: 46-53.
10. Wallberg AE, Yamamura S, Malik S, Spiegelman BM, and Roeder RG (2003) Coordination of p300-mediated chromatin remodeling and TRAP/mediator function through coactivator PGC-1alpha. Mol Cell 12: 1137-1149.
11. Chinsomboon J, Ruas J, Gupta RK, Thom R, Shoag J, et al. (2009) The transcriptional coactivator PGC-1alpha mediates exercise-induced angiogenesis in skeletal muscle. Proc Natl Acad Sci U S A 106: 21401-21406.
12. Miura S, Kai Y, Kamei Y, and Ezaki O (2008) Isoform-specific increases in murine

skeletal muscle peroxisome proliferator-activated receptor-gamma coactivator-1alpha (PGC-1alpha) mRNA in response to beta2-adrenergic receptor activation and exercise. Endocrinology 149: 4527-4533.

13. Ruas JL, White JP, Rao RR, Kleiner S, Brannan KT, et al. (2012) A PGC-1alpha isoform induced by resistance training regulates skeletal muscle hypertrophy. Cell 151: 1319-1331.
14. Yoshioka T, Inagaki K, Noguchi T, Sakai M, Ogawa W, et al. (2009) Identification and characterization of an alternative promoter of the human PGC-1alpha gene. Biochem Biophys Res Commun 381: 537-543.
15. Tadaishi M, Miura S, Kai Y, Kawasaki E, Koshinaka K, et al. (2011) Effect of exercise intensity and AICAR on isoform-specific expressions of murine skeletal muscle PGC-1alpha mRNA: a role of beta2-adrenergic receptor activation. Am J Physiol Endocrinol Metab 300: E341-349.
16. Lin J, Wu H, Tarr PT, Zhang CY, Wu Z, et al. (2002) Transcriptional co-activator PGC-1 alpha drives the formation of slow-twitch muscle fibres. Nature 418: 797-801.
17. Miura S, Kai Y, Ono M, and Ezaki O (2003) Overexpression of peroxisome proliferator-activated receptor gamma coactivator-1alpha down-regulates GLUT4 mRNA in skeletal muscles. J Biol Chem 278: 31385-31390.
18. Handschin C, Chin S, Li P, Liu F, Maratos-Flier E, et al. (2007) Skeletal muscle fiber-type switching, exercise intolerance, and myopathy in PGC-1alpha muscle-specific knock-out animals. J Biol Chem 282: 30014-30021.
19. Miura S, Tomitsuka E, Kamei Y, Yamazaki T, Kai Y, et al. (2006) Overexpression of peroxisome proliferator-activated receptor gamma co-activator-1alpha leads to muscle atrophy with depletion of ATP. Am J Pathol 169: 1129-1139.
20. Arany Z, Foo SY, Ma Y, Ruas JL, Bommi-Reddy A, et al. (2008) HIF-independent regulation of VEGF and angiogenesis by the transcriptional coactivator PGC-1alpha. Nature 451: 1008-1012.
21. Calvo JA, Daniels TG, Wang X, Paul A, Lin J, et al. (2008) Muscle-specific expression of PPARgamma coactivator-1alpha improves exercise performance and increases peak oxygen uptake. J Appl Physiol 104: 1304-1312.
22. Shimomura Y, Murakami T, Nakai N, Nagasaki M, and Harris RA (2004) Exercise

promotes BCAA catabolism: effects of BCAA supplementation on skeletal muscle during exercise. J Nutr 134: 1583S-1587S.

23. Shimomura Y, Obayashi M, Murakami T, and Harris RA (2001) Regulation of branched-chain amino acid catabolism: nutritional and hormonal regulation of activity and expression of the branched-chain alpha-keto acid dehydrogenase kinase. Curr Opin Clin Nutr Metab Care 4: 419-423.
24. Shimomura Y, Honda T, Shiraki M, Murakami T, Sato J, et al. (2006) Branched-chain amino acid catabolism in exercise and liver disease. J Nutr 136: 250S-253S.
25. Takahashi M, Kamei Y, Ehara T, Yuan X, Suganami T, et al. (2013) Analysis of DNA methylation change induced by Dnmt3b in mouse hepatocytes. Biochem Biophys Res Commun 434: 873-878.
26. Huang da W, Sherman BT, and Lempicki RA (2009) Systematic and integrative analysis of large gene lists using DAVID bioinformatics resources. Nat Protoc 4: 44-57.
27. Lachmann A, Xu H, Krishnan J, Berger SI, Mazloom AR, et al. (2010) ChEA: transcription factor regulation inferred from integrating genome-wide ChIP-X experiments. Bioinformatics 26:2438-2444.
28. Misawa K, Nosaka T, Morita S, Kaneko A, Nakahata T, et al. (2000) A method to identify cDNAs based on localization of green fluorescent protein fusion products. Proc Natl Acad Sci U S A 97: 3062-3066.
29. Kobayashi R, Shimomura Y, Otsuka M, Popov KM, and Harris RA (2000) Experimental hyperthyroidism causes inactivation of the branched-chain alpha-ketoacid dehydrogenase complex in rat liver. Arch Biochem Biophys 375: 55-61.
30. Shimomura Y, Fujii H, Suzuki M, Murakami T, Fujitsuka N, et al. (1995) Branched-chain alpha-keto acid dehydrogenase complex in rat skeletal muscle: regulation of the activity and gene expression by nutrition and physical exercise. J Nutr 125: 1762S-1765S.
31. Jeyaraj D, Scheer FA, Ripperger JA, Haldar SM, Lu Y, et al. (2012) Klf15 orchestrates circadian nitrogen homeostasis. Cell Metab 15: 311-323.
32. Shimizu N, Yoshikawa N, Ito N, Maruyama T, Suzuki Y, et al. (2011) Crosstalk between glucocorticoid receptor and nutritional sensor mTOR in skeletal muscle. Cell Metab 13: 170-182.

Legend

Figure 1

Pathway map of Val, Leu, and Ile degradation

Individual gene name of the KEGG pathway of Val, Leu, and Ile degradation extracted by pathway analysis is shown as a metabolic map. Red asterisks indicate increased gene expression by microarray of Tg mice. Gene names corresponding to enzyme numbers with red asterisks are as follows: 2.8.3.5, 3-oxoacid CoA transferase 1; 2.3.1.16, acetyl-Coenzyme A acyltransferase 2 (mitochondrial 3-oxoacyl-Coenzyme A thiolase); 1.3.8.1, acyl-Coenzyme A dehydrogenase, short chain; 2.6.1.42, branched chain aminotransferase 2, mitochondrial; 1.2.4.4, branched chain ketoacid dehydrogenase E1, alpha polypeptide; 1.8.1.4, dihydrolipoamide dehydrogenase; 1.1.1.35, hydroxyacyl-Coenzyme A dehydrogenase; 4.2.1.17, hydroxyacyl-Coenzyme A dehydrogenase/3-ketoacyl-Coenzyme A thiolase/enoyl-Coenzyme A hydratase (trifunctional protein), alpha subunit; 5.1.99.1, methylmalonyl CoA epimerase; 1.1.1.31, 3-hydroxyisobutyrate dehydrogenase.

Figure 2

Gene expression of BCAA metabolic enzyme in skeletal muscle of PGC-1α Tg mice

Expression of A) BCAT2, B) BCKDH, and C) BCKDK genes in WT (control; open columns, N = 9) and PGC-1α Tg (filled columns, N = 7) mice by quantitative real-time RT-PCR. RNA was obtained from mice with feeding condition. These samples were as used in [4]. In the sample, PGC-1α expression was 30 fold higher in Tg mice than in WT mice (Fig. 1 of [4]). The relative values are shown (the control is set as 100). *** $P < 0.001$.

Figure 3

Protein expression of PGC-1α and BCAA metabolic enzymes in skeletal muscle of PGC-1α -Tg mice

Total lysates from skeletal muscle were subjected to SDS-PAGE, followed by Western blot analysis with indicated antibodies. Typical blots are shown. Densitometric analysis was performed on the bands indicated (arrowheads). Molecular size marked was indicated on the left side of blots. Tg and WT mice were sacrificed at 12 weeks of age (N=3 for WT and N=3 for Tg mice). In these samples, we confirmed increased mRNA

expression of BCAT2 and BCKDH but not BCKDK as observed in Figure 1 (data not shown).

Figure 4

BCAA content in skeletal muscle and blood of PGC-1α Tg mice

Val, Leu, and Ile levels in (A) skeletal muscle and (B) blood. Open columns represent for WT (N = 4) and filled columns represent Tg (N=4). *** P< 0.001, ** P < 0.01. T.R., trace level.

Figure 5

Gene expression of BCAA metabolic enzymes in cultured C2C12 cells overexpressing PGC-1α.

Total RNA was isolated from the cells and analyzed by quantitative real-time RT-PCR with primers for A) PGC-1α, B) BCAT2, C) BCKDHa, and D) BCKDK. Open columns represent mock cells (N=3), and filled columns represent PGC-1α-overexpressed cells (N=3). Each value represents mean ± SE (N=3). The relative values are shown (the control is set as 100). For PGC-1α expression, the value was set as 100 in the PGC-1α overexpressed cells. *** P < 0.001, ** P < 0.01.

Table 1 Pathway analysis

Compared with WT mice, 315 genes were found to be up-regulated in PGC-1α Tg mice by microarray and classified into KEGG pathway analysis as described in Methods.

Table 2 Amino acid content in skeletal muscle of PGC-1α Tg mice

The samples were used as in Figure 4. *** P < 0.001, ** P < 0.01, * P < 0.05. TR, trace level. ND, not detected.

Table 3 Amino acid content in blood of PGC-1α Tg mice

The samples were used as in Figure 4. * P < 0.05.

Table 4 Amino acid content in C2C12 cells overexpressing of PGC-1α

The samples were used as in Figure 5. * P < 0.05. TR, trace level. ND, not detected.

Table 5 Bioinformatics analysis of transcription factors enriched in the BCAA metabolic pathway genes up-regulated in PGC-1α Tg mice

List of transcription factors, which are statistically identified as ones that can be recruited to the BCAA metabolic genes, up-regulated in PGC-1α Tg mice. Target genes were previously found in ChIP assay for interacting with indicated transcription factors in the literature [27]. Abbreviations of the transcription factors are as follows, KLF4, Krueppel-like factor 4; PPARG, Constitutive coactivator of peroxisome proliferator-activated receptor gamma (Constitutive coactivator of PPAR-gamma) (Constitutive coactivator of PPARG); EKLF, Krueppel-like factor 1 (Erythroid krueppel-like transcription factor); ESRRB, Steroid hormone receptor ERR2 (Estrogen receptor-like 2) (Estrogen-related receptor beta) (ERR-beta); PPARD, Peroxisome proliferator-activated receptor delta (PPAR-delta); ZFP42, Zinc finger protein 42; WT1, Wilms tumor protein; NR0B1, Nuclear receptor subfamily 0 group B member 1 (Nuclear receptor DAX-1); TET1, Methylcytosine dioxygenase TET1 (EC 1.14.11.n2) (CXXC-type zinc finger protein 6) (Ten-eleven translocation 1 gene protein homolog); GATA4, Transcription factor GATA-4 (GATA-binding factor 4).

Fig.1

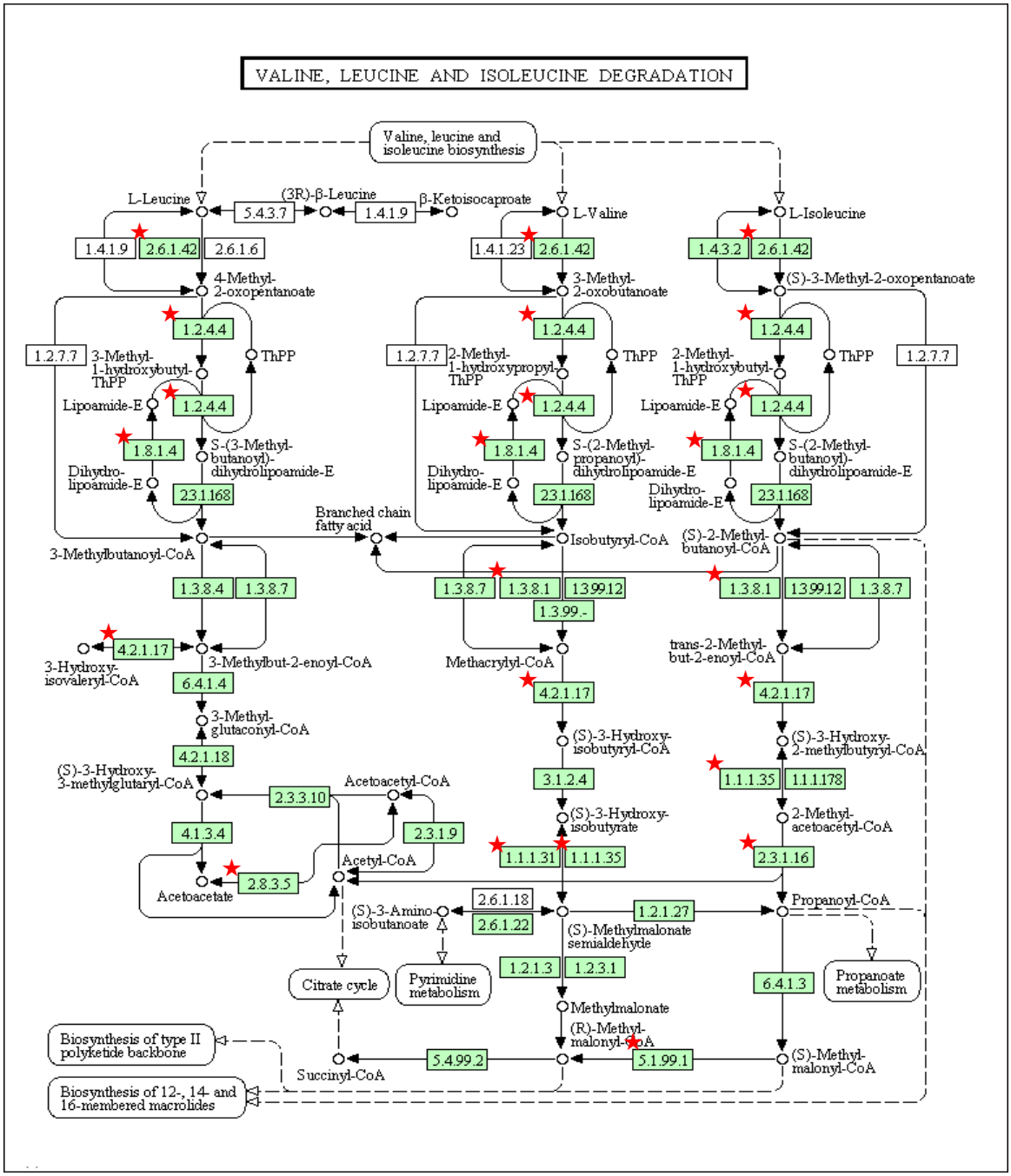
VALINE, LEUCINE AND ISOLEUCINE DEGRADATION
Valine, leucine and isoleucine biosynthesis
L-Leucine
(3R)-β-Leucine
β-Ketoisocaproate
L-Valine
L-Isoleucine
5.4.3.7
1.4.1.9
1.4.1.23
1.4.3.2
2.6.1.42
2.6.1.6
4-Methyl-2-oxopentanoate
3-Methyl-2-oxobutanoate
(S)-3-Methyl-2-oxopentanoate
1.2.4.4
1.2.7.7
3-Methyl-1-hydroxybutyl-ThPP
2-Methyl-1-hydroxypropyl-ThPP
2-Methyl-1-hydroxybutyl-ThPP
ThPP
Lipoamide-E
1.8.1.4
S-(3-Methyl-butanoyl)-dihydrolipoamide-E
S-(2-Methyl-propanoyl)-dihydrolipoamide-E
S-(2-Methyl-butanoyl)-dihydrolipoamide-E
Dihydro-lipoamide-E
23.1.168
Branched chain fatty acid
3-Methylbutanoyl-CoA
Isobutyryl-CoA
(S)-2-Methyl-butanoyl-CoA
1.3.8.4
1.3.8.7
1.3.8.1
1.3.99.12
1.3.99.-
4.2.1.17
3-Hydroxy-isovaleryl-CoA
3-Methylbut-2-enoyl-CoA
Methacrylyl-CoA
trans-2-Methyl-but-2-enoyl-CoA
6.4.1.4
3-Methyl-glutaconyl-CoA
(S)-3-Hydroxy-isobutyryl-CoA
(S)-3-Hydroxy-2-methylbutyryl-CoA
4.2.1.18
(S)-3-Hydroxy-3-methylglutaryl-CoA
Acetoacetyl-CoA
2.3.3.10
3.1.2.4
1.1.1.35
1.1.1.178
(S)-3-Hydroxy-isobutyrate
2-Methyl-acetoacetyl-CoA
4.1.3.4
2.3.1.9
2.3.1.16
Acetyl-CoA
Acetoacetate
2.8.3.5
1.1.1.31
2.6.1.18
2.6.1.22
(S)-3-Amino-isobutanoate
1.2.1.27
Propanoyl-CoA
(S)-Methylmalonate semialdehyde
Citrate cycle
Pyrimidine metabolism
1.2.1.3
1.2.3.1
6.4.1.3
Propanoate metabolism
Methylmalonate
(R)-Methyl-malonyl-CoA
Biosynthesis of type II polyketide backbone
5.4.99.2
5.1.99.1
(S)-Methyl-malonyl-CoA
Succinyl-CoA
Biosynthesis of 12-, 14- and 16-membered macrolides

Fig.2

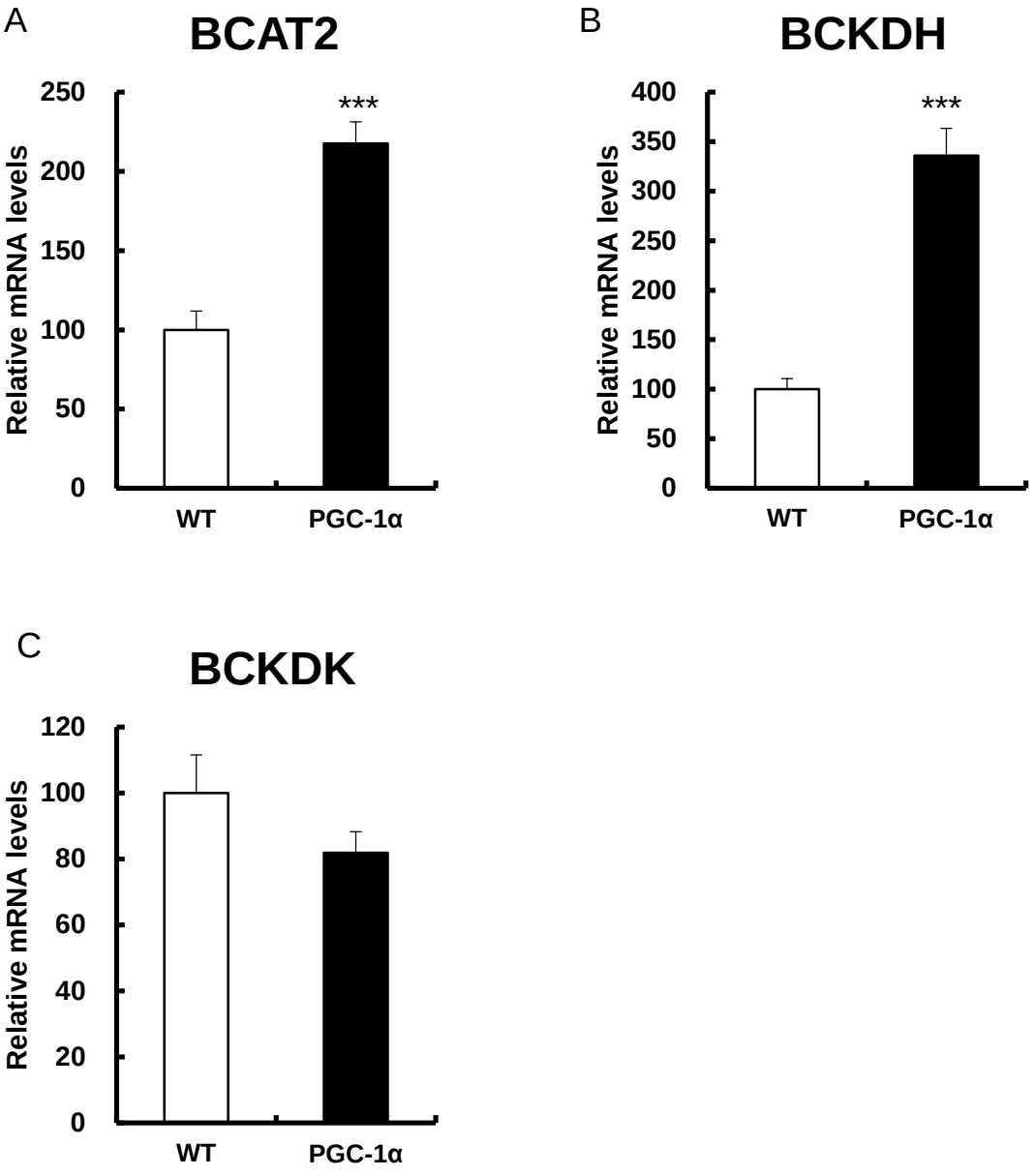
A
BCAT2
Relative mRNA levels
250
200
150
100
50
0
***
WT
PGC-1α
B
BCKDH
Relative mRNA levels
400
350
300
250
200
150
100
50
0
***
WT
PGC-1α
C
BCKDK
Relative mRNA levels
120
100
80
60
40
20
0
WT
PGC-1α

Fig.3

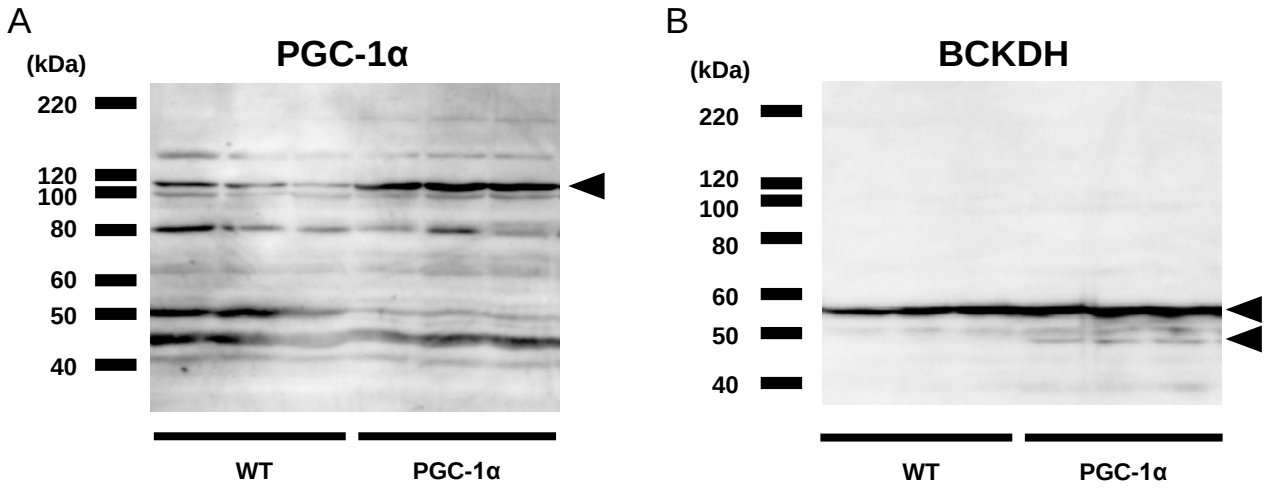
A
PGC-1α
(kDa)
220
120
100
80
60
50
40
WT
PGC-1α
B
BCKDH
(kDa)
220
120
100
80
60
50
40
WT
PGC-1α

Fig.4

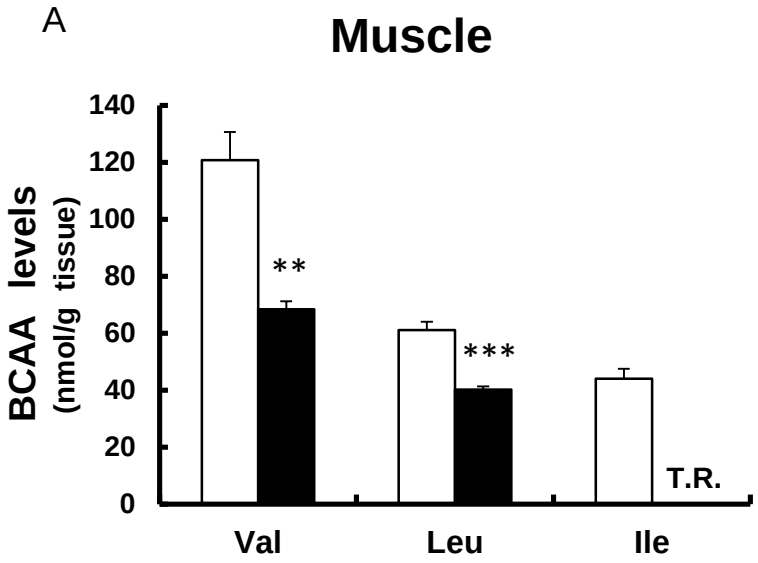
A
Muscle
BCAA levels
(nmol/g tissue)
140
120
100
80
60
40
20
0
**
***
T.R.
Val
Leu
Ile

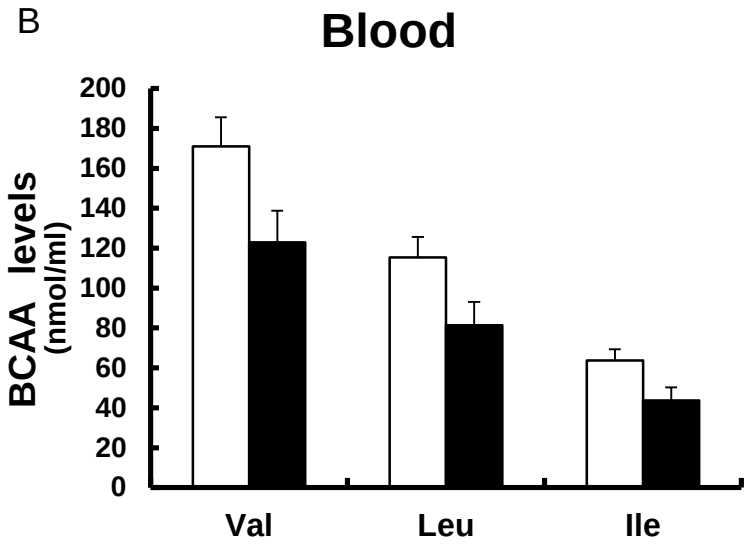
B
Blood
BCAA levels
(nmol/ml)
200
180
160
140
120
100
80
60
40
20
0
Val
Leu
Ile

Fig.5

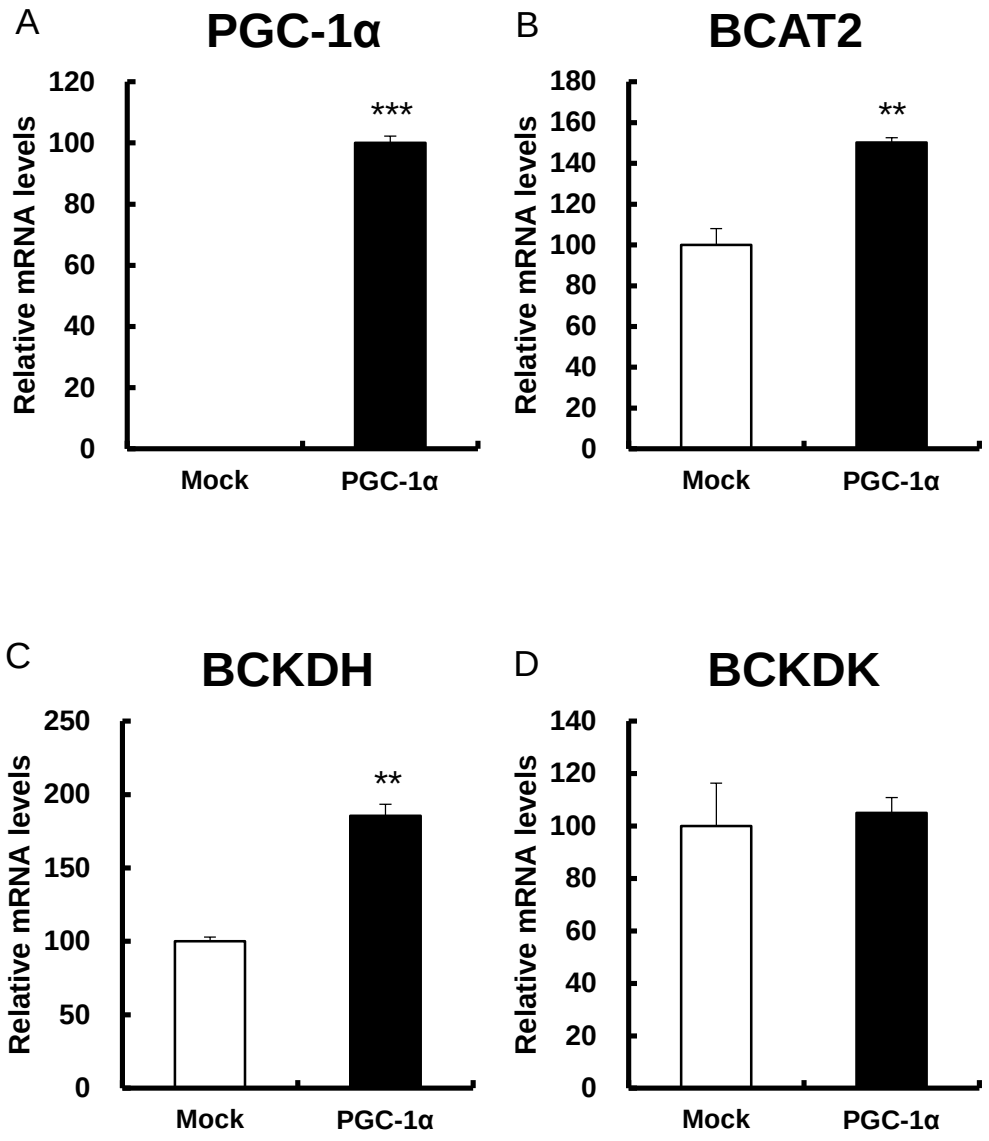
A
PGC-1α
Relative mRNA levels
120
100
80
60
40
20
0
***
Mock
PGC-1α
B
BCAT2
Relative mRNA levels
180
160
140
120
100
80
60
40
20
0
**
Mock
PGC-1α
C
BCKDH
Relative mRNA levels
250
200
150
100
50
0
**
Mock
PGC-1α
D
BCKDK
Relative mRNA levels
140
120
100
80
60
40
20
0
Mock
PGC-1α

Table 1

Categories of pathway analysis	P-Value	Benjamini
Oxidative phosphorylation	1.10E-13	1.00E-11
Parkinson's disease	1.70E-13	8.10E-12
Citrate cycle (TCA cycle)	3.10E-12	9.70E-11
Huntington's disease	9.10E-12	2.10E-10
Alzheimer's disease	5.30E-10	9.90E-09
Valine, leucine and isoleucine degradation	7.10E-09	1.10E-07
Fatty acid metabolism	9.10E-08	1.20E-06

Table 2

Amino acid	WT	PGC-1α Tg
Alanine	1768.3	1388.6
Arginine	218.1	446.4*
Asparagine	61.9	53.1
Aspartic acid	163.4	257.3**
Cystine	TR	TR
Glutamic acid	505.9	1237.5***
Glutamine	1341	1557.9
Glycine	3165.9	655.9**
Histidine	104.3	101.3
Isoleucine	44.4	TR
Leucine	61.1	40.3***
Lysine	574	1074.1*
Methionine	49.9	35.7
Phenylalanine	12.4	TR
Proline	169.1	ND
Serine	357.7	186.3*
Threonine	242.6	186.3
Tryptophan	ND	ND
Tyrosine	77	75
Valine	120.8	68.4**

(nmol/g tissue)

Table 3

Amino acid	WT	PGC-1α Tg
Alanine	381.4	313.9
Arginine	112.3	114.5
Asparagine	45.7	38.9
Aspartic acid	7.7	6.7
Cystine	8.7	5.1
Glutamic acid	42	35.2*
Glutamine	631.4	726
Glycine	306.2	334
Histidine	60.1	58
Isoleucine	63.7	43.6
Leucine	115.3	81.3
Lysine	277.7	256.4
Methionine	56.1	53.1
Phenylalanine	60.5	59.7
Proline	105	96.1
Serine	134.8	125.5
Threonine	117.2	121.6
Tryptophan	41.8	39.7
Tyrosine	99.4	82
Valine	171.1	122.9

(nmol/ml)

Table 4

Amino acid	Mock	PGC-1α
Alanine	35.7	62.7*
Arginine	ND	ND
Asparagine	ND	ND
Aspartic acid	44.3	55.3
Cystine	TR	TR
Glutamic acid	116.3	87.1
Glutamine	24.4	20.6
Glycine	67.1	61.3
Histidine	ND	ND
Isoleucine	TR	TR
Leucine	9	TR
Lysine	14.6	15.9
Methionine	ND	ND
Phenylalanine	ND	ND
Proline	ND	ND
Serine	9	9.5
Threonine	27.4	35.2
Tryptophan	ND	ND
Tyrosine	TR	TR
Valine	10.2	8.7

(nmol/10cm dish)

Table 5

Transcription factor	P-Value	Target gene
KLF4	2.80E-07	ACAA2;ACADS;BCAT2;BCKDHA;HADHA;MCEE;OXCT1
PPARG	3.68E-07	ACAA2;ACADS;BCAT2;HADHB
EKLF	5.14E-06	ACADS;BCAT2;HADH;HIBADH;OXCT1
ESRRB	1.04E-05	ACADS;DLD;HIBADH;MCEE;OXCT1
PPARD	1.16E-05	HADHA;HADHB;OXCT1
ZFP42	1.22E-05	ACADS;BCAT2;BCKDHA;HADHA;HADHB
WT1	4.22E-04	BCAT2;HADHB;HIBADH;OXCT1
NR0B1	4.49E-04	ACADS;BCAT2;HADHA;HADHB
TET1	6.17E-04	ACAA2;ACADS;HADHA;OXCT1
GATA4	9.09E-04	ACAA2;BCAT2;HADHA;HADHB

Chapter 2-2

Deletion of the transcriptional coactivator PGC-1α in skeletal muscles is associated with reduced expression of genes related to oxidative muscle function

Introduction:

Peroxisome proliferator-activated receptor (PPAR)γ coactivator 1α (PGC-1α) was identified as a nuclear receptor coactivator of PPARγ in brown adipose tissue and found to be up-regulated in brown adipose tissue and skeletal muscles in response to cold exposure (1). PGC-1α is now known to be involved not only in the regulation of thermogenesis, but also in energy metabolism and other biological processes that are critical for controlling the phenotypic characteristics of various organ systems (1-6). PGC-1α coactivates a broad range of transcription factors, including estrogen-related receptors (ERR), PPARs, glucocorticoid receptors (GR) (nuclear receptors), nuclear respiratory factors, and myocyte-enhancing factors (7-10).

PGC-1α expression is increased in skeletal muscles during exercise. The overexpression of PGC-1α in skeletal muscles causes increased mitochondrial biogenesis, TCA cycle activity, oxidative phosphorylation, BCAA metabolism, and exercise tolerance (4). Exercise training leads to adaptation of the body, including skeletal muscles, such as in terms of muscle oxidation capacity, muscle content, and muscle angiogenesis. In addition to performing a gain-of-function experiment, we created PGC-1α KO mice for a loss-of-function experiment. We previously showed that the PGC-1α level decreased in skeletal muscles, but not in the liver. In skeletal muscles of PGC-1α KO mice, leucine-activated mTOR activity was attenuated (11). In this study, global gene expression of PGC-1α KO mice, with exercise training, was analyzed. We observed opposite phenotypes between PGC-1α KO and previously analyzed PGC-1α Tg, and helped to further elucidate the role of PGC-1α in skeletal muscles.

Materials and Methods:

Knockout (KO) mice

KO mice with a deletion of PGC-1α in skeletal muscles (PGC-1α KO mice or just KO mice) were generated as previously described (12). In brief, the human α-skeletal actin promoter was used to express Cre recombinase in mouse skeletal muscles (C57BL6 background), and these mice were then crossed with floxed PGC-1α mice (13).

Ethics statement

The mice were cared for in accordance with the National Institutes of Health (NIH) Guide for the Care and Use of Laboratory Animals and our institutional guidelines. All animal experiments were performed with the approval of the Institutional Animal Care and Use Committee of Kyoto Prefectural University.

Quantitative real-time RT-PCR analysis

PGC-1α KO mice (male, 12 weeks old, n = 7) and wild-type control littermates (WT, n = 8) were placed in a wheel cage for 4 weeks. Then, the mice were forced to run on a treadmill for 30 min. Three hours after the last run, RNA was isolated from skeletal muscles (gastrocnemius) of PGC-1α KO and WT mice. Total RNA was prepared using TRIzol (Life Technologies Japan, Tokyo, Japan). cDNA was synthesized from 1 μg of total RNA using a QuantiTect Rev. Transcription Kit (QIAGEN K.K, Tokyo, Japan). Gene expression levels were measured as previously described (12). The following primers were used:

PGC-1α Fw, 5’-CGGAAATCATATCCAACCAG-3’; PGC-1α Rv, 5’-TGAGGACCGCTAGCAAGTTTG-3’; 36B4 Fw, 5’-GGCCCTGCACTCTCGCTTTC-3’; 36B4 Rv, 5’-TGCCAGGACGCGCTTGT -3’; PGC1β Fw, 5’-CAGCTGTGTGCTGACTTGCC-3’; PGC1β Rv, 5’- TCAAAGTCACTGGCGTCCAG -3’; PRC1 Fw, 5’- TGGACGCCTCCCTTATATCCC -3’; PRC1 Rv, 5’-TGTGAGCAGCGACATTTCATTC -3’; Sdhb Fw, 5’-CCTCGAATGCAGACGTACGA -3’; Sdhb Rv5’-CAACACCATAGGTCCGCACTT -3’; Mdh2 Fw, 5’-AAGGCTACCTTGGACCGGAG -3’; Mdh2 Rv, 5’-CATCACAACCTTTGAGGCAATCT3’;

cDNA microarray analysis

PGC-1α KO mice (male, 20 weeks old, n = 2) and wild-type control littermates (WT, n = 2) were placed in a wheel cage for 3 weeks. Then, the mice were moved to a normal (without wheel) cage and forced to run on a treadmill for 30 min during the next week. Three hours after the last run, RNA was isolated from skeletal muscles (gastrocnemius) of KO and WT mice. Samples from WT and KO mice were pooled and used. Each sample was labeled with cyanine 3-CTP using a Low Input Quick Amp Labeling Kit (Agilent Technologies, Inc., Santa Clara, CA) and hybridized to the Agilent whole mouse genome microarray (8 × 60), which contains 34000 genes including expressed sequence tags. Signal detection and data analysis were performed in accordance with the manufacturer's instructions (14).

Locomotor activity

Locomotor activity was recorded automatically every 10 min using an ARCO2000 (Neuroscience Co., Tokyo, Japan) located under each chamber.

Functional annotation analysis of genes down-regulated by PGC-1α KO

We conducted pathway analysis using the Kyoto Encyclopedia of Genes and Genomes (KEGG) database resource with DAVID version 6.7 (15), which is a web application providing a comprehensive set of functional annotation tools to understand the biological significance of a large list of genes. A list of symbols of genes that showed decreased expression in skeletal muscles of PGC-1α KO mice was submitted, and significantly overrepresented KEGG pathways were detected.

Bioinformatic analysis of transcription factors enriched among the genes down-regulated in PGC-1α KO mice

We employed ChIP Enrichment analysis (Enricher) software (16) to explore the transcription factors involved in the regulation of genes whose expression was decreased by PGC-1α KO. Enricher is a tool that computes overrepresentations of transcription factor targets from a database of ChIP-seq and ChIP-chip experiments (16).

Statistical analysis

Statistical analysis was performed using Student's t-tests. Data are expressed as the mean

± SE. A P-value <0.05 was considered to be significant. Standard P-values (Fisher’s exact test) and Benjamini P-values were evaluated for functional annotation analysis (Table 2). Fisher’s exact test with Bonferroni's correction was used for transcription factor search analysis (Table 3).

Results and Discussion

Phenotype of PGC-1α KO mice

First, we examined the PGC-1α mRNA level in various tissues of PGC-1α KO mice (Fig. 1A). Among skeletal muscles (gastrocnemius, soleus), liver, adipose tissue, brain, and kidney, a marked decrease of PGC-1α expression was observed in skeletal muscles (Fig. 1A). We examined the PGC-1α protein level in skeletal muscles of PGC-1α KO mice; however, we could not detect PGC-1α expression in both WT and KO mice, likely because the commercially available antibodies used were not sensitive enough (data not shown). We measured the gene expression of PGC1β and PRC, homologues of PGC-1α, in skeletal muscles of PGC-1α KO mice. Gene expression of PGC1β and PRC did not change, thus, there were no compensatory inductions of PGC1β and PRC (Fig. 1B). PGC-1α KO mice and WT control mice were forced to run on a treadmill. The duration that the PGC-1α KO mice could continue to run was shorter than that of WT mice (data not shown). Thus, exercise performance appeared to be lower in PGC-1α KO mice than in WT mice. However, locomotor activity did not differ between PGC-1α KO mice and WT mice (data not shown).

Microarray analysis in skeletal muscles of PGC-1α KO mice

To characterize the phenotype of KO mice skeletal muscles, we performed microarray analysis of gene expression and compared the WT and KO groups. As PGC-1α is a transcriptional coactivator, we focused on genes with decreased expression in KO mice compared with those in WT mice. In fact, there were no genes that showed increased expression in KO compared with those in WT. Table 1 lists the genes with decreased expression (by 0.75-fold) upon training in KO mice compared with training in WT mice (176 genes). Table 1 also provides a comparison of the data of previously examined gene expression changes in PGC-1α Tg mice. Most of the genes with decreased expression in KO mice (colored blue) showed an increased expression level (colored red) in PGC-1α Tg mice. We performed RT-qPCR to examine the representative gene expression of Sdhb (succinate dehydrogenase b) and Mdh2 (malate dehydrogenase 2). These gene expressions were decreased, which was consistent with microarray data. Meanwhile, Arany's group reported that gene expression and electron transfer chain activity in mitochondria was decreased in PGC-1α/PGC1β double KO mice (17). In addition, Kelly's group reported PGC-1α/PGC1β double KO mice (PGC-1α whole body KO and

PGC1β muscle-specific KO) showed diminution of muscle oxidative capacity (18). However, there was no report of microarray analysis data in PGC-1α muscle-specific KO mice, as far as we know.

Pathway analysis of genes with decreased expression in PGC-1α KO mice

To understand the function of these listed genes, we performed bioinformatic pathway analysis (as shown in Table 2). The TCA cycle (Fig. 2), oxidative phosphorylation, fatty acid metabolism, and BCAA degradation pathways were all revealed. These pathways were consistent with previously detected pathways associated with genes with increased expression in PGC-1α Tg mice. Additionally, these pathways are consistent with well-known PGC-1α functions, in that PGC-1α increases mitochondrial biogenesis and fatty acid oxidation (4). These results were also consistent with previous reports that PGC-1α increases the number of mitochondria and enhances their function (3, 5). In our previous study, we showed that PGC-1α Tg enhances BCAA metabolism (14) and activates the TCA cycle (12). These findings explain the decreased (KO) and increased (Tg mice) exercise performances, at least in part. As the PGC-1α KO microarray data in this study show opposing findings to the PGC-1α Tg data, a loss-of-function experiment, as well as a gain-of-function experiment, revealed PGC-1α function in skeletal muscles. Additionally, we observed pathway categories of Parkinson's disease, Huntington's disease, and Alzheimer's disease (Table 2), and found that individual genes with decreased expression in the categories were all related to mitochondrial functions.

Mitochondrial gene expression change

Rowe et al. have reported that gene expression of nuclear-encoded ETC genes (nduf5b, cycs, Cox5b, and Atp5o) of mitochondrial-encoded ETC genes (ND1, ND2, Cytb, Cox1, Cox2, and ATPb) were decreased approximately 0.5-fold in PGC-1α/PGC1β double KO mice, compared with WT mice (17). Zechner et al. also showed that mitochondrial-encoded ETC genes were decreased in PGC-1α/PGC1β double KO mice (18). In our microarray data, corresponding gene expression changes were as follows: Nuclear-encoded ETC genes (nduf5b; 0.79, cycs; 0.75, Cox5b; 0.68, and Atp5o; 0.72) and mitochondrial-encoded ETC genes (ND1; 0.74, ND2; 0.89, Cytb; 0.94, Cox1; 0.92, Cox2; 0.91, and ATPb; 0.88). Thus, nuclear-encoded ETC genes were clearly decreased (~0.7-fold), but mitochondrial-encoded ETC genes were only mildly decreased (~0.9-fold).

These findings indicate that PGC-1α may preferentially regulate nuclear-encoded ETC genes.

Muscle fiber type gene expression

Concerning the fiber type, gene expression of Myh1 (type IIx fiber) (0.6-fold) and Myh7b (type I fiber gene) (0.75-fold) were decreased in PGC-1α-KO mice compared with WT mice. Whereas, gene expression of Myh2 (type IIa) (0.96-fold) and Myh4 (type IIb) (1.08-fold) did not change between WT and PGC-1α-KO mice. Thus, in skeletal muscles of PGC-1α-KO mice, type I and type IIx, but not type IIa and type IIB fibers, are likely decreased, based on gene expression changes. Accordingly, gene expression of Myl2 (0.71-fold), Myl3 (0.73-fold), and Troponin I, which are all slow fiber genes, decreased in PGC-1α KO mice compared with WT mice.

Features of individual genes with changed expression

On examination of individual genes, multiple genes that were previously shown to be PGC-1α targets were included. For example, vascular endothelial growth factor (VEGF) (angiogenesis) (19), lactate dehydrogenase B (catalyzes the reaction of lactate to pyruvate) (20), branched-chain ketoacid dehydrogenase (BCAA degradation) (14), and ERRα (nuclear receptor) were included (7). PGC-1α is a coactivator of multiple nuclear receptors (7), and several nuclear receptors exhibited decreased expression in KO mice: RORγ, PPARα, LXRa, and ERRα. PPARα, LXR, and ERRα are important for lipid metabolism, which may mediate PGC-1α activity in skeletal muscles. Additionally, the myokine Irisin (Fndc5) (21) appeared on the list (Table 1). In addition to Irisin, several secretory proteins, including fibroblast growth factor 1 (FGF1) (22), were included, which may be myokines regulated by PGC-1α.

Possible nuclear receptors that mediate PGC-1α activity

Bioinformatic analysis also revealed that several nuclear receptors, including ERR and PPAR, are frequently recruited to genes down-regulated in skeletal muscles of PGC-1α KO mice (Table 3). These findings suggest that PGC-1α regulates gene expression through multiple nuclear receptors.

In this study, we investigated the role of PGC-1α regulation in murine skeletal muscles

by deleting PGC-1α. Our data showed that mitochondrion-related gene expression was down-regulated, which was the reverse of previous findings in PGC-1α Tg mice, supporting a critical role of PGC-1α during conditions that induce the expression of PGC-1α, such as exercise.

References

1. Puigserver P, Wu Z, Park CW, Graves R, Wright M, Spiegelman BM. - A cold-inducible coactivator of nuclear receptors linked to adaptive. Cell. 1998;92(6):829-39.

2. Liang H, Balas B, Tantiwong P, Dube J, Goodpaster BH, O'Doherty RM, DeFronzo RA, Richardson A, Musi N, Ward WF. Whole body overexpression of PGC-1alpha has opposite effects on hepatic and muscle insulin sensitivity. Am. J. Physiol. Endocrinol. Metab. 2009;296(4):E945-54.

3. Puigserver P, Spiegelman BM. Peroxisome proliferator-activated receptor-gamma coactivator 1 alpha (PGC-1 alpha): transcriptional coactivator and metabolic regulator. Endocrine Reviews. 2003;24(1):78-90.

4. Tadaishi M, Miura S, Kai Y, Kano Y, Oishi Y, Ezaki O. Skeletal muscle-specific expression of PGC-1alpha-b, an exercise-responsive isoform, increases exercise capacity and peak oxygen uptake. PloS One. 2011;6(12):e28290.

5. Wareski P, Vaarmann A, Choubey V, Safiulina D, Liiv J, Kuum M, Kaasik A. PGC-1alpha and PGC-1beta regulate mitochondrial density in neurons. J Biol Chem. 2009;284(32):21379-85.

6. Kamei Y, Hatazawa Y, Yoshimura R, Miura S. PGC-1α, a stimuli-inducible nuclear receptor coactivator: structural features and role in skeletal muscle metabolism gene regulation. RNA and Transcription. 2015;1(1):6-9.

7. Kamei Y, Ohizumi H, Fujitani Y, Nemoto T, Tanaka T, Takahashi N, Kawada T, Miyoshi M, Ezaki O and Kakizuka A. PPARgamma coactivator 1beta/ERR ligand 1 is an ERR protein ligand. Proc Natl Acad Sci USA. 2003;100(21):12378-83.

8. Kelly DP, Scarpulla RC. Transcriptional regulatory circuits controlling mitochondrial biogenesis and function. Genes & development. 2004;18(4):357-68.

9. Lin J, Puigserver P, Donovan J, Tarr P, Spiegelman BM. Peroxisome proliferator-activated receptor gamma coactivator 1beta (PGC-1beta), a novel PGC-1-related transcription coactivator associated with host cell factor. J Biol Chem. 2002;277(3):1645-8.

10. Rodgers JT, Lerin C, Gerhart-Hines Z, Puigserver P. Metabolic adaptations through the PGC-1 alpha and SIRT1 pathways. FEBS Letters. 2008;582(1):46-53.

11. Yoshimura R, Minami K, Matsuda J, Sawada N, Miura S, Kamei Y. Phosphorylation of 4EBP by oral leucine administration was suppressed in the skeletal muscle of PGC-1alpha knockout mice. Bioscience, Biotechnology, and Biochemistry.

2016;80(2):288-90.

12. Hatazawa Y, Senoo N, Tadaishi M, Ogawa Y, Ezaki O, Kamei Y, Miura S. Metabolomic Analysis of the Skeletal Muscle of Mice Overexpressing PGC-1alpha. PloS One. 2015;10(6):e0129084.

13. Sawada N, Jiang A, Takizawa F, Safdar A, Manika A, Tesmenitsky Y, Kang KT, Bischoff J, Kalwa H, Sartoretto JL, Kamei Y, Benjamin LE, Watada H, Ogawa Y, Higashikuni Y, Kessinger CW, Jaffer FA, Michel T, Sata M, Croce K, Tanaka R, Arany Z. Endothelial PGC-1alpha mediates vascular dysfunction in diabetes. Cell Metabolism. 2014;19(2):246-58.

14. Hatazawa Y, Tadaishi M, Nagaike Y, Morita A, Ogawa Y, Ezaki O, Takai-Igarashi T, Kitaura Y, Shimomura Y, Kamei Y, Miura S. PGC-1alpha-mediated branched-chain amino acid metabolism in the skeletal muscle. PloS One. 2014;9(3):e91006.

15. Huang da W, Sherman BT, Lempicki RA. Systematic and integrative analysis of large gene lists using DAVID bioinformatics resources. Nature Protocols. 2009;4(1):44-57.

16. Lachmann A, Xu H, Krishnan J, Berger SI, Mazloom AR, Ma'ayan A. ChEA: transcription factor regulation inferred from integrating genome-wide ChIP-X experiments. Bioinformatics. 2010;26(19):2438-44.

17. Rowe GC, Patten IS, Zsengeller ZK, El-Khoury R, Okutsu M, Bampoh S, Koulisis N, Farrell C, Hirshman MF, Yan Z, Goodyear LJ, Rustin P, Arany Z. Disconnecting mitochondrial content from respiratory chain capacity in PGC-1-deficient skeletal muscle. Cell Rep. 2013;3(5):1449-56.

18. Zechner C, Lai L, Zechner JF, Geng T, Yan Z, Rumsey JW, Collia D, Chen Z, Wozniak DF, Leone TC, Kelly DP. Total skeletal muscle PGC-1 deficiency uncouples mitochondrial derangements from fiber type determination and insulin sensitivity. Cell Metab. 2010;12(6):633-42.

19. Chinsomboon J, Ruas J, Gupta RK, Thom R, Shoag J, Rowe GC, Sawada N, Raghuram S, Arany Z. The transcriptional coactivator PGC-1alpha mediates exercise-induced angiogenesis in skeletal muscle. Proc Natl Acad Sci USA. 2009;106(50):21401-6.

20. Summermatter S, Santos G, Perez-Schindler J, Handschin C. Skeletal muscle PGC-1alpha controls whole-body lactate homeostasis through estrogen-related receptor alpha-dependent activation of LDH B and repression of LDH A. Proc Natl Acad Sci USA.

2013;110(21):8738-43.

21. Bostrom P, Wu J, Jedrychowski MP, Korde A, Ye L, Lo JC, Rasbach KA, Bostrom EA, Choi JH, Long JZ, Kajimura S, Zingaretti MC, Vind BF, Tu H, Cinti S, Hojlund K, Gygi SP, Spiegelman BM. A PGC1-alpha-dependent myokine that drives brown-fat-like development of white fat and thermogenesis. Nature. 2012;481(7382):463-8.

22. Narkar VA, Fan W, Downes M, Yu RT, Jonker JW, Alaynick WA, Banayo E, Karunasiri MS, Lorca S, Evans RM. Exercise and PGC-1alpha-independent synchronization of type I muscle metabolism and vasculature by ERRgamma. Cell Metabolism. 2011;13(3):283-93.

Legends

Figure 1

Expression of PGC-1α mRNA in various tissues of PGC-1α KO mice

A) The mRNA levels of PGC-1α in the tissues of WT and PGC-1α KO mice (male, 16 weeks of age). (n = 3 for WT, n = 4 for KO) B) The mRNA levels of PGC-1β and PRC in the tissues of WT and PGC-1α KO mice (male, 12 weeks of age). (n = 8 for WT, n = 7 for KO). C) The mRNA levels of Sdhb and Mdh2 in the tissues of WT and PGC-1α KO mice. These mice are the same as Fig. 1B. Relative mRNA levels are shown. The white bar shows WT mice and the black bar shows PGC-1α KO mice. Values are expressed as the mean ± SE. **p < 0.01, ***p < 0.001.

Figure 2

Pathway map of TCA cycle (citrate cycle)

Individual gene names (enzyme numbers) of the KEGG pathway of the TCA cycle extracted by pathway analysis are shown as a metabolic map. The red asterisks indicate decreased (< 0.75-fold) gene expression as determined by microarray analysis of KO mice. Gene names corresponding to enzyme numbers with red asterisks are as follows: 2.3.1.12, dihydrolipoamide S-acetyltransferase (E2 component of the pyruvate dehydrogenase complex); 4.2.1.2, fumarate hydratase 1; 1.1.1.42, isocitrate dehydrogenase 2 (NADP+), mitochondrial; 1.1.1.41, isocitrate dehydrogenase 3 (NAD+), gamma; 1.1.1.37, malate dehydrogenase 2, NAD (mitochondrial); 1.2.4.2, oxoglutarate dehydrogenase (lipoamide); 1.2.4.1, pyruvate dehydrogenase E1 alpha 1; 1.3.5.1, succinate dehydrogenase complex, subunit C, integral membrane protein; 6.2.1.4 and 6.2.1.5, succinate-CoA ligase, GDP-forming, alpha subunit.

Table 1

List of genes down-regulated in KO mice as determined by microarray analysis

RNA obtained from WT and KO mice was pooled and used for microarray analysis as described in the Methods. Hybridized signals outside the linear range were excluded, and values were normalized by the 75th percentile calculation. Genes with a calculated value less than 100 in WT mice were deleted. Genes down-regulated less than 0.75-fold in KO mice are listed. The previously determined change in gene expression of Tg mice (14) is shown alongside. Up-regulated genes are shown in red and down-regulated genes in blue.

Darker red shows higher gene expression.

Table 2

Pathway analysis

Compared with those in WT mice, 176 genes were found to be down-regulated (< 0.75-fold) in PGC-1α KO mice by microarray analysis and classified into the KEGG pathway analysis as described in the Methods.

Table 3

Bioinformatic analysis of transcription factors enriched among the genes down-regulated in PGC-1α KO mice

A list of the transcription factors that were identified as ones that were recruited to the down-regulated genes in PGC-1α KO mice. Target genes were previously found by an ChIP assay to interact with the indicated transcription factors (16). Abbreviations of the transcription factors are as follows: PPARG, constitutive coactivator of peroxisome proliferator-activated receptor gamma (constitutive coactivator of PPAR-gamma) (constitutive coactivator of PPARG); ESRRB, steroid hormone receptor ERR2 (estrogen receptor-like 2) (estrogen-related receptor beta) (ERR-beta); PPARD, NR0B1, nuclear receptor subfamily 0 group B member 1 (nuclear receptor DAX-1).

Fig.1

A

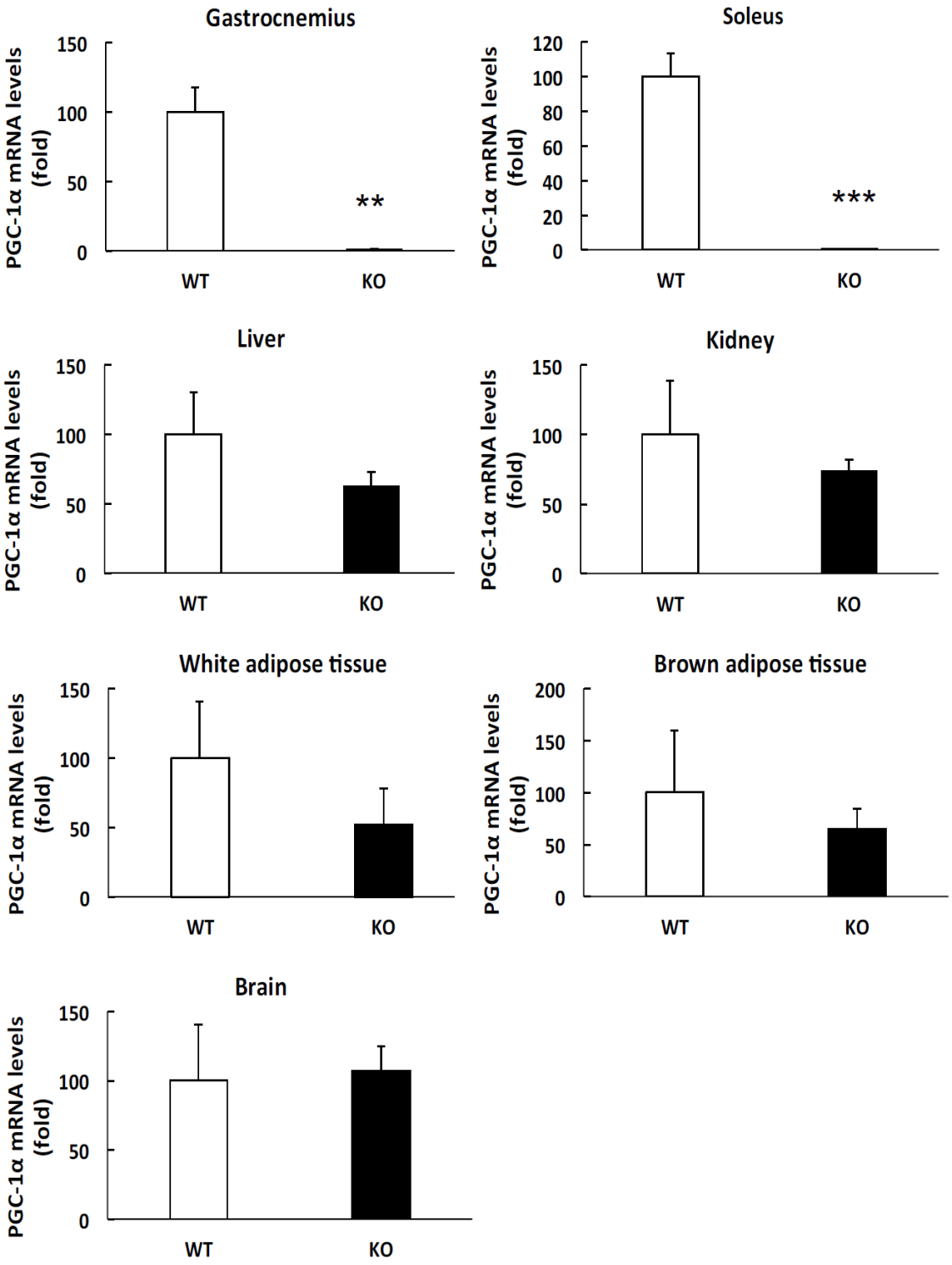
Gastrocnemius
PGC-1α mRNA levels (fold)
150
100
50
0
**
WT
KO
Soleus
PGC-1α mRNA levels (fold)
120
100
80
60
40
20
0
***
WT
KO
Liver
PGC-1α mRNA levels (fold)
150
100
50
0
WT
KO
Kidney
PGC-1α mRNA levels (fold)
150
100
50
0
WT
KO
White adipose tissue
PGC-1α mRNA levels (fold)
150
100
50
0
WT
KO
Brown adipose tissue
PGC-1α mRNA levels (fold)
200
150
100
50
0
WT
KO
Brain
PGC-1α mRNA levels (fold)
150
100
50
0
WT
KO

Fig.1

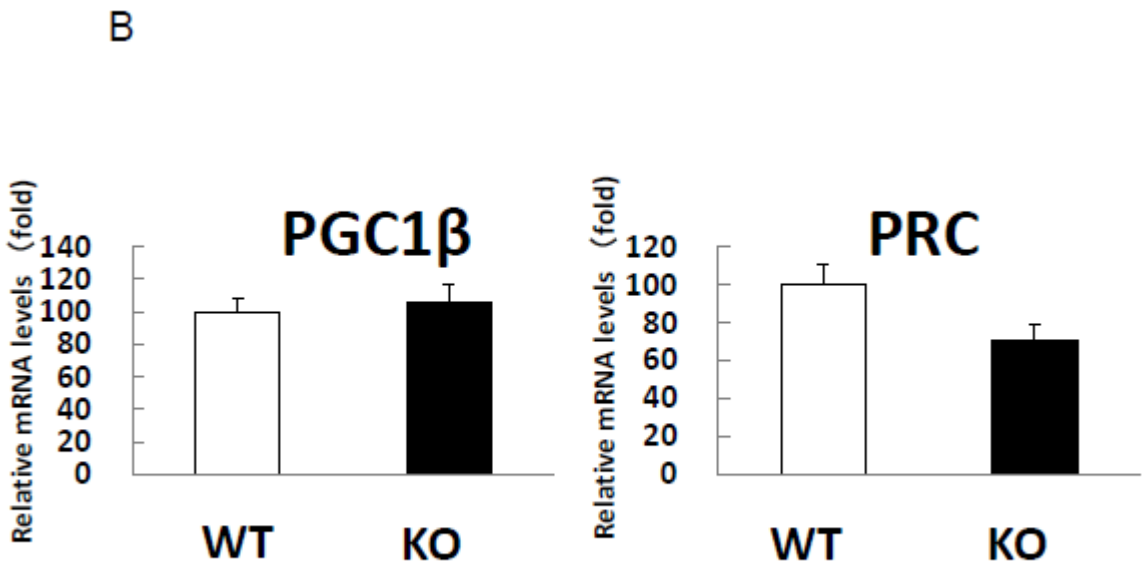
B
PGC1β
Relative mRNA levels (fold)
140
120
100
80
60
40
20
0
WT
KO
PRC
Relative mRNA levels (fold)
120
100
80
60
40
20
0
WT
KO

Fig.1

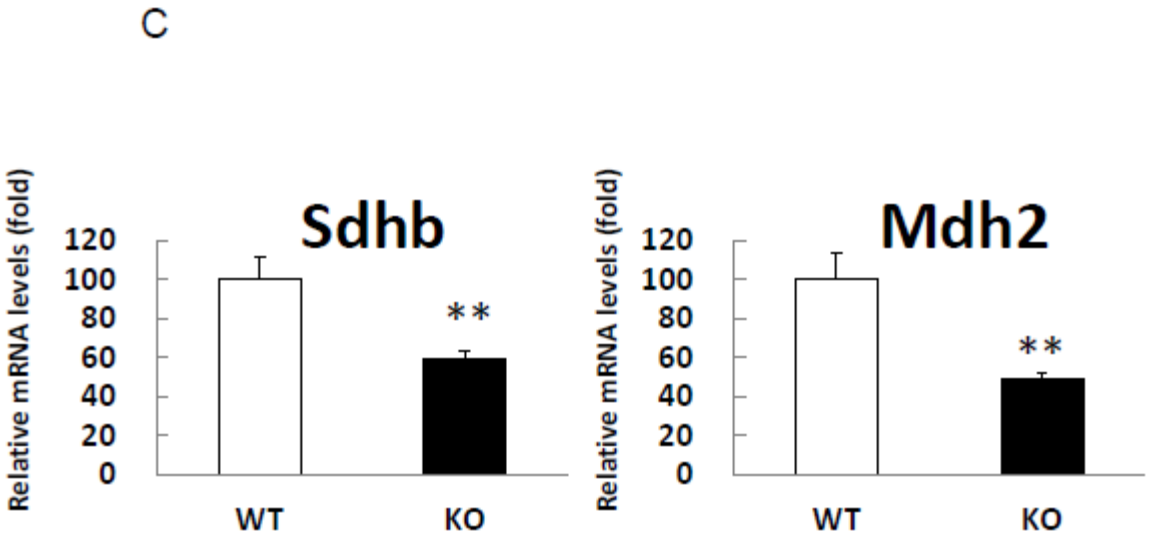
C
Relative mRNA levels (fold)
120
100
80
60
40
20
0
Sdhb
**
WT
KO
Relative mRNA levels (fold)
120
100
80
60
40
20
0
Mdh2
**
WT
KO

Fig.2

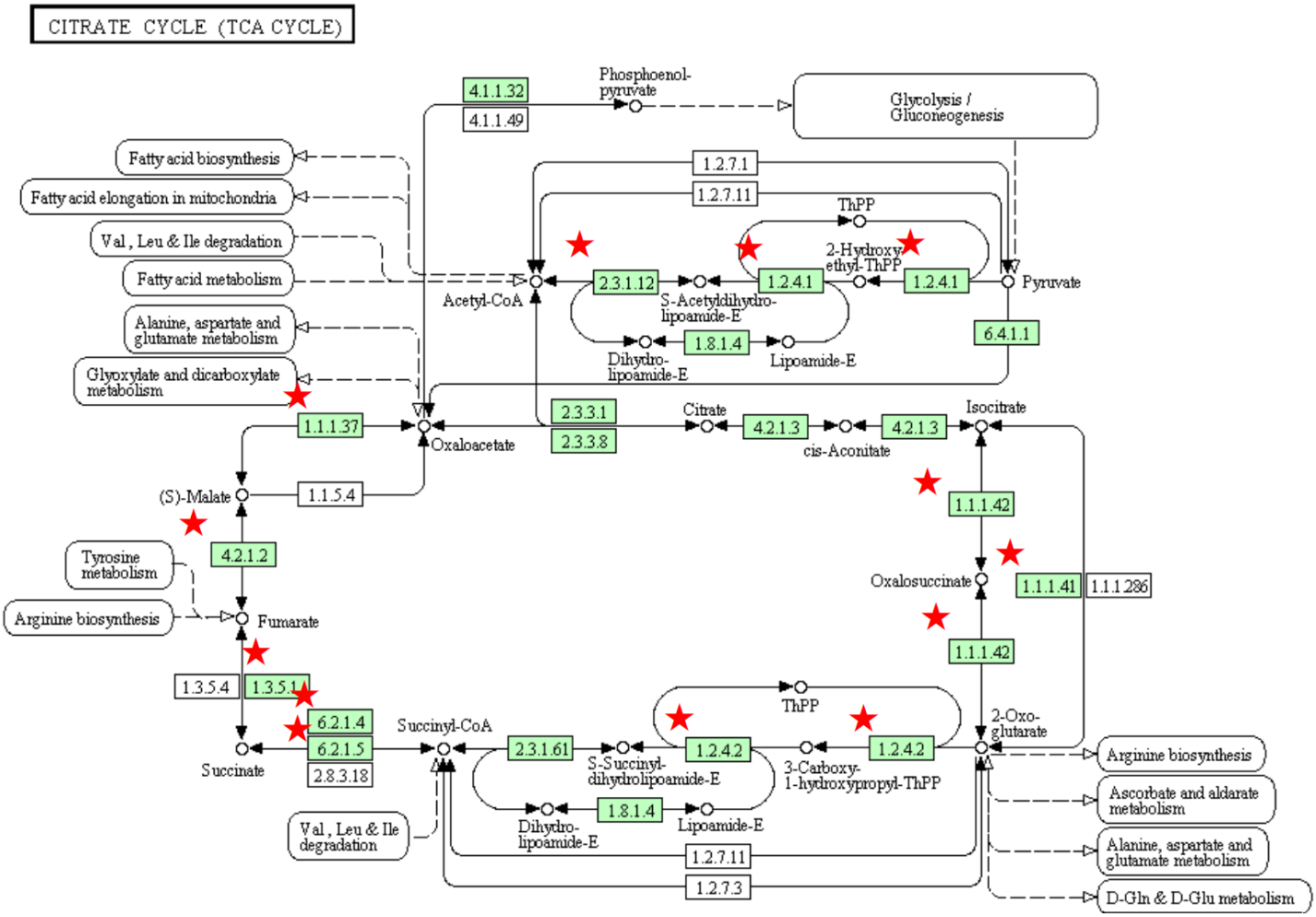
CITRATE CYCLE (TCA CYCLE)
Phosphoenol-pyruvate
4.1.1.32
4.1.1.49
Glycolysis / Gluconeogenesis
Fatty acid biosynthesis
Fatty acid elongation in mitochondria
Val, Leu & Ile degradation
Fatty acid metabolism
Alanine, aspartate and glutamate metabolism
Glyoxylate and dicarboxylate metabolism
1.2.7.1
1.2.7.11
ThPP
2-Hydroxy-ethyl-ThPP
2.3.1.12
1.2.4.1
1.2.4.1
Pyruvate
Acetyl-CoA
S-Acetyldihydro-lipoamide-E
1.8.1.4
Dihydro-lipoamide-E
Lipoamide-E
6.4.1.1
1.1.1.37
Oxaloacetate
2.3.3.1
2.3.3.8
Citrate
4.2.1.3
4.2.1.3
cis-Aconitate
Isocitrate
(S)-Malate
1.1.5.4
1.1.1.42
Tyrosine metabolism
4.2.1.2
Oxalosuccinate
1.1.1.41
1.1.1.286
Arginine biosynthesis
Fumarate
1.1.1.42
1.3.5.4
1.3.5.1
ThPP
6.2.1.4
6.2.1.5
2.8.3.18
Succinyl-CoA
2.3.1.61
1.2.4.2
1.2.4.2
2-Oxo-glutarate
Succinate
S-Succinyl-dihydrolipoamide-E
3-Carboxy-1-hydroxypropyl-ThPP
Arginine biosynthesis
Ascorbate and aldarate metabolism
Alanine, aspartate and glutamate metabolism
D-Gln & D-Glu metabolism
Val, Leu & Ile degradation
1.8.1.4
Dihydro-lipoamide-E
Lipoamide-E
1.2.7.11
1.2.7.3

Table 1

GeneName	SystematicName	Description	KO / WT	TG / WT
Hbb-b1	NM_008220	hemoglobin, beta adult major chain (Hbb-b1)	0.38	2.67
ENSMUST00000081342	NM_001177544	histone cluster 1, H2ap	0.38	–
Hbb-b2	NM_016956	hemoglobin, beta adult minor chain (Hbb-b2)	0.41	–
Ostn	NM_198112	osteocrin (Ostn)	0.45	0.27
Beta-s	NM_001278161	hemoglobin subunit beta-1-like (Beta-s)	0.45	–
Smpx	NM_001252591	small muscle protein, X-linked (Smpx), transcript variant 1	0.45	–
Phyh	NM_010726	phytanoyl-CoA hydroxylase (Phyh)	0.45	4.08
Fndc5	NM_027402	fibronectin type III domain containing 5 (Fndc5)	0.46	4.29
Rasd2	NM_029182	RASD family, member 2 (Rasd2)	0.46	–
Hba-a1	NM_008218	hemoglobin alpha, adult chain 1 (Hba-a1)	0.47	3.43
Lactb	NM_030717	lactamase, beta (Lactb)	0.48	0.86
Cox7a1	NM_009944	cytochrome c oxidase subunit VIIa 1 (Cox7a1)	0.48	1.97
Got2	NM_010325	glutamate oxaloacetate transaminase 2, mitochondrial (Got2)	0.49	4.05
Me3	NM_181407	malic enzyme 3, NADP(+)-dependent, mitochondrial (Me3)	0.50	1.70
Dlat	NM_145614	dihydrolipoamide S-acetyltransferase (E2 component of pyruvate dehydrogenase complex) (Dlat)	0.51	3.49
Hba-a2	NM_001083955	hemoglobin alpha, adult chain 2 (Hba-a2)	0.52	–
Ckmt2	NM_198415	creatine kinase, mitochondrial 2 (Ckmt2)	0.53	4.43
Aldh5a1	NM_172532	aldhehyde dehydrogenase family 5, subfamily A1 (Aldh5a1)	0.53	2.97
Scn4b	NM_001013390	sodium channel, type IV, beta (Scn4b)	0.54	–
Ablim3	NM_198649	actin binding LIM protein family, member 3 (Ablim3), transcript variant 1	0.54	0.85
Got1	NM_010324	glutamate oxaloacetate transaminase 1, soluble (Got1)	0.55	4.36
TC1733495	TC1733495	amylase	0.57	–
Ushbp1	NM_181418	Usher syndrome 1C binding protein 1 (Ushbp1)	0.58	2.45
Gpr116	NM_001081178	G protein-coupled receptor 116 (Gpr116)	0.59	–
Mss51	NM_029104	MSS51 mitochondrial translational activator (Mss51)	0.59	–
Klhl31	NM_172925	kelch-like 31 (Klhl31)	0.59	0.36
Mustn1	NM_181390	musculoskeletal, embryonic nuclear protein 1 (Mustn1)	0.59	3.03
Amy1	NM_007446	amylase 1, salivary (Amy1), transcript variant 1	0.59	1.60
S100a1	NM_011309	S100 calcium binding protein A1 (S100a1)	0.59	4.08
Myh1	NM_030679	myosin, heavy polypeptide 1, skeletal muscle, adult (Myh1)	0.60	3.52
Pde5a	NM_153422	phosphodiesterase 5A, cGMP-specific (Pde5a)	0.60	–
Chmp4b	NM_029362	charged multivesicular body protein 4B (Chmp4b)	0.61	1.17
Kcnc4	NM_145922	potassium voltage gated channel, Shaw-related subfamily, member 4 (Kcnc4)	0.61	0.81
Vapb	NM_019806	vesicle-associated membrane protein, associated protein B and C (Vapb)	0.62	0.80
Scd1	NM_009127	stearoyl-Coenzyme A desaturase 1 (Scd1)	0.62	1.04
Acaa2	NM_177470	acetyl-Coenzyme A acyltransferase 2 (mitochondrial 3-oxoacyl-Coenzyme A thiolase) (Acaa2)	0.62	3.95
Il6ra	NM_010559	interleukin 6 receptor, alpha (Il6ra)	0.63	0.79
Cdc42ep1	NM_027219	CDC42 effector protein (Rho GTPase binding) 1 (Cdc42ep1)	0.63	1.78
Smtnl1	NM_024230	smoothelin-like 1 (Smtnl1)	0.63	3.08
Akr1b10	NM_172398	aldo-keto reductase family 1, member B10 (aldose reductase) (Akr1b10)	0.63	1.62
Rorc	NM_011281	RAR-related orphan receptor gamma (Rorc)	0.63	2.00
Ldhb	NM_008492	lactate dehydrogenase B (Ldhb)	0.63	5.01
Ppara	NM_011144	peroxisome proliferator activated receptor alpha (Ppara), transcript variant 1	0.63	3.44
Msrb2	NM_029619	methionine sulfoxide reductase B2 (Msrb2)	0.63	4.61
Cnbp	ENSMUST000001	cellular nucleic acid binding protein	0.64	–
Dlx3	NM_010055	distal-less homeobox 3 (Dlx3)	0.64	–
Plbd1	NM_025806	phospholipase B domain containing 1 (Plbd1)	0.64	4.36
Mb	NM_013593	myoglobin (Mb), transcript variant 2	0.64	3.10
Csrp3	NM_013808	cysteine and glycine-rich protein 3 (Csrp3), transcript variant 1	0.65	0.47
Mtfp1	NM_026443	mitochondrial fission process 1 (Mtfp1)	0.65	3.82
Dgat2	NM_026384	diacylglycerol O-acyltransferase 2 (Dgat2)	0.65	3.34
Uqcrc1	NM_025407	ubiquinol-cytochrome c reductase core protein 1 (Uqcrc1)	0.66	2.61
Lmcd1	NM_144799	LIM and cysteine-rich domains 1 (Lmcd1)	0.66	2.01
Tmem37	NM_019432	transmembrane protein 37 (Tmem37)	0.66	7.13
Copa	NM_009938	coatomer protein complex subunit alpha (Copa)	0.66	1.01
Fgf1	NM_010197	fibroblast growth factor 1 (Fgf1)	0.66	3.57
Aldh1a1	NM_013467	aldehyde dehydrogenase family 1, subfamily A1 (Aldh1a1)	0.66	0.88
Rcan2	NM_001286653	regulator of calcineurin 2 (Rcan2), transcript variant 1	0.66	–
Fam195a	NM_026633	family with sequence similarity 195, member A (Fam195a)	0.66	3.43
Dusp26	NM_025869	dual specificity phosphatase 26 (putative) (Dusp26)	0.66	0.44
Tmem246	NM_025944	transmembrane protein 246 (Tmem246)	0.66	1.20
Egfl7	NM_178444	EGF-like domain 7 (Egfl7), transcript variant a	0.66	2.17
Gpihbp1	NM_026730	GPI-anchored HDL-binding protein 1 (Gpihbp1)	0.66	2.49
Padi2	NM_008812	peptidyl arginine deiminase, type II (Padi2)	0.66	2.18
Neu2	NM_001160165	neuraminidase 2 (Neu2), transcript variant 3	0.67	–
Slco3a1	NM_001038643	solute carrier organic anion transporter family, member 3a1 (Slco3a1), transcript variant 2	0.67	–
Mfn1	NM_024200	mitofusin 1 (Mfn1)	0.67	2.20
Cdh5	NM_009868	cadherin 5 (Cdh5)	0.67	1.39
Nnt	NM_008710	nicotinamide nucleotide transhydrogenase (Nnt)	0.67	0.76
Nos3	NM_008713	nitric oxide synthase 3, endothelial cell (Nos3)	0.67	2.14
Gadd45b	NM_008655	growth arrest and DNA-damage-inducible 45 beta (Gadd45b)	0.67	0.78
Tnni1	NM_021467	troponin I, skeletal, slow 1 (Tnni1), transcript variant 1	0.67	1.08
Adamts1	NM_009621	a disintegrin-like and metallopeptidase (reprolysin type) with thrombospondin type 1 motif, 1 (Adamts1)	0.67	0.93
Nr1h3	NM_013839	nuclear receptor subfamily 1, group H, member 3 (Nr1h3), transcript variant 1	0.67	1.33
Pdha1	NM_008810	pyruvate dehydrogenase E1 alpha 1 (Pdha1)	0.67	2.08
Sdhb	NM_023374	succinate dehydrogenase complex, subunit B, iron sulfur (Ip) (Sdhb)	0.68	3.33
Pdk2	NM_133667	pyruvate dehydrogenase kinase, isoenzyme 2 (Pdk2)	0.68	1.54
Bckdha	NM_007533	branched chain ketoacid dehydrogenase E1, alpha polypeptide (Bckdha)	0.68	3.17
2310002L09Rik	NM_027981	RIKEN cDNA 2310002L09 gene (2310002L09Rik)	0.68	–
Vegfb	NM_011697	vascular endothelial growth factor B (Vegfb)	0.68	3.30
Esrra	NM_007953	estrogen related receptor, alpha (Esrra)	0.68	2.91
Gpt	NM_182805	glutamic pyruvic transaminase, soluble (Gpt)	0.68	3.55
Sirt3	NM_022433	sirtuin 3 (silent mating type information regulation 2, homolog) 3 (S. cerevisiae) (Sirt3)	0.68	3.14
Tmem52	NM_027161	transmembrane protein 52 (Tmem52)	0.68	–
Acadl	NM_007381	acyl-Coenzyme A dehydrogenase, long-chain (Acadl)	0.68	3.63
Dok7	ENSMUST000001	docking protein 7	0.68	–
Echs1	NM_053119	enoyl Coenzyme A hydratase, short chain, 1, mitochondrial (Echs1)	0.68	2.41
Rgma	NM_177740	RGM domain family, member A (Rgma)	0.69	0.65
Ankrd2	NM_020033	ankyrin repeat domain 2 (stretch responsive muscle) (Ankrd2)	0.69	1.11
Cyc1	NM_025567	cytochrome c-1 (Cyc1)	0.69	2.73
Acat1	NM_144784	acetyl-Coenzyme A acetyltransferase 1 (Acat1)	0.69	1.56
Apoo	NM_001199337	apolipoprotein O (Apoo), transcript variant 2	0.69	–
D10Jhu81e	NM_138601	DNA segment, Chr 10, Johns Hopkins University 81 expressed (D10Jhu81e)	0.70	2.33
Idh3g	NM_008323	isocitrate dehydrogenase 3 (NAD+), gamma (Idh3g)	0.70	1.92
Ivd	NM_019826	isovaleryl coenzyme A dehydrogenase (Ivd)	0.70	1.67
Rnf128	NM_023270	ring finger protein 128 (Rnf128), transcript variant 1	0.70	1.44

Table 1

Ciapin1	NM_134141	cytokine induced apoptosis inhibitor 1 (Ciapin1)	0.70	5.84
Cmss1	NM_025599	cms small ribosomal subunit 1 (Cmss1)	0.70	1.99
Acot7	NM_133348	acyl-CoA thioesterase 7 (Acot7), transcript variant 2	0.70	2.01
Idh2	NM_173011	isocitrate dehydrogenase 2 (NADP+), mitochondrial (Idh2)	0.70	2.85
Ndufv1	NM_133666	NADH dehydrogenase (ubiquinone) flavoprotein 1 (Ndufv1)	0.70	2.07
Mdh2	NM_008617	malate dehydrogenase 2, NAD (mitochondrial) (Mdh2)	0.70	2.27
Rgcc	NM_025427	regulator of cell cycle (Rgcc)	0.70	1.67
Hist1h2ag	NM_178186	histone cluster 1, H2ag (Hist1h2ag)	0.71	–
Myl2	NM_010861	myosin, light polypeptide 2, regulatory, cardiac, slow (Myl2)	0.71	0.64
Plin5	NM_001077348	perilipin 5 (Plin5), transcript variant 2	0.71	7.15
Tango2	NM_138583	transport and golgi organization 2 (Tango2)	0.71	3.89
Atp5sl	NM_025504	ATP5S-like (Atp5sl)	0.71	2.92
Tnnt1	NM_001277903	troponin T1, skeletal, slow (Tnnt1)	0.71	–
Mcf2l	NM_178076	mcf.2 transforming sequence-like (Mcf2l), transcript variant 1	0.71	1.35
Cyp2r1	NM_177382	cytochrome P450, family 2, subfamily r, polypeptide 1 (Cyp2r1)	0.71	–
Mid1ip1	NM_001166635	Mid1 interacting protein 1 (gastrulation specific G12-like (zebrafish)) (Mid1ip1), transcript variant 1	0.71	–
Aldh2	NM_009656	aldehyde dehydrogenase 2, mitochondrial (Aldh2)	0.71	2.07
Ndufa8	NM_026703	NADH dehydrogenase (ubiquinone) 1 alpha subcomplex, 8 (Ndufa8)	0.71	2.15
Atp1b1	NM_009721	ATPase, Na+/K+ transporting, beta 1 polypeptide (Atp1b1)	0.71	3.18
Slc9a3r2	NM_023055	solute carrier family 9 (sodium/hydrogen exchanger), member 3 regulator 2 (Slc9a3r2), transcript variant A	0.71	–
Sdha	NM_023281	succinate dehydrogenase complex, subunit A, flavoprotein (Fp) (Sdha)	0.71	2.52
Aqp1	NM_007472	aquaporin 1 (Aqp1)	0.72	2.10
Cox5b	NM_009942	cytochrome c oxidase subunit Vb (Cox5b)	0.72	–
Ppip5k1	NM_178795	diphosphoinositol pentakisphosphate kinase 1 (Ppip5k1)	0.72	2.42
LOC100046079	XM_006542973	cytochrome c oxidase subunit 5B, mitochondrial-like	0.72	–
Flt1	NM_010228	FMS-like tyrosine kinase 1 (Flt1)]	0.72	2.09
Atp5g1	NM_001161419	ATP synthase, H+ transporting, mitochondrial F0 complex, subunit c1 (subunit 9) (Atp5g1)	0.72	–
Vwa8	NM_173758	von Willebrand factor A domain containing 8 (Vwa8), transcript variant 2	0.72	–
Ndufa9	NM_025358	NADH dehydrogenase (ubiquinone) 1 alpha subcomplex, 9 (Ndufa9)	0.72	2.43
Stab2	NM_138673	stabilin 2 (Stab2)	0.72	1.81
Atp5b	NM_016774	ATP synthase, H+ transporting mitochondrial F1 complex, beta subunit (Atp5b)	0.72	2.10
Alas1	NM_001291835	aminolevulinic acid synthase 1 (Alas1)	0.72	–
Rgs5	NM_009063	regulator of G-protein signaling 5 (Rgs5)	0.72	1.74
Sdhc	NM_025321	succinate dehydrogenase complex, subunit C, integral membrane protein (Sdhc)	0.72	1.95
Ptges2	NM_133783	prostaglandin E synthase 2 (Ptges2)	0.73	2.31
Sod2	NM_013671	superoxide dismutase 2, mitochondrial (Sod2)	0.73	2.89
Myl3	NM_010859	myosin, light polypeptide 3 (Myl3)	0.73	0.47
Pdlim1	NM_016861	PDZ and LIM domain 1 (elfin) (Pdlim1)	0.73	1.21
Ndufs1	NM_145518	NADH dehydrogenase (ubiquinone) Fe-S protein 1 (Ndufs1)	0.73	2.03
Cyth1	NM_011180	cytohesin 1 (Cyth1), transcript variant 1	0.73	2.69
Coq9	NM_026452	coenzyme Q9 homolog (yeast) (Coq9)	0.73	2.12
Midn	NM_021565	midnolin (Midn)	0.73	2.23
Tox4	NM_023434	TOX high mobility group box family member 4 (Tox4)	0.73	0.76
Cpt1b	NM_009948	carnitine palmitoyltransferase 1b, muscle (Cpt1b)	0.73	2.40
Mpc2	NM_027430	mitochondrial pyruvate carrier 2 (Mpc2)	0.73	2.86
Fdft1	NM_010191	farnesyl diphosphate farnesyl transferase 1 (Fdft1)	0.73	2.37
Fxyd6	NM_022004	FXYD domain-containing ion transport regulator 6 (Fxyd6)	0.73	0.91
Cab39	NM_133781	calcium binding protein 39 (Cab39)	0.73	0.63
Kank3	NM_030697	KN motif and ankyrin repeat domains 3 (Kank3)	0.73	1.80
Sema7a	NM_011352	sema domain, immunoglobulin domain (Ig), and GPI membrane anchor, (semaphorin) 7A (Sema7a)	0.73	2.67
Hibadh	NM_145567	3-hydroxyisobutyrate dehydrogenase (Hibadh)	0.73	2.55
Cd36	NM_007643	CD36 antigen (Cd36), transcript variant 2	0.73	3.16
Adh1	NM_007409	alcohol dehydrogenase 1 (class I) (Adh1)	0.73	2.26
Myom3	NM_001085509	myomesin family, member 3 (Myom3)	0.73	–
TC1627788	TC1627788	Atp5b protein (Fragment), partial (30%)	0.74	2.32
Atp5c1	NM_001112738	ATP synthase, H+ transporting, mitochondrial F1 complex, gamma polypeptide 1 (Atp5c1)	0.74	–
Ogdh	NM_001252287	oxoglutarate (alpha-ketoglutarate) dehydrogenase (lipoamide) (Ogdh), transcript variant 3	0.74	–
Etfa	NM_145615	electron transferring flavoprotein, alpha polypeptide (Etfa)	0.74	2.22
Tnnc1	NM_009393	troponin C, cardiac/slow skeletal (Tnnc1)	0.74	1.01
Hspb7	NM_013868	heat shock protein family, member 7 (cardiovascular) (Hspb7)	0.74	1.19
Abhd11	NM_145215	abhydrolase domain containing 11 (Abhd11)	0.74	1.64
Ldhd	NM_027570	lactate dehydrogenase D (Ldhd), nuclear gene encoding mitochondrial protein	0.74	3.09
Uqcrc2	NM_025899	ubiquinol cytochrome c reductase core protein 2 (Uqcrc2)	0.74	2.13
Inf2	NM_198411	inverted formin, FH2 and WH2 domain containing (Inf2)	0.74	1.55
Acadvl	NM_017366	acyl-Coenzyme A dehydrogenase, very long chain (Acadvl)	0.74	4.20
Thap4	NM_025920	THAP domain containing 4 (Thap4)	0.74	1.40
Slc25a3	NM_133668	solute carrier family 25 (mitochondrial carrier, phosphate carrier), member 3 (Slc25a3)	0.74	2.55
Vegfa	NM_001025250	vascular endothelial growth factor A (Vegfa)	0.75	2.98
9430020K01Rik	NM_001081963	RIKEN cDNA 9430020K01 gene (9430020K01Rik)	0.75	–
Eci1	NM_010023	enoyl-Coenzyme A delta isomerase 1 (Eci1)	0.75	2.79
Acot13	NM_025790	acyl-CoA thioesterase 13 (Acot13)	0.75	1.95
Fh1	NM_010209	fumarate hydratase 1 (Fh1)	0.75	1.51
Suclg1	NM_019879	succinate-CoA ligase, GDP-forming, alpha subunit (Suclg1)	0.75	2.29
Enpp4	NM_199016	ectonucleotide pyrophosphatase/phosphodiesterase 4 (Enpp4)	0.75	0.66
Ehd2	ENSMUST000000	EH-domain containing 2	0.75	–
Ptprb	NM_029928	protein tyrosine phosphatase, receptor type, B (Ptprb)	0.75	1.47
Myh7b	NM_001085378	myosin, heavy chain 7B, cardiac muscle, beta (Myh7b)	0.75	–
Vgll2	NM_153786	vestigial like 2 homolog (Drosophila) (Vgll2)	0.75	0.85
Ptp4a3	NM_008975	protein tyrosine phosphatase 4a3 (Ptp4a3)	0.75	1.87

Table 2

Categories of pathway analysis	P-Value	Benjamini
Citrate cycle (TCA cycle)	4.20E-12	3.10E-10
Oxidative phosphorylation	1.40E-09	5.10E-08
Parkinson's disease	1.90E-09	4.60E-08
Huntington's disease	1.50E-08	2.80E-07
Alzheimer's disease	1.10E-07	1.60E-06
Pyruvate metabolism	1.00E-06	1.20E-05
Fatty acid metabolism	2.00E-06	2.10E-05
Cardiac muscle contraction	8.80E-06	8.20E-05
Valine, leucine and isoleucine degradation	3.20E-05	2.60E-04
PPAR signaling pathway	4.20E-03	2.60E-02

Table 3

Transcription factor	P-Value	Adjusted P-value	Z-score	Combined score	Target gene
ESRRB	1.62E-27	5.99E-25	-1.99	111.22	SLC25A3;MIDN;DLX3;ALAS1;HIBADH;ATP5C1;ETFA;COX5B;COX7A1;D10JHU81E;ACAT1;SLC9A3R2;ATP5B;ABHD11;ACADL;NNT;MFN1;TNNI1;ME3;ENPP4;CYC1;DLAT;NDUFV1;NDUFA9;MDH2;PTGES2;VEGFB;SDHC;COQ9;SDHA;SOD2;ATP1B1;FH1;SIRT3;THAP4;ALDH5A1;RNF128;UQCRC1;OGDH;NDUFS1;SUCLG1;UQCRC2;CIAPIN1
TAF7L	1.01E-10	6.73E-09	-2.86	53.9	ESRRA;ACADVL;ECHS1;ACAA2;ACOT7;S100A1;NOS3;RORC;NR1H3;IL6RA;ETFA;COQ9;SOD2;CPT1B;VEGFA;ACADL;CIAPIN1;SCD1;DLAT;LMCD1
NR0B1	4.36E-14	8.05E-12	-1.95	49.85	SLC25A3;MIDN;ATP5C1;ETFA;COX5B;FGF1;ATP5G1;PDLIM1;LDHB;ATP5B;ABHD11;MB;ENPP4;SCD1;ESRRA;PHYH;GOT1;PTGES2;GOT2;VEGFB;SDHC;SDHA;ATP1B1;SDHB;FH1;SIRT3;TMEM37;UQCRC1;OGDH;MSRB2;PADI2
ESR1	8.39E-09	3.44E-07	-2.52	37.51	PDHA1;ECHS1;ACAA2;GOT1;GOT2;RORC;ETFA;SIRT3;ADH1;ALDH2;CYP2R1;NDUFS1;PPARA
PPARG	6.63E-07	0.00001631	-2.99	32.99	ACADVL;ACAA2;ACADL;NOS3;NR1H3;SDHC;CD36;NDUFV1;VEGFA

Chapter 3

Metabolomic analysis of the skeletal muscle of mice overexpressing PGC-1α

Introduction

Peroxisome proliferator-activated receptor (PPAR) γ coactivator 1α (PGC-1α) is a coactivator of various nuclear receptors and other transcription factors, which is involved in the regulation of energy metabolism, thermogenesis, and other biological processes that control phenotypic characteristics of various organ systems, including the skeletal muscle [1-5]. PGC-1α in the skeletal muscle is thought to be involved in contractile protein function, mitochondrial function, metabolic regulation, intracellular signaling, and transcriptional responses, and its levels increase in the skeletal muscle with exercise. Animal and cellular genetic models with altered expression of the PGC-1α gene indicate the role of PGC-1α in fiber-type specificity [6, 7]. We have previously demonstrated that transgenic overexpression of PGC-1α in the skeletal muscle of mice (PGC-1α-Tg mice) increases mitochondrial biogenesis and capillary density, contributing to improved exercise capacity [4]. Meanwhile, in a previous study, a microarray analysis revealed that the BCAA catabolic pathway was coordinately activated in the skeletal muscle of PGC-1α-Tg mice. It was apparent that PGC-1α stimulates the metabolism of branched chain amino acids (BCAA) with an increase in the expression of enzymes involved [8].

Considering that PGC-1α changes the expression of various genes in the skeletal muscle, including those involved in muscle metabolism, metabolites are also expected to change; however, little is known about the global changes in metabolites in PGC-1α-Tg mice. Global information of metabolite level change may reveal connections in the biological network of the skeletal muscle in these mice. Thus, we analyzed metabolic profiles by coupling capillary electrophoresis with electrospray ionization time-of-flight mass spectrometry (CE-TOFMS). In the present study, combined with microarray data [8], we analyzed global changes of metabolites in the skeletal muscle of PGC-1α-Tg mice to investigate the modified metabolic pathways related to PGC-1α expression.

Materials and Methods

Transgenic (Tg) mice

Tg mice overexpressing PGC-1α in the skeletal muscle (PGC-1α-Tg mice) were generated as described [22]. In brief, the human α-skeletal actin promoter was used to

express PGC-1α in the skeletal muscle (C57BL/6 background). We used PGC1α-b (B) mice [4], which is same to PGC1α-b (03-2) mice [22]. Two independent lines of Tg mice (PGC1α-b (B)/ PGC1α-b (03-2) mice and PGC1α-b (A)/ PGC1α-b (02-1) mice) [22] showed similar phenotypes in a previous study [4]. The mice were maintained in a controlled environment with a constant temperature of 24°C, with fixed artificial light (12-h light–dark cycle).

Metabolomic analysis

Gastrocnemius muscles of male PGC-1α-Tg mice and sex-matched WT control mice littermates were used for metabolomic analysis (Human Metabolome Technologies Inc., Tsuruoka, Japan) [23, 24]. The age of mice used were: WT1, 13 weeks; WT2, 10 weeks; WT3, 9 weeks; Tg1, 13 weeks; Tg2, 10 weeks; and Tg3, 9 weeks of age. Three mice each were used in the PGC-1α-Tg and WT groups. Frozen mice muscle samples were transferred into 500 µl of methanol containing 50 mM of the external standard. After homogenization by BMSM10N21 (BMS, Tokyo) at 1,500 rpm for 120 s performed five times, 500 µl of chloroform and 200 µl of ultrapure water were added to the homogenate and mixed well and centrifuged at 2,300 g for 5 min at 4°C. The resultant water phase was ultrafiltrated by the Millipore Ultrafree-MC PLHCC HMT Centrifugal Filter Device, 5 kDa (Millipore, Billerica, MA). The filtrates were then dried and dissolved in 50 µl of ultrapure water. The samples obtained were then subjected to capillary electrophoresis time-of-flight mass spectrometry (CE-TOFMS) analysis using the Agilent CE-TOFMS system (Agilent Technologies, Santa Clara, CA) at 4°C. The detected peaks were aligned according to their m/z values and normalized migration times. The peaks were mean-centered and scaled using their standard deviations on a per-peak basis as a pretreatment. After applying autoscaling, a principal component analysis (PCA) and a hierarchical clustering analysis (HCA) were conducted using JMP ver. 11 software (SAS Institute, Cary, North Carolina, USA). In the PCA, a score plot of the first and second principal components was generated. In the HCA, the resulting data sets from each genotype were clustered by Euclidean distance using Ward's method [25]. Heat maps were generated by coloring the values of all data across their value ranges. The relative area of each peak was calculated and used for the comparison between the PGC1α-Tg and WT groups.

Ethics Statement

Mice were cared for in accordance with the National Institutes of Health (NIH) Guide for the Care and Use of Laboratory Animals and our institutional guidelines. All animal experiments were performed with the approval of the Institutional Animal Care and Use Committees of the University of Shizuoka and Kyoto Prefectural University. All surgery was performed under sodium pentobarbital anesthesia, and all efforts were made to minimize suffering.

cDNA microarray analysis

cDNA microarray data were collected as described previously [8]. Briefly, RNA was isolated from skeletal muscle (gastrocnemius) of PGC-1α-Tg mice and age- and sex-matched WT control mice. Samples from WT and PGC-1α-Tg mice (N=5) were pooled and used. Each sample was labeled with a cyanine 3-CTP using the Low Input Quick Amp Labeling Kit (Agilent Technologies, Inc., Santa Clara, CA) and hybridized to the Agilent whole mouse genome microarray (4× 44K), which contains 41,534 genes including expressed sequence tags. Signal detection and data analysis were performed according to the manufacturer's instructions. The microarray data was submitted to GEO database (accession No. GSE67049).

Quantitative real-time RT-PCR analysis

Total RNA was prepared usnig TRIzol (Life Technologies Japan, Tokyo, Japan). cDNA was synthesized from 1 μg of total RNA using the ReverTra Ace qPCR RT Master Mix. Transcription Kit (TOYOBO, Tokyo, Japan). Gene expression levels were measured as described [8]. The mouse-specific primer pairs used were as shown in Table 1.

Results and Discussion

Metabolomic analysis was conducted in the skeletal muscle of PGC-1α-Tg mice with age- and sex-matched wild-type (WT) mice littermates. Average body weights were 26.2 ± 3.0 g in PGC-1α-Tg mice and 25.7 ± 2.0 g in WT mice. Average weights of the gastrocnemius muscles were 115 ± 10 mg in PGC-1α-Tg mice and 138 ± 17 mg in WT mice. Consistent with previous reports [4], the weights of the gastrocnemius muscles in PGC-1α-Tg mice were significantly lower than those in WT littermates. Skeletal muscles of PGC-1α-Tg mice showed a red color characteristic of oxidative muscle. In the metabolomic analysis, 211 peaks (126 cations and 85 anions) were detected by the anion and cation modes of CE-TOFMS. The results of principal component analysis (PCA) in these detected peaks are shown in Fig. 1. The first principal component effectively and distinctly separated the mice based on genotype (x axis), suggesting that overexpression of PGC-1α in the skeletal muscle caused a significant change in the overall metabolite profile of the muscle. Furthermore, a hierarchical cluster analyses (HCA) was conducted, followed by heat map analysis (Fig. 2). As demonstrated from the heat map analysis, skeletal muscle samples from individual WT and PGC-1α-Tg mice segregated into tight clusters, indicating that PGC-1α has profound effects on the systemic metabolite profile of the skeletal muscle. From the results of PCA (Fig. 1) and HCA (Fig. 2), it was observed that PGC-1α overexpression had a significant influence in the metabolite profiles of the skeletal muscle because the two groups (WT and PGC-1α-Tg) were clearly distinguishable. In the following subsections, we discuss the results of the metabolomic analysis.

TCA cycle

Metabolic products of the TCA cycle increased in PGC-1α-Tg mice. The levels of citrate (2.3-fold), succinate (2.2-fold), fumarate (2.8-fold), and malate (2.3-fold) increased (Fig. 3). Consistent with the increased metabolic product levels of the TCA cycle, the gene expression of citrate synthase (2.6-fold), aconitase (2.7-fold), isocitrate dehydrogenase (2.8-fold), succinate dehydrogenase (3.3-fold), and malate dehydrogenase 2 (2.3-fold) increased in PGC-1α-Tg mice (Fig. 3). These data suggest that the TCA cycle was activated in PGC-1α-Tg mice, probably, in part, due to the increase of mitochondria content [4].

Pentose phosphate pathway

The pentose phosphate pathway is initiated when glucose 6-phosphate, a metabolic intermediate of glycolysis, is metabolized to 6-phosphogluconate. The pentose phosphate pathway produces ribose 5-phosphate that is required for nucleotide biosynthesis. In addition, the pathway produces NADPH, a reducing agent required for de novo lipogenesis (Fig. 4) [9, 10]. In this study, metabolic products associated with the pentose phosphate pathway increased in PGC-1α-Tg mice; the levels of 6-phosphogluconate (1.4-fold), ribulose 5-phosphate (3.6-fold), ribose 5-phosphate (2.4-fold), NADPH (2.0-fold), ADP-ribose (3.6-fold), and sedoheptulose 7-phosphate (1.3-fold) increased in PGC-1α-Tg mice compared with WT mice (Fig. 4). Glyceraldehyde 3-phosphate was not detected in WT mice, but detected in one mouse among three PGC-1α-Tg mice. However, the gene expression of enzymes associated with this pathway was not changed, consistent with previous reports that PGC-1α promoted the pentose phosphate pathway by enzymatic activity (glucose 6-phosphate dehydrogenase), but not gene expression [11]. Thus, PGC-1α-Tg mice in this study are likely to have a more active pentose phosphate pathway, as previously reported [11]. As suggested in this previous report, an increase in NADPH content observed in our PGC-1α-Tg mice may contribute to the stimulation of lipogenesis in the skeletal muscle.

Nucleotide biosynthesis

Ribose 5-phosphate, derived from the pentose phosphate pathway, is a starting material for nucleotide biosynthesis, including pyrimidines and purines [9, 10]. We observed a change in metabolite levels of these pathways. For pyrimidine biosynthesis, ribose 5-phosphate (2.4-fold) is metabolized to 5-phosphoribosyl pyrophosphate (PRPP) (0.5-fold), uridine monophosphate (UMP) (detected only in PGC-1α-Tg mice, but not in WT mice), uridine diphosphate (UDP) (detected only in PGC-1α-Tg mice, but not in WT mice), uridine triphosphate (UTP) (1.0-fold), and cytidine triphosphate (CTP) (0.7-fold) (Fig. 5). For purine biosynthesis, ribose 5-phosphate (2.4-fold) is metabolized to inosine monophosphate (IMP) (5.4-fold), which is used in the purine nucleotide cycle (described in the next paragraph). IMP is metabolized to AMP (detected only in PGC-1α-Tg mice, but not in WT control mice), ADP (3.4-fold), and ATP (0.7-fold). IMP is also metabolized

to GMP (16-fold), GDP (detected only in PGC-1α-Tg mice, but not in WT mice), and GTP (1.3-fold) (Fig. 5). Among them, UTP, CTP, ATP, and GTP may be used for RNA synthesis, which is consistent with the previous report that RNA synthesis is stimulated in PGC-1α-Tg mice [11]. Because many of the associated metabolites are increased, the nucleotide biosynthesis pathway appears to be activated in PGC-1α-Tg mice.

Purine nucleotide cycle

The purine nucleotide cycle is a metabolic pathway that contributes to the energy requirement in the skeletal muscle, and is very active during exercise [12]. An outline of the purine nucleotide cycle is shown in Fig. 6.

In the activated purine nucleotide cycle, fumarate is supplied to the TCA cycle, enhancing the capacity of acetyl-CoA oxidation. As shown in Fig. 6, adenylosuccinate is the product of Asp and IMP (generated from AMP), which is then metabolized into fumarate. Metabolic product levels related to this pathway were changed in PGC-1α-Tg mice. The levels of GDP and AMP were detected in PGC-1α-Tg mice but not in WT mice (Fig. 6). Consistently, increasing AMP levels were observed in a previous study using a different line of PGC-1α-Tg mice [13]. Meanwhile, in the metabolome data, adenylosuccinate (12-fold), fumarate (2.8-fold), IMP (5.4-fold), Asp (2.2-fold), GTP (1.3-fold), and ADP (3.4-fold) levels increased in PGC-1α-Tg mice (Fig. 6). Microarray data show an increase in related enzyme gene expression: AMP deaminase (AMP $\rightarrow$ IMP) (1.8-fold), adenylosuccinate lyase (adenylosuccinate $\rightarrow$ fumarate + AMP) (1.7-fold), and adenylate kinase (AMP + ATP $\longleftrightarrow$ 2ADP) (2-fold). Thus, the purine nucleotide cycle appears to be activated in PGC-1α-Tg mice. This is consistent with increased activity of the pentose phosphate pathway and nucleotide synthesis, as the metabolites derived from those pathways, such as IMP, are used for purine nucleotide cycle. Also, this is consistent with an increased mitochondria level in PGC-1α-Tg mice [4], as ADP derived from purine nucleotide cycle is usable for ATP production in the mitochondria.

BCAA metabolism and malate-aspartate shuttle

We have previously reported that BCAA metabolism was enhanced in PGC-1α-Tg mice [8]; in accordance, levels of BCAA (Val, Leu, and Ile) decreased in the present metabolomic analysis (Fig. 7) (Val, 0.7-fold; Leu, 0.8-fold; and Ile, 0.7-fold). Leu and Ile

are degraded, producing acetyl-CoA, and enters the TCA cycle [9, 10]. The level of acetyl-CoA was more increased in PGC-1α-Tg mice than in WT mice (detected only in PGC-1α-Tg mice, and not in WT mice). Val and Ile are converted into succinyl-CoA and enters the TCA cycle [9, 10]. Thus, this metabolomic analysis further supports our previous study of increased BCAA metabolism, which is likely to be used in the TCA cycle [8]. Meanwhile, Val is known to be converted into methylmalonic acid semialdehyde, followed by the production of β-amino isobutyric acid (BAIBA). BAIBA was detected only in PGC-1α-Tg mice, but not in WT mice (data not shown), consistent with previous reports that the level of BAIBA increased in cells overexpressing PGC-1α [14].

On the other hand, the increased amino acids in PGC-1α-Tg mice in the metabolomic analysis were as follows: Glu (3.1-fold), Asp (2.2-fold), Arg (1.7-fold), Gln (1.7-fold), and Lys (1.6-fold) (data not shown). As shown in Fig. 7, in the mitochondria, Asp is converted from oxaloacetate and is then transported from the mitochondria to the cytosol via the Slc25a13 transporter. Asp in the cytosol is then converted to oxaloacetate and malate. Furthermore, malate is transported from the cytosol to the mitochondria via Slc25a11 [15] and is converted to oxaloacetate, which is a part of the TCA cycle [9, 10]. This metabolic pathway is known as the malate–aspartate shuttle (known to be associated with BCAA metabolism during exercise) [16]. The gene expression of enzymes and transporters involved in this process were upregulated in PGC-1α-Tg mice; glutamate oxalate transaminase (GOT2) (catalyzes oxaloacetate to Asp in mitochondria) was upregulated by 4.1-fold, Slc25a13 (a transporter of Asp) [15] by 10.7-fold, GOT1 (Asp to oxaloacetate in cytosol) by 4.4 fold, malate dehydrogenase 1 (oxaloacetate to malate in cytosol) by 4.4-fold, Slc25a11 (a transporter of malate) [15] by 2.2-fold, and malate dehydrogenase 2 (malate to oxaloacetate in mitochondria) by 2.3-fold. Concerning mitochondrial Asp, GOT2 metabolization of Asp results in Glu conversion to α-keto-glutarate. Meanwhile, BCAA is converted to α-keto-acid, which is catalyzed by branched chain aminotransferase 2 [9, 10] (2.5-fold upregulated). Consistently, BCAA levels decreased as previously mentioned (Val, 0.7-fold; Leu, 0.8-fold; and Ile, 0.7-fold), and Glu (3.1-fold) levels increased (Fig. 7). Thus, BCAA and related amino acid metabolism as well as the malate-aspartate shuttle appear coordinately regulated in PGC-1α-Tg mice. These results suggest that deamination was promoted with an increase in BCAA

metabolism and the activation of the malate-aspartate shuttle, which may contribute to the improvement of exercise capacity of PGC-1α-Tg mice.

Metabolism of other amino acids with decreased levels

Some amino acid levels decreased, including Thr (0.7-fold), Met (0.8-fold), Ala (0.7-fold), Ser (0.7-fold), Pro (0.4-fold), and Gly (0.3-fold) in PGC-1α-Tg mice compared with WT mice (data not shown). Some of these can be converted into pyruvate [9, 10] (Fig. 8). Ala is metabolized into pyruvate by alanine amino transferase (ALT). Thr is converted into Gly by threonine aldolase, Gly is subsequently converted into Ser by serine hydroxymethyltransferase, and Ser is subsequently converted into pyruvate by serine dehydratase [9, 10] (Fig. 8). The enzymes related to the metabolism of these amino acids increased in this study. Expression of ALT (3.6-fold), threonine aldolase (2.1-fold), serine hydroxymethyltransferase (2.3-fold), and serine dehydratase (12.6-fold) increased. Pyruvate may be converted into acetyl-CoA by pyruvate dehydrogenase (2.5-fold) (Fig. 8). Consistently, although there is an increased level of pyruvate dehydrogenase kinase 4, which suppresses pyruvate dehydrogenase activity, pyruvate dehydrogenase activity is enhanced in PGC-1α-Tg mice [17]. In the previous study, we reported that glycolysis was suppressed in PGC-1α-Tg mice, and the respiration quotient was low [4], suggesting that glucose was not used as an energy source. Meanwhile, as the respiration quotient due to the use of amino acids as an energy source is lower than that of glucose, the idea that these amino acids are used for the TCA cycle, via pyruvate and acetyl-CoA, does not contradict with previous findings (suppressed glycolysis and low respiration quotient in PGC-1α-Tg mice) [4].

β-alanine

Metabolic products related to β-alanine metabolism decreased in PGC-1α-Tg mice (Fig. 9). This includes the levels of β-alanine (0.15-fold), anserine (dipeptide of β-alanine and methylhistidine) (0.08-fold), and carnosine (dipeptide of β-alanine and histidine) (0.04-fold). β-Ala–Lys (dipeptide of β-alanine and lysine) was detected in WT mice but not in PGC-1α-Tg mice (Fig. 9). β-alanine is metabolized by 4-aminobutyrate transaminase (4.0-fold in microarray) to malonate semialdehyde. Furthermore, acetyl-CoA (detected only in PGC-1α-Tg mice, but not in WT mice) is produced from malonate-semialdehyde

by malonate-semialdehyde dehydrogenase (the probe for this enzyme was not present in the microarray). Thus, β-alanine is likely to be converted into acetyl-CoA and enter the TCA cycle.

Other metabolite changes previously noted in the literature: neurotransmitters

The level of gamma-aminobutyric acid (GABA), a neurotransmitter, was reported to be increased in myocytes overexpressing PGC-1α [14]. In this study, it was also observed that there was an increased level of GABA (12-fold) in PGC-1α-Tg mice (data not shown). PGC-1α-Tg is known to activate neural muscular junction function, including increased acetylcholine receptor gene expression [18]. In our microarray, we also observed increased acetylcholine receptor gene expression (Chnra1, 2.8-fold). Consistently, we observed increased acetylcholine levels in PGC-1α-Tg mice (detected only in PGC-1α-Tg mice, and not in WT mice). In addition, although the significance in skeletal muscle is not clear, we observed that another neurotransmitter, serotonin, was increased in PGC-1α-Tg mice (2.4-fold). The functional significance of increased neurotransmitters in PGC-1α-Tg mice needs to be investigated.

Other metabolite changes previously noted in the literature: creatine

Brown et al. reported that PGC-1α up-regulates creatine transporter expression and creatine uptake in myotubes [19]. We observed increased creatine (1.2-fold), and decreased phosphocreatine (0.2-fold) and creatinine (0.6-fold) levels (data not shown). Although creatine transporter gene expression did not change in our microarray, expression of creatine kinase (mitochondrial 2, Ckmt2) (creatine phosphate + ADP ⟷ creatine + ATP) increased in PGC-1α-Tg mice (4.4-fold). Creatine plays an important role in skeletal muscle energy production during exercise [19, 20]. PGC-1α may be involved in the metabolism of creatine/phosphocreatine.

Possible metabolic effect of long-term-exercise-induced PGC1α

We have to be careful that the expression level of PGC1α driven by the PGC1α transgene in PGC1α-Tg mice remains high after birth. The results of the metabolomic analysis conducted in this study may not be applicable to the metabolic changes by physiological increases in PGC1α level observed in other contexts, such as exercise in wild-type mice.

On the other hand, Egan et al. reported that exercise-induced increases in mRNA levels are a temporary response and are not translated into protein during the bout of exercise. Superimposition of repeated exercise bouts results in the general accumulation of protein in response to repeated, pulsed increases in relative mRNA expression [21]. The PGC1α-Tg mice in this study may be an appropriate model of the effects of long-term exercise. This remains clarified in future study.

PGC1α-b and other isoforms of PGC1α

We used PGC1α-b transgenic mice in this study, as described in the Methods section. PGC1α-b is an isoform of PGC1α. The PGC1α-b, which is considered to be similar to PGC1α-a (the originally found to be full-length PGC-1α) [1] in function, structurally differs by 16 amino acids at its amino terminus. Moreover, transcriptional activity did not differ among PGC1α-a, PGC1α-b, and PGC1α-c in a reporter assay [22]. Furthermore, gene expression changes were similar among lines of PGC1α-a and PGC1α-b mice (data not shown). We consider that changes in the PGC1α-b Tg mice are representative of the effects of full-length PGC1α (not isoform-specific). However, we cannot exclude the possibly that there may be some PGC1α-b isoform-specific effects. This remains to be clarified in a future study.

Conclusion

In this study, it was observed that many metabolic product levels changed in the skeletal muscle of PGC-1α-Tg mice (Fig. 10). Many of these changes are related to mitochondrial metabolism. Increased coordinal regulation of the TCA cycle and amino acid metabolism, including BCAA, suggests that PGC-1α plays important roles in energy metabolism. Moreover, activation of the purine nucleotide pathway, malate–aspartate shuttle as well as creatine metabolism, which are known to be active during exercise, further suggests that PGC-1α regulates metabolism in exercise. In this study, we evaluated the role of PGC-1α in the skeletal muscle at the metabolic level.

References

1. Puigserver P, Wu Z, Park CW, Graves R, Wright M, Spiegelman BM. A cold-inducible coactivator of nuclear receptors linked to adaptive thermogenesis. Cell. 1998;92(6):829-39. Epub 1998/04/07. PubMed PMID: 9529258.

2. Liang H, Balas B, Tantiwong P, Dube J, Goodpaster BH, O'Doherty RM, et al. Whole body overexpression of PGC-1alpha has opposite effects on hepatic and muscle insulin sensitivity. American journal of physiology Endocrinology and metabolism. 2009;296(4):E945-54. Epub 2009/02/12. doi: 10.1152/ajpendo.90292.2008. PubMed PMID: 19208857; PubMed Central PMCID: PMCPmc2670619.

3. Puigserver P, Spiegelman BM. Peroxisome proliferator-activated receptor-gamma coactivator 1 alpha (PGC-1 alpha): transcriptional coactivator and metabolic regulator. Endocrine reviews. 2003;24(1):78-90. Epub 2003/02/18. doi: 10.1210/er.2002-0012. PubMed PMID: 12588810.

4. Tadaishi M, Miura S, Kai Y, Kano Y, Oishi Y, Ezaki O. Skeletal muscle-specific expression of PGC-1alpha-b, an exercise-responsive isoform, increases exercise capacity and peak oxygen uptake. PloS one. 2011;6(12):e28290. Epub 2011/12/17. doi: 10.1371/journal.pone.0028290. PubMed PMID: 22174785; PubMed Central PMCID: PMCPmc3234261.

5. Wareski P, Vaarmann A, Choubey V, Safiulina D, Liiv J, Kuum M, et al. PGC-1{alpha} and PGC-1{beta} regulate mitochondrial density in neurons. The Journal of biological chemistry. 2009;284(32):21379-85. Epub 2009/06/23. doi: 10.1074/jbc.M109.018911. PubMed PMID: 19542216; PubMed Central PMCID: PMCPmc2755862.

6. Lin J, Wu H, Tarr PT, Zhang CY, Wu Z, Boss O, et al. Transcriptional co-activator PGC-1 alpha drives the formation of slow-twitch muscle fibres. Nature. 2002;418(6899):797-801. Epub 2002/08/16. doi: 10.1038/nature00904. PubMed PMID: 12181572.

7. Miura S, Kai Y, Ono M, Ezaki O. Overexpression of peroxisome proliferator-activated receptor gamma coactivator-1alpha down-regulates GLUT4 mRNA in skeletal muscles. The Journal of biological chemistry. 2003;278(33):31385-90. Epub 2003/06/05. doi: 10.1074/jbc.M304312200. PubMed PMID: 12777397.

8. Hatazawa Y, Tadaishi M, Nagaike Y, Morita A, Ogawa Y, Ezaki O, et al. PGC-1alpha-mediated branched-chain amino acid metabolism in the skeletal muscle. PloS one. 2014;9(3):e91006. Epub 2014/03/19. doi: 10.1371/journal.pone.0091006. PubMed PMID: 24638054; PubMed Central PMCID: PMCPmc3956461.

9. Salway JG. Metabolism at glance. Blackwell Science Ltd. 1999.

10. Robert A Horton, Laurence A. Moran, Scrimgeour G, Perry M. Principles of Biochemistry 2005.
11. Summermatter S, Baum O, Santos G, Hoppeler H, Handschin C. Peroxisome proliferator-activated receptor {gamma} coactivator 1{alpha} (PGC-1{alpha}) promotes skeletal muscle lipid refueling in vivo by activating de novo lipogenesis and the pentose phosphate pathway. The Journal of biological chemistry. 2010;285(43):32793-800. Epub 2010/08/19. doi: 10.1074/jbc.M110.145995. PubMed PMID: 20716531; PubMed Central PMCID: PMCPmc2963391.
12. Arabadjis PG, Tullson PC, Terjung RL. Purine nucleoside formation in rat skeletal muscle fiber types. The American journal of physiology. 1993;264(5 Pt 1):C1246-51. Epub 1993/05/01. PubMed PMID: 8498484.
13. Miura S, Tomitsuka E, Kamei Y, Yamazaki T, Kai Y, Tamura M, et al. Overexpression of peroxisome proliferator-activated receptor gamma co-activator-1alpha leads to muscle atrophy with depletion of ATP. The American journal of pathology. 2006;169(4):1129-39. Epub 2006/09/28. PubMed PMID: 17003473; PubMed Central PMCID: PMCPmc1780180.
14. Roberts LD, Bostrom P, O'Sullivan JF, Schinzel RT, Lewis GD, Dejam A, et al. beta-Aminoisobutyric acid induces browning of white fat and hepatic beta-oxidation and is inversely correlated with cardiometabolic risk factors. Cell metabolism. 2014;19(1):96-108. Epub 2014/01/15. doi: 10.1016/j.cmet.2013.12.003. PubMed PMID: 24411942; PubMed Central PMCID: PMCPmc4017355.
15. Palmieri F. The mitochondrial transporter family SLC25: identification, properties and physiopathology. Molecular aspects of medicine. 2013;34(2-3):465-84. Epub 2012/12/26. doi: 10.1016/j.mam.2012.05.005. PubMed PMID: 23266187.
16. She P, Zhou Y, Zhang Z, Griffin K, Gowda K, Lynch CJ. Disruption of BCAA metabolism in mice impairs exercise metabolism and endurance. Journal of applied physiology (Bethesda, Md : 1985). 2010;108(4):941-9. Epub 2010/02/06. doi: 10.1152/japplphysiol.01248.2009. PubMed PMID: 20133434; PubMed Central PMCID: PMCPmc2853195.
17. Kiilerich K, Adser H, Jakobsen AH, Pedersen PA, Hardie DG, Wojtaszewski JF, et al. PGC-1alpha increases PDH content but does not change acute PDH regulation in mouse skeletal muscle. American journal of physiology Regulatory, integrative and comparative physiology. 2010;299(5):R1350-9. Epub 2010/08/20. doi: 10.1152/ajpregu.00400.2010. PubMed PMID: 20720174.
18. Handschin C, Kobayashi YM, Chin S, Seale P, Campbell KP, Spiegelman BM. PGC-1alpha regulates the neuromuscular junction program and ameliorates Duchenne

muscular dystrophy. Genes & development. 2007;21(7):770-83. Epub 2007/04/04. doi: 10.1101/gad.1525107. PubMed PMID: 17403779; PubMed Central PMCID: PMCPmc1838529.

19. Brown EL, Snow RJ, Wright CR, Cho Y, Wallace MA, Kralli A, et al. PGC-1alpha and PGC-1beta increase CrT expression and creatine uptake in myotubes via ERRalpha. Biochimica et biophysica acta. 2014;1843(12):2937-43. Epub 2014/09/01. doi: 10.1016/j.bbamcr.2014.08.010. PubMed PMID: 25173818.

20. Salway JG. Medical Biochemistry at a Glance. Blackwell Science Ltd. 2007.

21. Egan B, Zierath JR. Exercise metabolism and the molecular regulation of skeletal muscle adaptation. Cell metabolism. 2013;17(2):162-84. Epub 2013/02/12. doi: 10.1016/j.cmet.2012.12.012. PubMed PMID: 23395166.

22. Miura S, Kai Y, Kamei Y, Ezaki O. Isoform-specific increases in murine skeletal muscle peroxisome proliferator-activated receptor-gamma coactivator-1alpha (PGC-1alpha) mRNA in response to beta2-adrenergic receptor activation and exercise. Endocrinology. 2008;149(9):4527-33. Epub 2008/05/31. doi: 10.1210/en.2008-0466. PubMed PMID: 18511502.

23. Soga T, Heiger DN. Amino acid analysis by capillary electrophoresis electrospray ionization mass spectrometry. Analytical chemistry. 2000;72(6):1236-41. Epub 2000/03/31. PubMed PMID: 10740865.

24. Soga T, Ueno Y, Naraoka H, Matsuda K, Tomita M, Nishioka T. Pressure-assisted capillary electrophoresis electrospray ionization mass spectrometry for analysis of multivalent anions. Analytical chemistry. 2002;74(24):6224-9. Epub 2003/01/04. PubMed PMID: 12510742.

25. Ward HJ. Hierarchical Grouping to Optimize an Objective Function. Journal of the American Statistical Association. 1963;58:236–44.

Legend

Fig. 1 Principal component analysis (PCA) of the metabolomic datasets of the skeletal muscle of PGC-1α-Tg mice and WT mice

Three mice were used in each group (WT1, WT2, and WT3 for wild-type and Tg1, Tg2, and Tg3 for PGC-1α-Tg mice). PCA was conducted with the determined data peaks by using SampleStat ver. 3.14. Plots of WT (open circles) and PGC-1α-Tg mice (filled circles) are clearly distinguished on the PC1 axis (X-axis).

Fig. 2 A heat map of hierarchical cluster analysis comparing the metabolite changes between PGC-1α-Tg mice and WT mice

Horizontal axis shows sample names corresponding to the samples used in Fig. 1 (WT1, WT2, and WT3 for wild-type and Tg1, Tg2, and Tg3 for PGC-1α-Tg mice). The heat map patterns between WT (upper three lanes) and PGC-1α-Tg (lower three lanes) are clearly distinguishable. The color red demonstrates that the relative content of metabolites is high and green demonstrates that they are low.

Fig. 3 Observed metabolite changes mapped onto the pathways involved in the TCA cycle

Changes in the metabolite levels in the skeletal muscle of PGC-1α-Tg mice and WT mice are shown. Relative metabolite changes shown in the graphs were obtained by CE-TOFMS (data not shown). Open bars, WT and filled bars, PGC-1α-Tg (N = 3). Data are expressed as the mean ± SD. Asterisks indicate statistically significant differences (***$p < 0.001$, **$p < 0.01$). Microarray data of gene expression change of enzymes in the related metabolic process are shown in the scheme.

Fig. 4 Observed metabolite changes mapped onto the pathways involved in the pentose phosphate pathway

Changes in the metabolite levels in the skeletal muscle of PGC-1α-Tg mice and WT mice are shown. Relative metabolite changes shown in the graphs were obtained by CE-TOFMS (data not shown). Open bars, WT and filled bars, PGC-1α-Tg (N = 3). Data are expressed as the mean ± SD. Asterisks indicate statistically significant differences (**p <

0.01, *p < 0.05). Microarray data of gene expression change of enzymes in the related metabolic process are shown in the scheme.

Fig. 5 Observed metabolite changes mapped onto the pathways involved in nucleotide synthesis

Changes in the metabolite levels in the skeletal muscle of PGC-1α-Tg mice and WT mice are shown. Relative metabolite changes shown in the graphs were obtained by CE-TOFMS (data not shown). Open bars, WT and filled bars, PGC-1α-Tg (N = 3). Data are expressed as the mean ± SD. Asterisks indicate statistically significant differences (**p < 0.01, *p < 0.05).

Fig. 6 Observed metabolite changes mapped onto the pathways involved in the purine nucleotide cycle

Changes in the metabolite levels in the skeletal muscle of PGC-1α-Tg mice and WT mice are shown. Relative metabolite changes shown in the graphs were obtained by CE-TOFMS (data not shown). Open bars, WT and filled bars, PGC-1α-Tg (N = 3). Data are expressed as the mean ± SD. Asterisks indicate statistically significant differences (**p < 0.01). Microarray data of gene expression change of enzymes and transporter in the related metabolic process are shown in the scheme.

Fig. 7 Observed metabolite changes mapped onto the pathways associated with BCAA metabolism and the malate-aspartate shuttle

Changes in the metabolite levels in the skeletal muscle of PGC-1α-Tg mice and WT mice are shown. Relative metabolite changes shown in the graphs were obtained by CE-TOFMS (data not shown). Open bars, WT and filled bars, PGC-1α-Tg (N = 3). Data are expressed as the mean ± SD. Asterisks indicate statistically significant differences (***p < 0.001, **p < 0.01). Microarray data of gene expression change of enzymes and transporter in the related metabolic process are shown in the scheme.

Fig. 8 Observed metabolite changes mapped onto the pathways associated with glycine, threonine, serine, and alanine metabolism

Changes in the metabolite levels in the skeletal muscle of PGC-1α-Tg mice and WT mice

are shown. Relative metabolite changes shown in the graphs were obtained by CE-TOFMS (data not shown). Open bars, WT and filled bars, PGC-1α-Tg (N = 3). Data are expressed as the mean ± SD. Asterisks indicate statistically significant differences (***p < 0.001, **p < 0.01, *p < 0.05). Microarray data of gene expression change of enzymes and transporter in the related metabolic process are shown in the scheme.

Fig. 9 Observed metabolite changes mapped onto the pathways associated with β-alanine metabolism

Changes in the metabolite levels in the skeletal muscle of PGC-1α-Tg mice and WT mice are shown. Relative metabolite changes shown in the graphs were obtained by CE-TOFMS (data not shown). Open bars, WT and filled bars, PGC-1α-Tg (N = 3). Data are expressed as the mean ± SD. Asterisks indicate statistically significant differences (***p < 0.001, **p < 0.01, *p < 0.05). Microarray data of gene expression change of enzymes and transporter in the related metabolic process are shown in the scheme.

Fig. 10 Schematic representation of metabolic pathway changes in PGC-1α-Tg mice

The levels of many metabolic products are changed in the skeletal muscle of PGC-1α-Tg mice. Many of these changes are associated with mitochondrial metabolism, in particular the TCA cycle. Increased mitochondrial content due to PGC-1α-overexpression appears to activate the TCA cycle (Fig. 3); therefore, there must be more substrates available for the TCA cycle. For instance, the activated pentose phosphate pathway (Fig. 4) stimulates nucleotide synthesis (Fig. 5), which is followed by activation of the purine nucleotide cycle (Fig. 6), supplying fumarate for the TCA cycle. Meanwhile, activation of the malate-aspartate shuttle supplies other substrates (Fig. 7). In addition, amino acids are also likely to be used as substrates (Figs. 7, 8, 9). Increased coordinated regulation of the TCA cycle and amino acid metabolism, including BCAA, suggests that PGC-1α plays important roles in energy metabolism. Moreover, activation of the purine nucleotide pathway and malate–aspartate shuttle, which are known to be active during exercise, further suggests that PGC-1α regulates metabolism in exercise.

Table 1

Mouse-specific primer pairs used for quantitative real-time RT-PCR

Fig.1

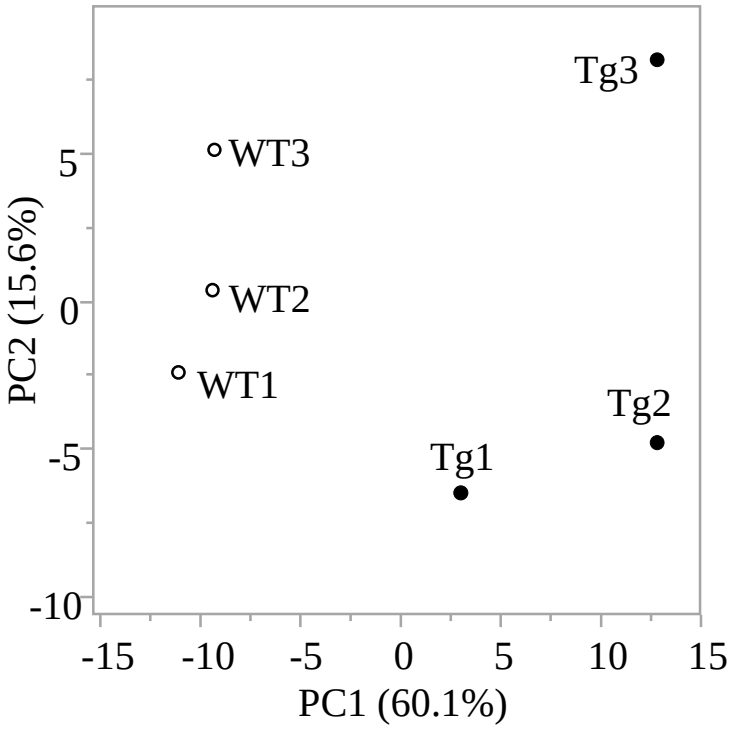

Fig.2

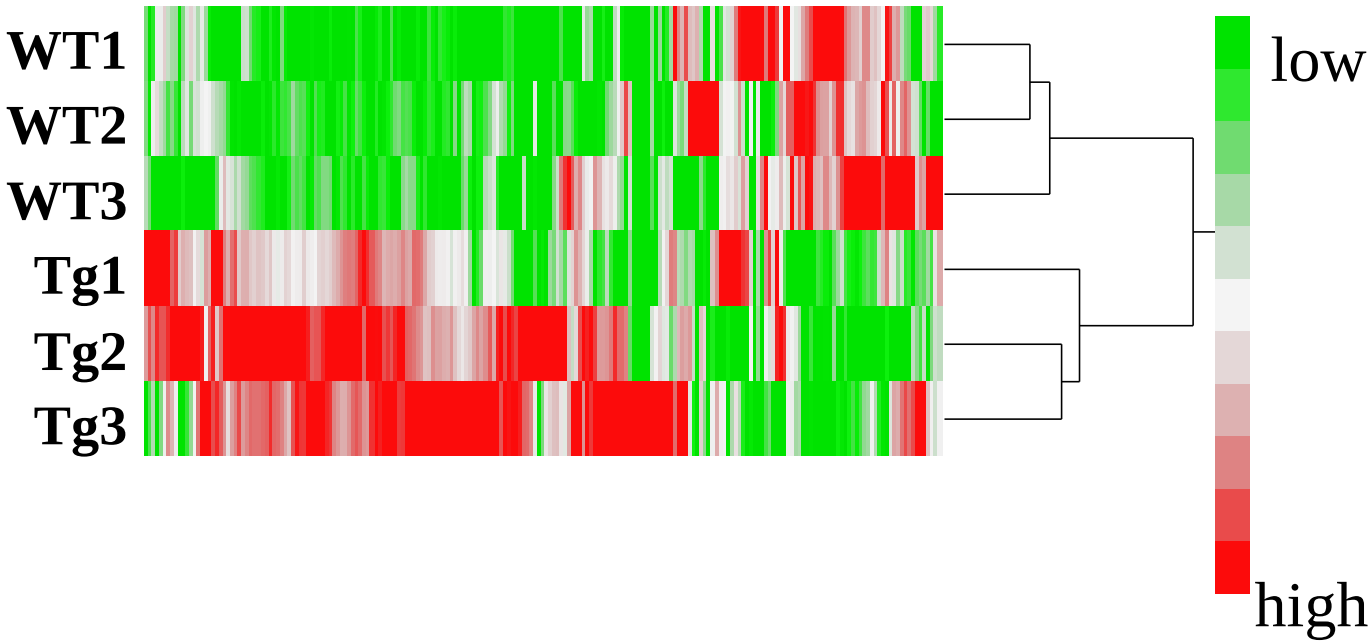

Fig.3

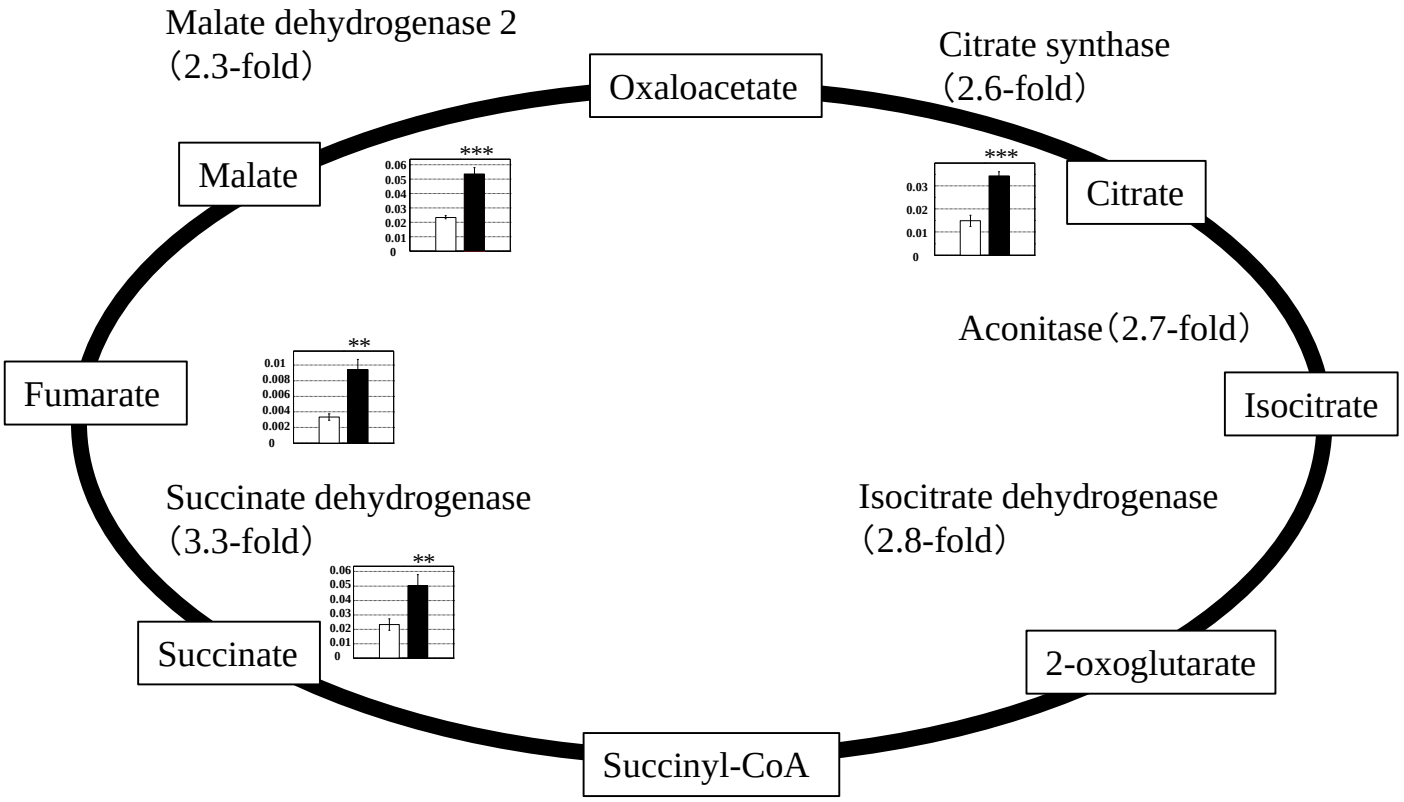

mitochondria

Fig.4

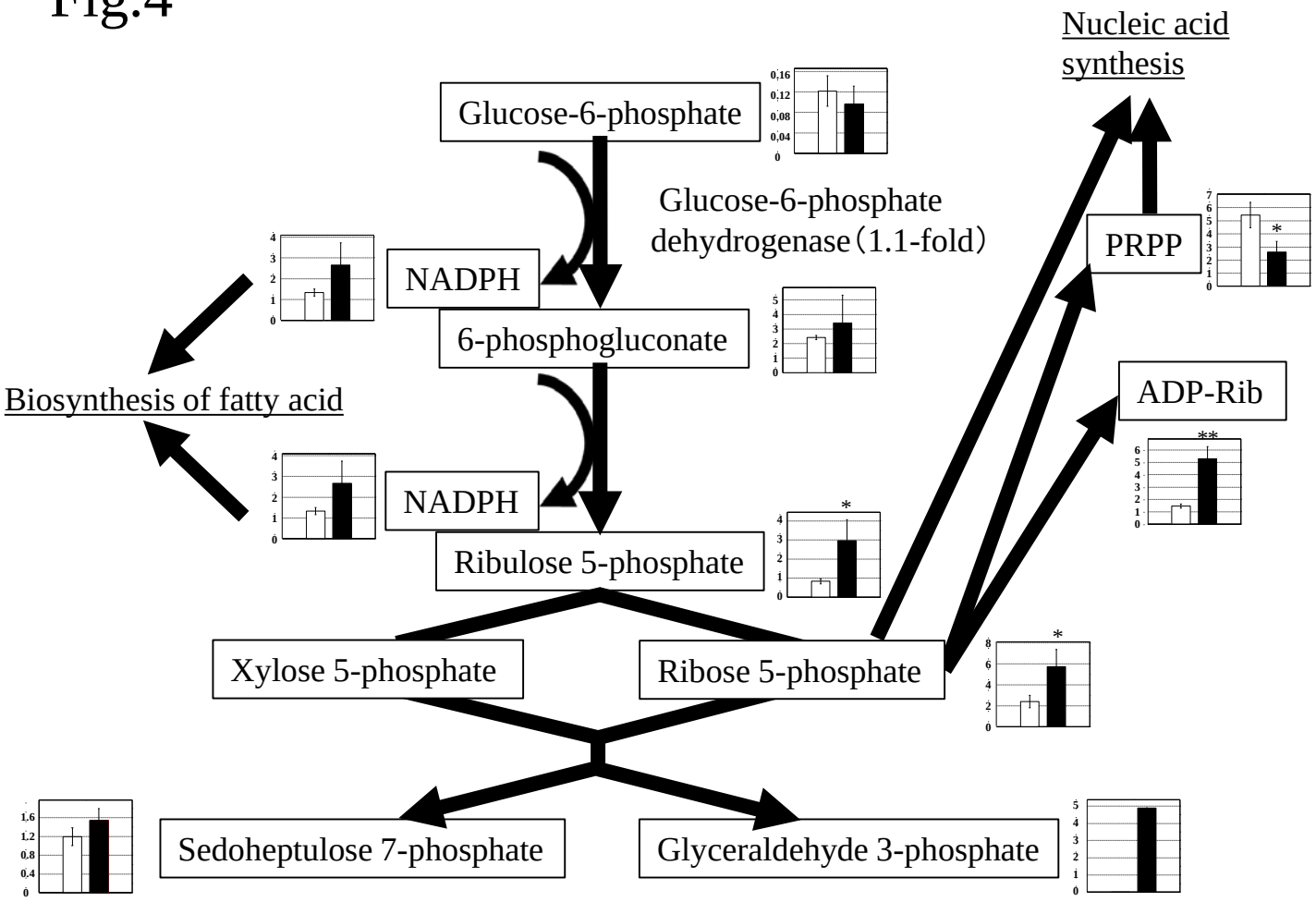
Nucleic acid synthesis
Glucose-6-phosphate
Glucose-6-phosphate dehydrogenase（1.1-fold）
PRPP
NADPH
6-phosphogluconate
ADP-Rib
Biosynthesis of fatty acid
NADPH
Ribulose 5-phosphate
Xylose 5-phosphate
Ribose 5-phosphate
Sedoheptulose 7-phosphate
Glyceraldehyde 3-phosphate

Fig.5

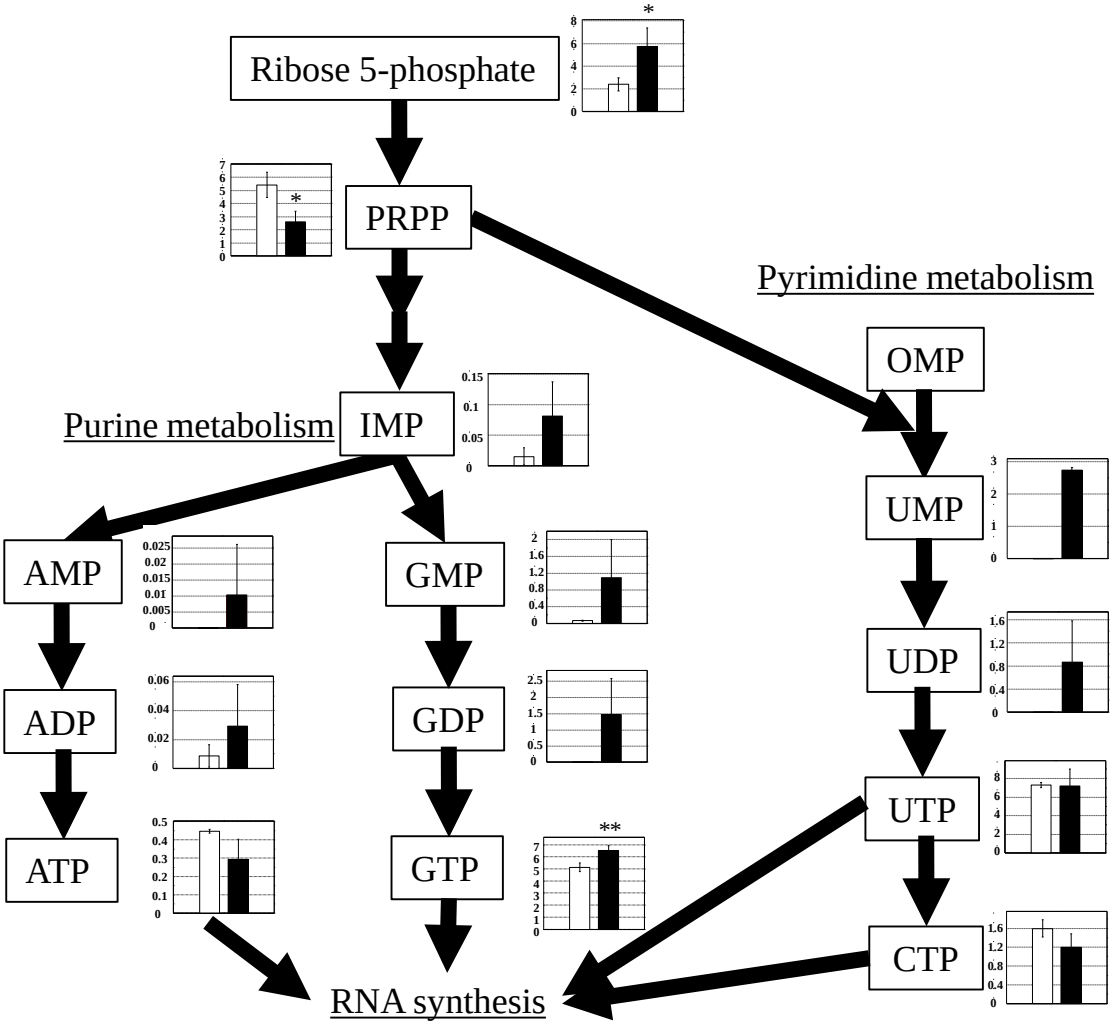
Ribose 5-phosphate
PRPP
IMP
Purine metabolism
Pyrimidine metabolism
OMP
UMP
UDP
UTP
CTP
AMP
ADP
ATP
GMP
GDP
GTP
RNA synthesis
*
*
*
**

Fig.6

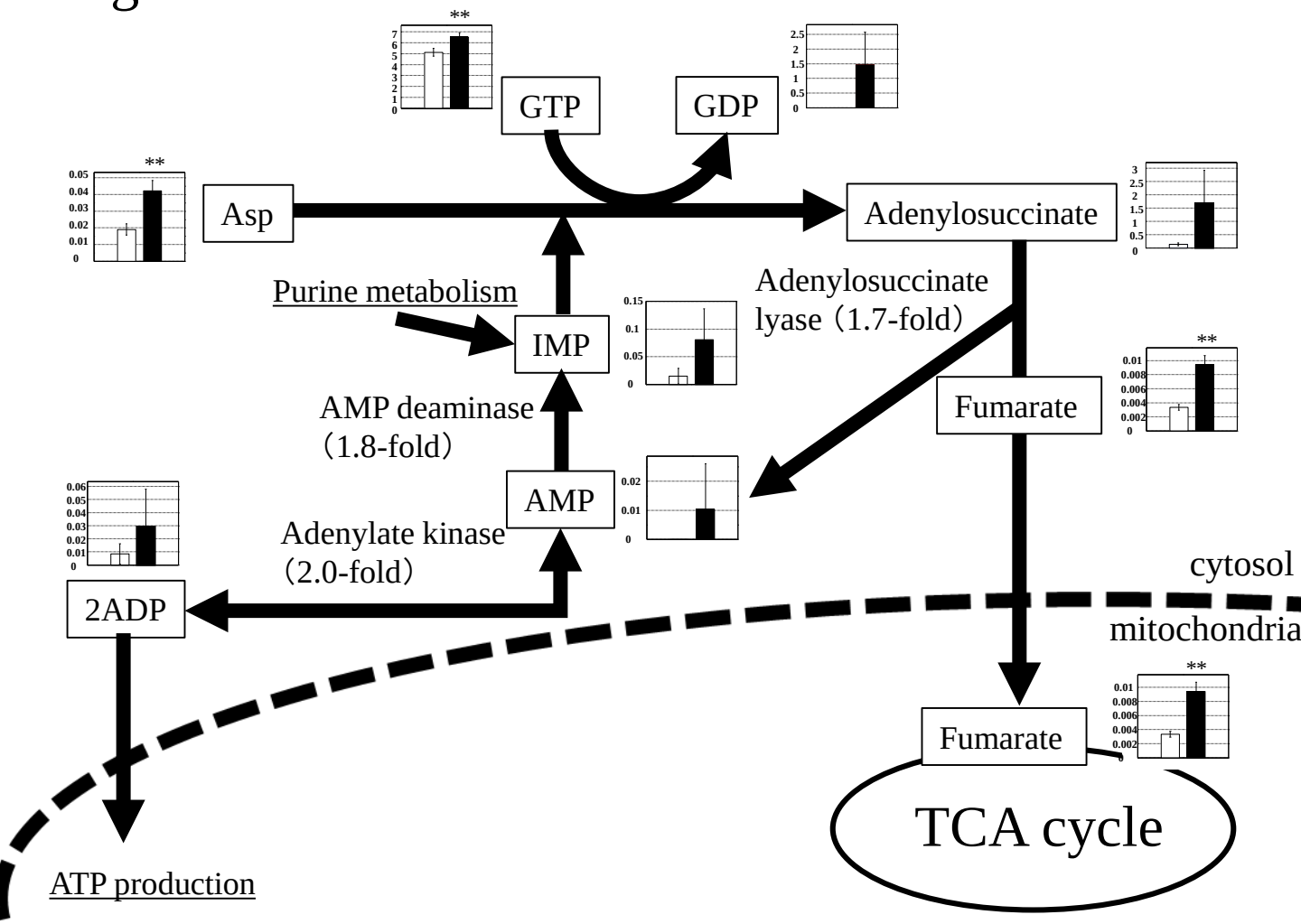
**
GTP
GDP
**
Asp
Adenylosuccinate
Purine metabolism
Adenylosuccinate
lyase（1.7-fold）
IMP
**
AMP deaminase
（1.8-fold）
Fumarate
AMP
Adenylate kinase
（2.0-fold）
cytosol
mitochondria
2ADP
**
Fumarate
TCA cycle
ATP production

Fig.7

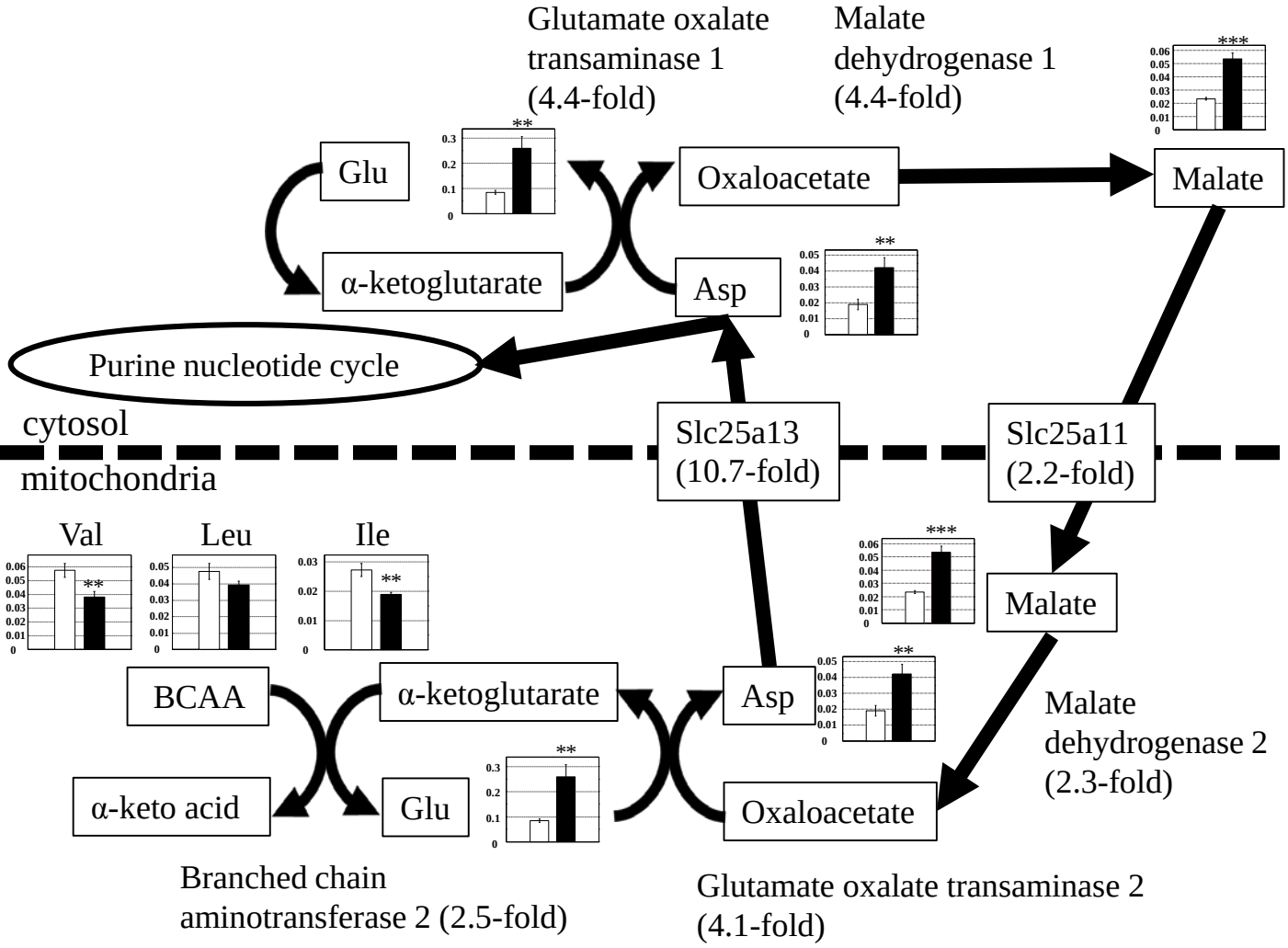
Glutamate oxalate transaminase 1 (4.4-fold)
Malate dehydrogenase 1 (4.4-fold)
Glu
α-ketoglutarate
Oxaloacetate
Asp
Malate
Purine nucleotide cycle
cytosol
mitochondria
Slc25a13 (10.7-fold)
Slc25a11 (2.2-fold)
Val
Leu
Ile
BCAA
α-keto acid
Malate dehydrogenase 2 (2.3-fold)
Branched chain aminotransferase 2 (2.5-fold)
Glutamate oxalate transaminase 2 (4.1-fold)

Fig.8

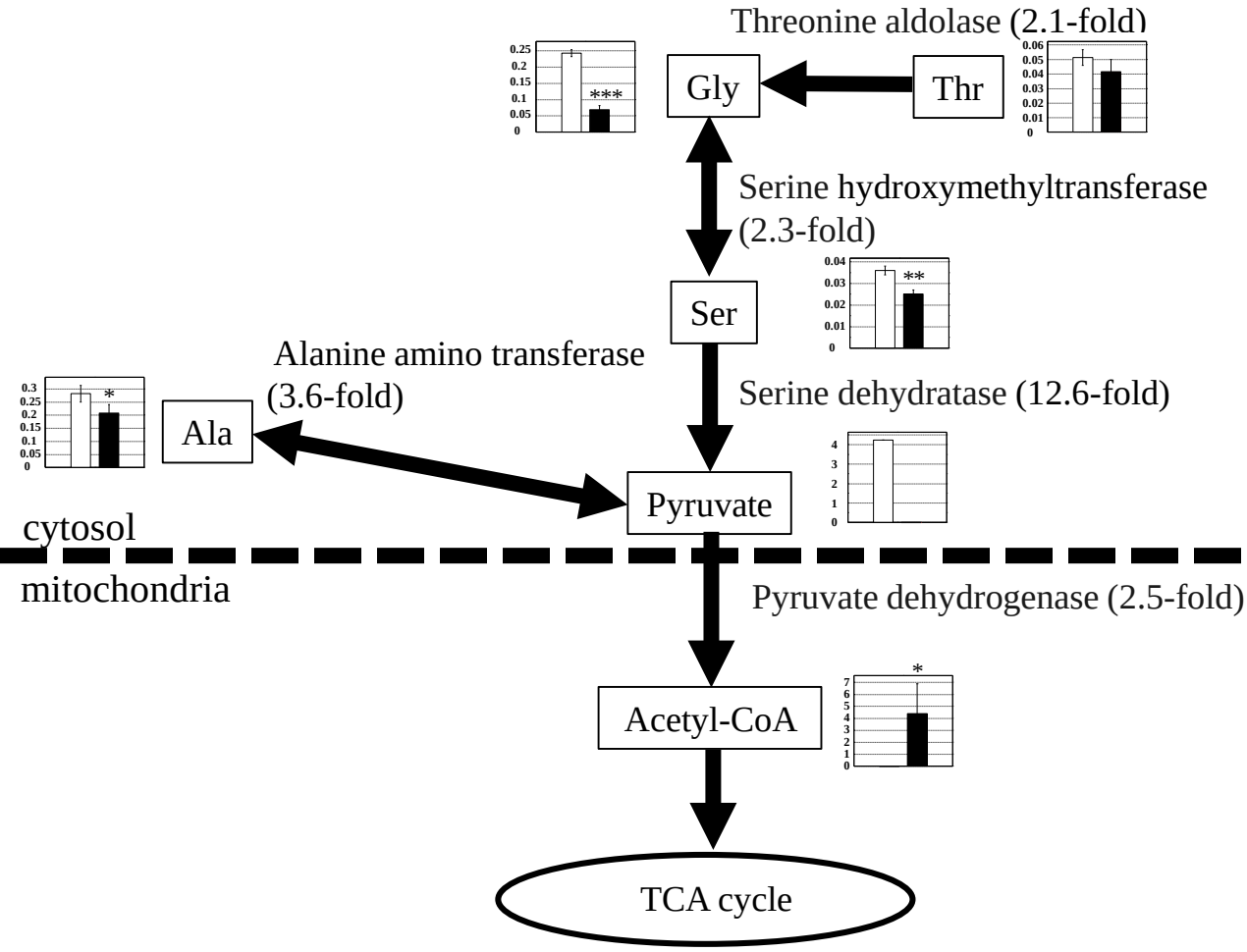
Threonine aldolase (2.1-fold)
Gly
Thr
***
Serine hydroxymethyltransferase
(2.3-fold)
Ser
**
Alanine amino transferase
(3.6-fold)
Ala
*
Serine dehydratase (12.6-fold)
Pyruvate
cytosol
mitochondria
Pyruvate dehydrogenase (2.5-fold)
Acetyl-CoA
*
TCA cycle

Fig.9

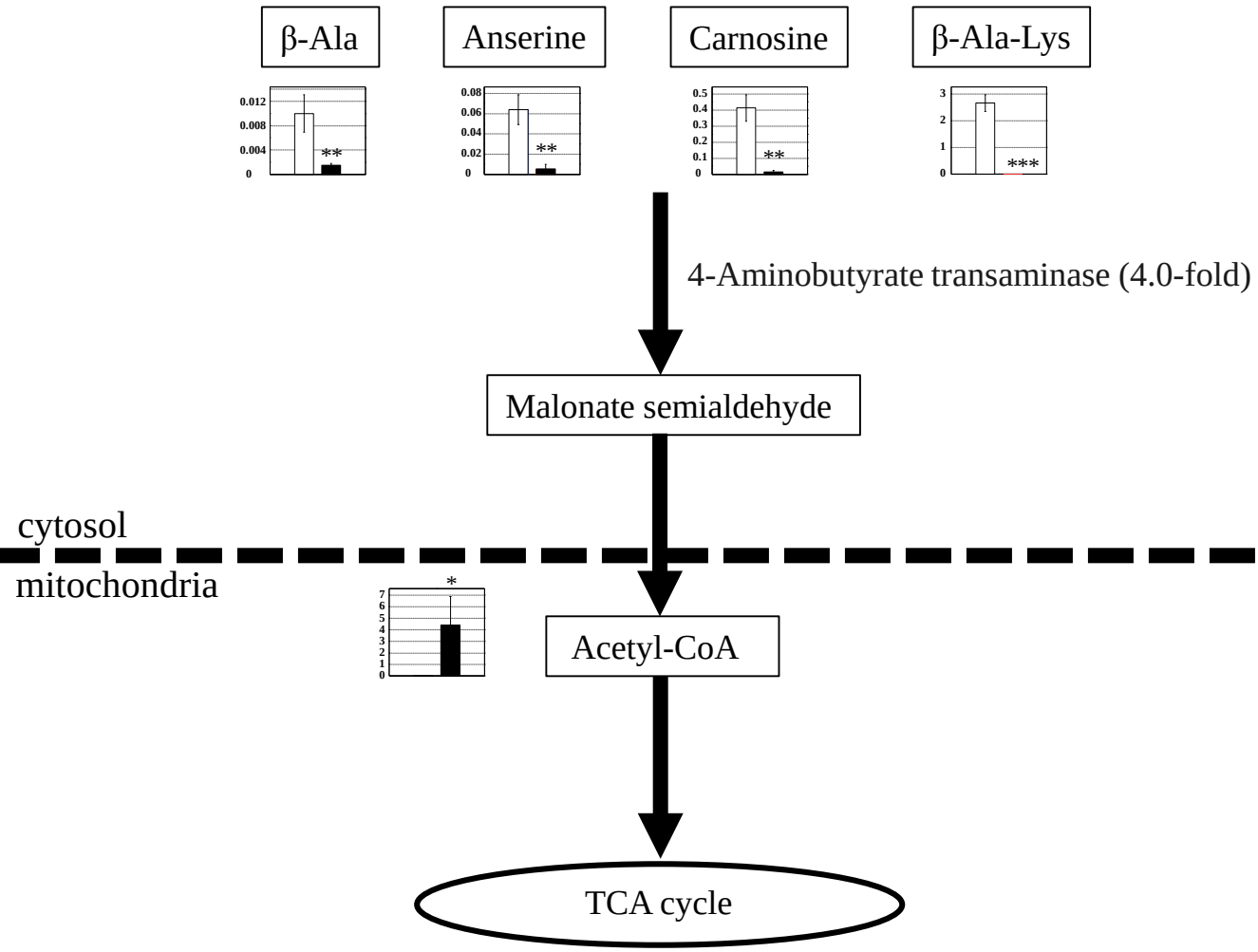
β-Ala
Anserine
Carnosine
β-Ala-Lys
0.012
0.008
0.004
0
**
0.08
0.06
0.04
0.02
0
**
0.5
0.4
0.3
0.2
0.1
0
**
3
2
1
0
***
4-Aminobutyrate transaminase (4.0-fold)
Malonate semialdehyde
cytosol
mitochondria
*
7
6
5
4
3
2
1
0
Acetyl-CoA
TCA cycle

Fig.10

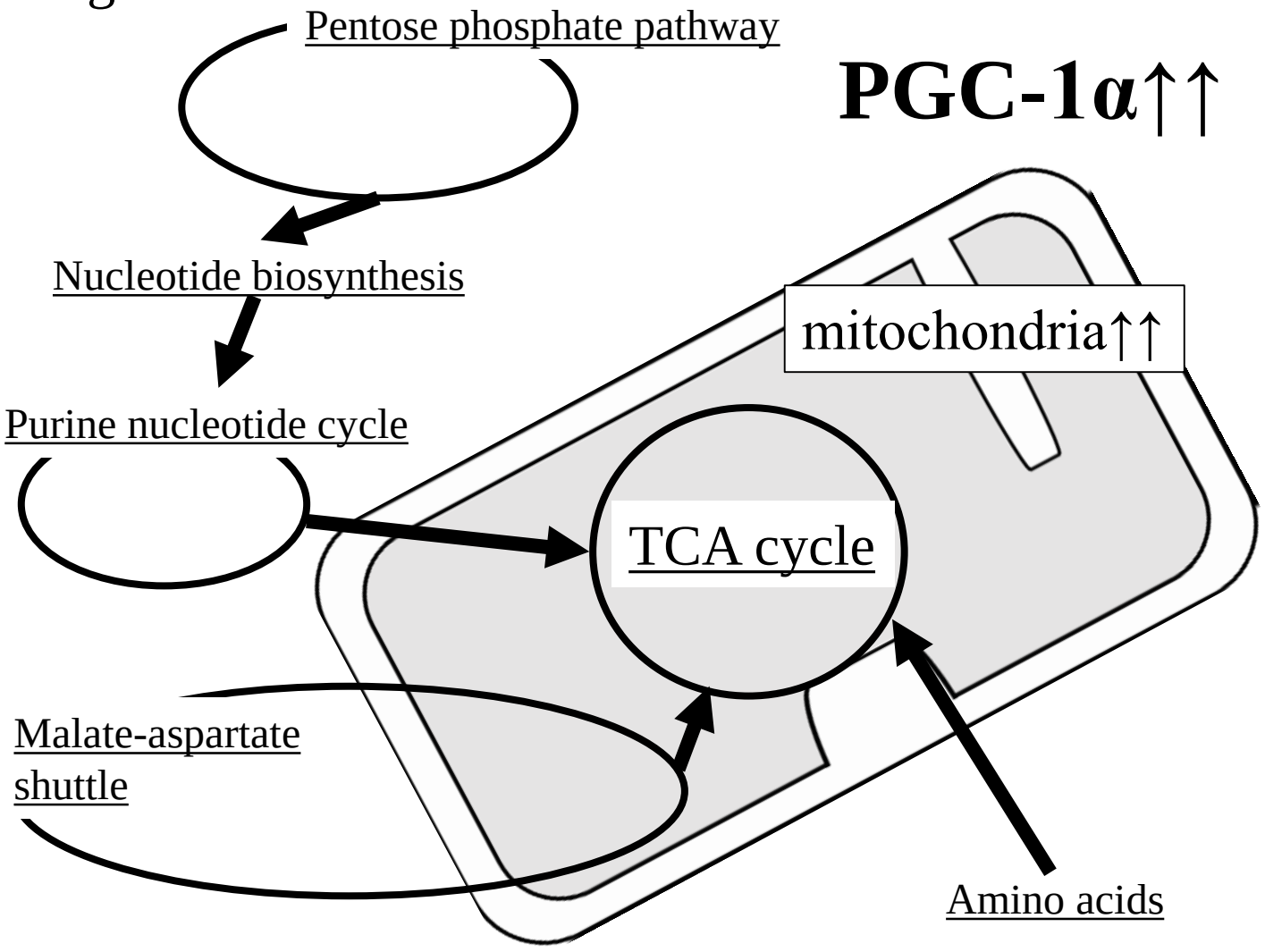
Pentose phosphate pathway
PGC-1α↑↑
Nucleotide biosynthesis
mitochondria↑↑
Purine nucleotide cycle
TCA cycle
Malate-aspartate shuttle
Amino acids

Table 1

Gene	Forward	Reverse
PGC1a	CGGAAATCATATCCAACCAG	TGAGGACCGCTAGCAAGTTTG
Citrate synthase	AAGTTGGCAAAGACGTGTCAG	TACTGCATGACCGTATCCTGG
Aconitase	TGGCTGCCAGTATGACCAAGT	ATGTGGCTTTAGCTCATTGAGGTT
Isocitrate dehydrogenase	ATTTTGTGGTAGATCGAGCTGG	CCTCCGGCAGGGAAGTTATAC
Succinate dehydrogenase	CCTCGAATGCAGACGTACGA	CAACACCATAGGTCCGCACTT
Malate dehydrogenase 2	AAGGCTACCTTGGACCGGAG	CATCACAACCTTTGAGGCAATCT
Glucose-6-phosphate dehydrogenase	ATCATCATGGGTGCATCGG	GGTAGGATAGATCTTCTTCTTGGCC
Adenylosuccinate lyase	TCTGCCCACGTTAGGTTTCAC	CGCTTCAAGTTCTGGAGATCC
AMP deaminase 3	GTGGAGATTACTGTGCAGGGATC	TGGCAGCCTGCTCATAGTCTT
Adenylate kinase 3	TCACGAGCTCAAAACCCTTACC	GGAAATCCATCCAACAGCCA
Glutamate oxalate transaminase 1	CCAACCTGGGAGAACCATAATG	CCAGTAGCAATAGGGCCGAAT
Malate dehydrogenase 1	TGTTGTACAGTATTGGAAATGGATCTG	TGATGGGCTGGTCTTTCCC
Slc25a13	ACTCTGGCTGGCAACAGGAA	CCAAAGCGAACTCCTCCTTAGTC
Slc25a11	ACACTGGGCTGTCAGCTGGT	CGAGTAGTGGTGTAGGTGGCCT
Branched chain aminotransferase 2	CGGACCCTTCATTCGTCAGA	CCATAGTTCCCCCCCAACTT
Glutamate oxalate transaminase 2	GATCCGTCCCCTGTATTCCA	CACCTCTTGCAACCATTGCTT
Threonine aldorase	GGAGGTGCTACCAAGGGACC	GAGTCCTTTAGCGAATCTCTGGG
Serine hydroxylmethyltransferase	AGTGATGCCGAGGTTTACAGC	CCGAGGCAATCAGCTCTAATC
Serine dehydratase	GTCTCCCCGTTTGACCATCC	GGGGTCCCTAGTGACTCCTTC
Alanine transaminase	GCGCCAGGGTGTGAAGAA	GCTTGTGCATCCCCAATATTG
Pyruvate dehydratase	TCAGCACTCGCAATGCTTTG	ATAAGTCCTTTTGCATCCTCGG
4-Aminobutyrate transaminase 2	TTGTTGATTACCCGACGGCT	GAGGTGGAGGTTTTTCTGGGA

Chapter 4

Reduced Dnmt3a increases Gdf5 expression with suppressed satellite cell differentiation and impaired skeletal muscle regeneration

Introduction

Epigenetic events contribute to skeletal muscle remodeling in a variety of physiological and pathophysiological conditions (1). DNA methylation occurs as 5-methylcytosines mainly at cytosine-guanine dinucleotides, so-called CpG sites, and such methylation is a well-studied epigenetic mechanism for transcriptional regulation (2, 3). Generally, DNA methylation of the gene promoter is correlated with transcriptional repression (2, 3). Genomic DNA methylation patterns are established by the actions of the *de novo* methyltransferases Dnmt3a and Dnmt3b, and are maintained by the methyltransferase Dnmt1 (4). DNA methylation has long been known to be involved in muscle formation. Treatment of fibroblasts with the DNA methylation inhibitor 5-azacytidine caused muscle differentiation (5). On the other hand, deletion of *Dnmt1* in skeletal muscles is reported to reduce the differentiation capacity of myogenic cells (6). Expression of Dnmt3a mRNA is relatively high in skeletal muscles (7). Also, denervation in skeletal muscles decreased expression of Dnmt3a (8), suggesting Dnmt3a plays a role in skeletal muscle physiology/pathophysiology, such as atrophy.

Muscle atrophy is associated with aging (sarcopenia) and chronic unloading (such as immobilization with casts), as well as nerve injury (denervation). During atrophy, the muscle regeneration capacity after injury (e.g., falling, trauma, or extreme exercise) is known to be decreased (9-11). However, the mechanism involved is largely unknown.

Satellite cells, the resident stem cells of adult skeletal muscles, are critical for regeneration (9), supplying myonuclei for homeostasis, hypertrophy, and replication (12). Satellite cell growth and differentiation are controlled by numerous secreted proteins, such as the bone morphogenic protein (Bmp) and growth differentiation factor (Gdf), which form a family of proteins that share the characteristic features of the TGFβ family (13). Bmp/Gdf is known to activate gene expression of *Id* (inhibitor of differentiation or DNA binding) and suppress muscle differentiation (12). Previously, we examined the role of Bmp signaling in regulating satellite cell function. Blockade of Bmp signaling promoted, and Bmp4 inhibited, myogenic differentiation of satellite cells. Collectively, these findings suggest that Bmp signaling suppresses satellite cell differentiation (12).

Expression of *Gdf5/Bmp14* was shown to be regulated by DNA methylation at the promoter (14). Increased Gdf5 may suppress satellite cell differentiation and reduce muscle regeneration. In this study, we used mice with ablation of Dnmt3a in skeletal muscles as well as satellite cells, and attempted to clarify the role of DNA methylation in muscle function.

Materials and Methods

Denervation of skeletal muscle

For the denervation model, a 4−5 mm section of sciatic nerve in the hindlimb of WT mice was removed. After 14 days, skeletal muscle was collected.

Plaster cast

Plaster casts of mice were performed as previously described (15). The hindlimb skeletal muscles of WT mice (9 weeks old, male) were immobilized (unloaded) by a plaster cast. After 11 days, skeletal muscles were collected.

Quantitative RT-PCR analysis

Total RNA was prepared using TRIzol (Thermo Fisher, Waltham, MA, USA). cDNA was synthesized from 500 ng of total RNA using ReverTra Ace qPCR RT MasterMix with gDNA Remover (Toyobo, Osaka, Japan). mRNA expression levels were measured on an ABI PRISM 7000 system using Thunderbird SYBR qPCR Mix (Toyobo, Osaka, Japan).

Dnmt3a-KO mice

We used a Cre-loxP recombination system to generate skeletal muscle-specific Dnmt3a knockout mice (Dnmt3a-KO). Dnmt3a-flox mice, originally generated in Massachusetts General Hospital (Boston, MA), were provided by the RIKEN BRC through the National Bio-Resource Project of MEXT, Japan. Briefly, mice in which exon 19 of

Dnmt3a was flanked by loxP sites (16) were crossed with transgenic mice expressing Cre recombinase specifically in skeletal muscles using the human α-actin promoter (17). In addition to crossing mice homozygous for the Dnmt3a lox allele with Cre transgene (heterozygous) mice, mice homozygous for the Dnmt3a lox allele were crossed with mice without the Cre transgene. Genotyping of the Dnmt3a lox allele was performed as previously described (16), and the Cre transgene was detected with the following PCR primers. 5'-CGCCGCATAACCAGTGAAAC-3' and 5'-ATGTCCAATTTACTGACCG-3'. Offspring of these crosses, Dnmt3a flox/flox with Cre (Dnmt3a-KO) and Dnmt3a flox/flox without Cre (WT), were used for experiments.

Western blotting analysis

Western blotting analysis was performed as previously described (15) using anti-Dnmt3a (H-295; Santa Cruz Biotechnology, Inc., Santa Cruz, CA, USA) and anti-GAPDH (C14C10; Cell Signaling Technology Japan, Tokyo, Japan).

Histological analyses

Skeletal muscles were frozen in liquid nitrogen-cooled isopentane. Transverse serial sections were prepared and stained with hematoxylin and eosin (HE), modified Gomori trichrome, or NADH stain, as previously described (18).

Glucose and insulin tolerance tests

Glucose tolerance tests and insulin tolerance tests were performed as previously

described (15).

Muscle regeneration following cardiotoxin (CTX)-induced muscle injury

Mice were injected with 50 or 100 µl of 10 µM CTX (C9759, Sigma-Aldrich, St. Louis, MO, USA) into the tibialis anterior or gastrocnemius muscle. Two weeks after injection, mice were sacrificed by cervical dislocation to harvest muscle samples.

Immunostaining of skeletal muscles and satellite cells

Skeletal muscles were dissected and stained for collagen type I (red), laminin (red), and MyHC (green). Nuclei were counterstained with DAPI (blue) (Southern Biotech, Birmingham, AL). Immunocytochemistry of satellite cells and isolated single fibers was performed as previously described (12). Antibodies and suppliers are as follows: mouse anti-MyHC (MF20) (R&D Systems, Minneapolis, MN), rat anti-laminin α2 (Alexis, San Diego, CA), goat anti-collagen type I (Southern Biotech), anti-Pax7 (Santa Cruz Biotechnology, Santa Cruz, CA) and anti-myogenin (F5D) (DSHB, Iowa City, IA).

Primary satellite cell isolation and culture

Adult (8–12-week-old) male mice were sacrificed by cervical dislocation, and the EDL muscles isolated and digested in type I collagenase as previously described (19). Satellite cells were obtained from isolated myofibers by trypsinization in a 0.125% trypsin–EDTA solution for 10 min at 37°C. Satellite cells were cultured in growth medium (GlutaMax DMEM (Thermo Fisher) supplemented with 30% FBS, 1% chicken

embryo extract, 10 ng/ml bFGF, and 1% penicillin-streptomycin). Myogenic differentiation was induced in differentiation medium (GlutaMax DMEM supplemented with 2% horse serum and 1% penicillin-streptomycin) (19).

Fluorescent reporter mice (Rosa-stop-YFP mice) of Cre expression

The Rosa-stop-YFP mouse is a reporter system that expresses Yellow Fluorescent Protein (YFP) only in cells expressing Cre recombinase, and their daughter cells. It was created by inserting YFP cDNA preceded by a loxP flanked “stop” sequence into the ubiquitously expressed ROSA26 locus (20). Mice with the Cre transgene driven by the α-actin promoter were crossed with fluorescent reporter mice (Rosa-stop-YFP mice). Muscle fibers were isolated as previously described (12). Satellite cells were stained with the cell marker Pax7. Mouse anti-Pax7 was used for immunostaining. Pax7-positive cells on muscle fibers from actin-Cre/Rosa-YFP floxed mice emitting a strong YFP signal were considered to be satellite cells with an active Cre system.

Analysis of cell proliferation

In experiments measuring cell proliferation, the Click-iT Plus EdU Alexa Fluor 488 Flow Cytometry Assay Kit (Invitrogen, Life Technologies, Paisley, UK) was used as per the manufacturer’s instructions. Ten mM EdU stock solution was added to the culture up to a 10 μM final concentration and subsequently cultured for an additional 6 h. Immunostained myofibers and plated myoblasts were viewed on an Inverted Laboratory Microscope with LED Illumination Leica DM IL LED. Digital images were acquired

with a Leica DFC3000 G system using Leica LAS Image Overlay software (ver. 4.6), optimized, and assembled into figures using ImageJ software.

cDNA microarray analysis

RNA was isolated from satellite cells from Dnmt3a-KO or WT mice. Each sample was labeled with cyanine 3-CTP using the Low Input Quick Amp Labeling Kit (Agilent Technologies, Inc., Santa Clara, CA, USA) and hybridized to the Agilent whole mouse genome (4 × 44K) microarray. Signal detection and data analysis were performed as previously described (21).

Functional annotation analysis in genes regulated by Dnmt3a-KO

We conducted pathway analysis using the Kyoto Encyclopedia of Genes and Genomes (KEGG) database resource with DAVID v6.8, which is a web application providing a comprehensive set of functional annotation tools to understand the biological meaning of a large list of genes (21). A list of gene symbols that showed changed expression in satellite cells of Dnmt3a-KO mice was submitted, and a significant overrepresentation of the KEGG pathway was detected (21).

Gdf5 protein concentration analysis

Concentrations of Gdf5 in culture medium, which was precipitated with trichloroacetic acid and dissolved in water, were measured by an enzyme-linked immunosorbent assay (ELISA) kit (Mouse GDF-5 DuoSet, R & D Systems, Minneapolis, MN, USA).

Bisulfite DNA methylation analysis

Genomic DNA was isolated by a standard procedure using proteinase K treatment. Bisulfite DNA methylation analysis was performed as previously described (22). PCR amplification of the genes of interest was performed using specific primers: Gdf5 forward: TTTTAGGAGGTGGAGGTGAAAATT, reverse: ACTTATATAAAACTAAAAAATTTTTCCAAAAA; IAP forward: TTGATAGTTGTGTTTTAAGTGGTAAATAAA, reverse: AAAACACCACAAACCAAAATCTTCTAC. QUMA (a web-based quantification tool for methylation analysis) (http://quma.cdb.riken.jp/) (23) was used for bisulfite sequencing analysis of CpG methylation. Representative data of 3 independent experiments with similar results are shown in the Figures.

Treatment of satellite cells by DNA methylation inhibitor 5-azacytidine

Satellite cells were isolated from the EDL of WT mice (8 weeks old, male). After isolation, satellite cells were cultured for 6 days. On day 4, 5-azacytidine was treated with medium (5 μg/ml). On day 6, satellite cells were replated and cultured in differentiation medium containing 5 μg/ml 5-azacytidine for 1 day.

Gdf5 recombinant protein

Satellite cells were cultured in growth medium for 6 days, replated, and cultured in differentiation medium containing 10 ng/ml or 100 ng/ml Gdf5 recombinant protein

(Peprotech, Rockyhill, NJ, USA) for 2 days.

A genome-wide analysis of DNA methylation (MIAMI)

Microarray-Based Integrated Analysis of Methylation by Isoschizomers (MIAMI) analysis, a genome-wide analysis of DNA methylation using a gene array and methylation-sensitive restriction enzymes, was performed as previously described (22). Briefly, genomic DNA from the two samples was digested using the methylation-sensitive *Hpa*II and methylation-insensitive *Msp*I, followed by adaptor ligation and PCR-amplification. Amplified DNA from one sample was labeled with Cy3 and the other with Cy5; further, they were cohybridized in the gene arrays containing 41,332 probes. The difference in the *Hpa*II/*Msp*I signal was used to determine the degree of methylation (22).

Statistical analyses

Sample sizes were not based on power calculations. No animals were excluded from analyses. Statistical comparison of 2 groups was performed by a Student's two-tailed unpaired t-test or a one-way analysis of variance followed by Tukey's post hoc test for more groups. Data was checked for normality and equal variances between groups. $P < 0.05$ was considered to be significant and the significance is marked by $*P < 0.05$, $**P < 0.01$, and $***P < 0.001$. The number of animals in each experiment is stated in the respective figure legends. All *in vitro* experiments were replicated 2–4 times and the main animal experiments were conducted twice.

Results and Discussion

Results

Decreased Dnmt3a mRNA expression in multiple skeletal muscle atrophy models

Histochemical analysis (HE staining) of the atrophied skeletal muscles from different mouse models (denervation, plaster cast, and aging) demonstrated a reduction in muscle fiber size. We examined the mRNA expression levels of DNA methyltransferases (Dnmt1, Dnmt3a, and Dnmt3b), and histone methylases (Ehmt1, Ehmt2, and Ezh2) in skeletal muscles of multiple atrophy models by RT-qPCR. Dnmt3a mRNA expression was decreased in all atrophy models (denervation, plaster cast, and aging), while expression levels of Dnmt1, Dnmt3b, and histone methylases were not significantly altered (Figure 1A, B, C). Previous study showed a decrease in Dnmt3a protein expression in muscle after denervation (8). Also, our Western blot data revealed a decrease in Dnmt3a protein expression in an aging-caused muscle atrophy (data not shown). Thus, Dnmt3a may play a role in skeletal muscle biology.

Creation of mice with deletion of Dnmt3a specifically in skeletal muscles

To examine the role of Dnmt3a in skeletal muscles, we produced skeletal muscle-specific Dnmt3a knockout mice (Dnmt3a-KO mice). We used a Cre-loxP recombination system; transgenic mice expressing Cre recombinase using the human *α-actin* promoter. A typical genotyping result is shown in Figure 2A. In skeletal muscles of Dnmt3a-KO mice, Dnmt3a mRNA expression was reduced to ~10% of WT levels (Figure 2B). On the other hand, mRNA expression of Dnmt3a was not decreased in

other tissues (Figure 2B). We then confirmed decreased Dnmt3a protein expression in skeletal muscles, but not the liver (Figure 2C). Expression of Dnmt1 and Dnmt3b mRNAs did not differ between WT and Dnmt3a-KO mice in skeletal muscles (Figure 2D). The *α-actin* promoter driving the *Cre* transgene in our Dnmt3a-KO mice acts after birth (17). Indeed, decreased Dnmt3a mRNA expression was not observed in the whole embryo at E13.5 or in hindlimbs (containing skeletal muscles) at E18.5 of Dnmt3a-KO mice (data not shown).

Skeletal muscles of Dnmt3a-KO mice appear normal

We did not observe gross morphological differences between Dnmt3a-KO and WT mice. Body and tissue weights (including of the gastrocnemius and quadriceps muscles, liver, and white adipose tissue) did not differ between WT and Dnmt3a-KO mice (Figure 3A), and there were no gross structural abnormalities in skeletal muscle tissue sections stained with HE (Figure 3B). Similarly, additional histological analyses using modified Gomori trichrome and NADH staining did not reveal marked differences in skeletal muscles of Dnmt3a-KO mice compared to WT mice (Figure 3C, D). We also did not observe signs of muscle degeneration in Dnmt3a-KO mice. Moreover, Dnmt3a-KO mice have a similar capacity to WT mice for glucose metabolism in skeletal muscles (Figure 3E, F).

Suppressed regeneration of skeletal muscles in Dnmt3a-KO mice

DNA methylation is known to be involved in muscle cell differentiation (5). Thus, we

focused on a condition where the activity of muscle cell (satellite cell) differentiation is high, such as muscle regeneration. During atrophy, Dnmt3a expression is decreased, and muscle regeneration is impaired (9). We then injected cardiotoxin (CTX) in skeletal muscles of Dnmt3a-KO mice to activate satellite cells. Centronuclear cells, which appear during muscle regeneration (24), were observed in muscle sections from WT mice following CTX injection (Figure 3G), indicating normal regeneration. In muscle samples from Dnmt3a-KO mice, centronuclear cells were surrounded by more stromal cells (Figure 3G). Collagen type I, a marker of fibrogenesis, was observed in skeletal muscles of Dnmt3a-KO mice following CTX injection (Figure 3H), indicating impaired regeneration. Laminin and myosin heavy chain (MyHC) staining showed muscle fiber size was smaller in Dnmt3a-KO mice than in WT mice, followed by CTX injection (Figure 3H). We quantified the cross-sectional area of the muscle fibers containing centralized nuclei (a feature of nascent myofibers) using laminin/DAPI staining. Fibers with centralized nuclei were smaller in Dnmt3a-KO mice than in WT mice (Figure 3H). Moreover, the decrease in muscle mass following CTX injection was larger in Dnmt3a-KO mice than in WT mice (Figure 3I), also indicating suppressed regeneration in Dnmt3a-KO mice.

Deletion of Dnmt3a in satellite cells from Dnmt3a-KO mice

Next, we examined whether Dnmt3a is deleted in satellite cells. Thus, we examined the expression of Dnmt3a in satellite cells isolated from Dnmt3a-KO mice. We observed a marked decrease in Dnmt3a mRNA in Dnmt3a-KO satellite cells compared to WTs

(Figure 4A), as well as reduced Dnmt3a protein expression (Figure 4B), while neither Dnmt1 nor Dnmt3b mRNA levels differed significantly between genotypes (Figure 4A). We also observed Cre mRNA expression in Dnmt3a-KO satellite cells (Figure 4A).

There are no reports that the *α-actin* promoter is active in satellite cells. We next examined whether *α-actin* promoter-driven Cre is functional in satellite cells *in vivo* using a reporter system (20). Almost all Pax7-positive satellite cells in muscle fibers from *α-actin*-Cre/Rosa-YFP floxed mice emitted strong YFP fluorescence, indicating that the *α-actin* promoter was active in satellite cells (Figure 4C). This suggests that the Cre-loxP system works successfully in satellite cells derived from Dnmt3a-KO mice *in vivo*. A genome-wide analysis of DNA methylation using a gene array (MIAMI analysis) showed a reduction in the extent of DNA methylation in several gene regions in the satellite cells of Dnmt3a-KO mice (data not shown), confirming that the Dnmt3a deletion is indeed functional. Thus, Dnmt3a-KO mice show Dnmt3a deletion in satellite cells, as well as in skeletal muscles.

Cell morphology in satellite cells of Dnmt3a-KO mice

Because Dnmt3a is absent in satellite cells obtained from Dnmt3a-KO mice (Figure 4A, B), we compared the phenotype of satellite cells isolated from Dnmt3a-KO mice with that of satellite cells isolated from WT mice. The morphology of the satellite cells obtained from Dnmt3a-KO mice appeared distinct from those of WT mice, *in vitro* (Figure 5A). To determine the phenotype of the satellite cells from Dnmt3a-KO mice, we performed immunostaining of the cell stage markers. Cell proliferation (assessed by

Edu incorporation, in Pax7-positive-satellite cells; Figure 5B), and myogenin staining (commitment marker of myocyte; (25), Figure 5C), were similar between Dnmt3a-KO and WT cells. Meanwhile, Dnmt3a-KO cells had a decreased number of nuclei in the myotubes (myonuclei) (Figure 5D, E), suggesting that fusion index is lower in Dnmt3a-KO than in WT cells. Cell length of MyHC-positive myotubes was shorter in Dnmt3a-KO than WT cells (Figure 5D, E). In addition, the MyHC-positive myotube area per microscopic field was smaller (Figure 5D, E), suggesting myogenic differentiation was impaired/delayed in Dnmt3a-KO compared to WT cells. As myotube formation was delayed (smaller cell area) in Dnmt3a-KO cells, muscle regeneration was likely impaired.

Gdf5 expression in satellite cells of Dnmt3a-KO mice

To examine gene expression changes in satellite cells derived from Dnmt3a-KO mice, we performed microarray analysis. The list of genes showing a greater than 2-fold increase in Dnmt3a-KO compared to WT-derived satellite cells is shown in Table 1A. Expression of growth differentiation factor 5 (Gdf5)/ bone morphogenic protein 14 (Bmp14) mRNA was most markedly increased in satellite cells derived from Dnmt3a-KO mice compared to WT mice. As Gdf5 is the most markedly up-regulated gene in satellite cells of Dnmt3a-KO mice, we focused on Gdf5. We observed increased Gdf5 mRNA expression in satellite cells of Dnmt3a-KO mice, by RT-qPCR (Figure 6A). Furthermore, we performed bioinformatics analysis to understand the function of these listed genes. In the list of up-regulated genes, we detected the TGF beta signaling

pathway (Table 1C). As Gdf5 belongs to the TGF beta-superfamily, these data also support our focus on Gdf5 as an important factor for the Dnmt3a-related phenotype. In addition, we confirmed the mRNA expression of the receptors for Gdf5 in the satellite cells (data not shown). Moreover, the Gdf5 protein concentration was higher in the medium of satellite cell cultures from Dnmt3a-KO mice than that of WT mice, as measured by ELISA (Figure 6B), suggesting that reduced Dnmt3a expression enhances Gdf5 protein expression and secretion.

DNA methylation level of the *Gdf5* gene promoter in satellite cells of Dnmt3a-KO mice

Generally, DNA methylation of the gene promoter is correlated with transcriptional repression (2, 3). The human *GDF5* promoter was reported to be regulated by DNA methylation. The proximal promoter region of the *GDF5* gene (from −0.5 to 0 kb relative to the transcription start site) in particular is thought to strongly regulate gene expression (14). A homology search between the human *GDF5* and mouse *Gdf5* promoter at −0.5 kb showed high homology, and included most CpG sequences (data not shown). We then compared the DNA methylation level of the *Gdf5* promoter in satellite cells derived from Dnmt3a-KO and WT mice. Interestingly, bisulfite analysis revealed much lower DNA methylation of the *Gdf5* promoter in satellite cells derived from Dnmt3a-KO mice compared to WT mice (Figure 6C, D), whereas, the IAP region remained methylated in satellite cells of both Dnmt3a-KO and WT mice (Figure 6C, E). Deletion of Dnmt3a did not reduce DNA methylation nonspecifically in satellite cells.

We then treated WT satellite cells with 5-azacytidine, a DNA methylation inhibitor (5). 5-Azacytidine treatment increased the expression of Gdf5 mRNA, but did not affect the expression of other-unrelated genes such as those of ribosomal 36B4 and muscle pyruvate kinase (PKM) (Figure 6F). Thus, DNA methylation appears, at least in part, to be involved in the regulation of *Gdf5* expression in satellite cells.

Gene expression in satellite cells of Dnmt3a-KO mice

The list of genes down-regulated to less than 0.5-fold in Dnmt3a-KO compared to WT-derived satellite cells, by microarray analysis, is shown in Table 1B. The mRNA expression levels of the mature muscle marker proteins, i.e., myosin heavy chain 6 (Myh6), Myh7 (26), and fibroblast growth factor receptor 4 (FGFR4) (27), were reduced in satellite cells derived from Dnmt3a-KO mice compared to WT mice. RT-qPCR of individual genes confirmed the microarray results. Expression levels of Myh6, Myh7, and FGFR4 were reduced in satellite cells derived from Dnmt3a-KO mice compared to WT mice (Figure 6G). In addition, we observed increased mRNA expression of Id4 (Figure 6G), a target gene of Gdf5 and inhibitor of muscle cell differentiation (12). After performing bioinformatics analysis of the down-regulated genes, we detected a tight-junction pathway (Table 1D), which may reflect changes in the morphology of the satellite cells from Dnmt3a-KO mice. The data suggest that differentiation was suppressed in satellite cells of Dnmt3a-KO mice compared to WT mice.

Effect of Gdf5 recombinant protein on gene expression in WT satellite cells

As shown in Figure 7A, the addition of recombinant Gdf5 protein to the culture medium of WT satellite cells reduced myotube formation. Gdf5 treatment affected neither cell proliferation, assessed by Edu incorporation (Figure 7B), nor the number of myogenin positive cells (Figure 7C). Nucleus number per myotube (myonuclei, fusion index) decreased with Gdf5 treatment (Figure 7D, E). Length and area of MyHC-positive myotubes decreased in Gdf5-treated cells (Figure 7D, E), suggesting suppressed differentiation. Furthermore, the mRNA expression level of Id4 was increased, and Myh6 was reduced (Figure 7F). This is consistent with increased Id4 and decreased Myh6 mRNA expression in satellite cells of Dnmt3a-KO mice with increased Gdf5 mRNA expression. These data suggest that Gdf5 suppresses satellite cell differentiation by increasing Id expression. Together, phenotypes of Dnmt3a-KO cells (Figure 5) and Gdf5-treated WT cells (Figure 7) were similar. Thus, Dnmt3a-KO may cause the effects that are, at least in part, mediated by Gdf5.

Discussion

During atrophy, such as sarcopenia and unloading, muscle regeneration capacity after injury is decreased (9-11). We observed decreased muscle regeneration by denervation (data not shown). This decreased muscle regeneration capacity is believed to interfere with muscle mass recovery after injury and lead to impaired muscle function as well as severer sarcopenia with lower quality of life (28). We present a plausible model for the decreased regeneration capacity of atrophied skeletal muscles involving

down-regulation of the DNA methyltransferase Dnmt3a in satellite cells and ensuing up-regulation of Gdf5/Bmp14, and suppression of satellite cell differentiation. It is better to analyze DNA methylation levels and/or Dnmt3a expression in satellite cells from aged or other atrophy models. However, it is technically difficult, because isolation of skeletal muscles and culturing satellite cells in a dish may change their features; for example, loss of connection with extracellular signals causing atrophy. These issues remain to be solved.

Differences in the *Gdf5* promoter methylation level between satellite cells and skeletal muscles of Dnmt3a-KO mice

Under normal conditions, we did not observe gross morphological differences in skeletal muscles between Dnmt3a-KO and WT mice. The DNA methylation level of the *Gdf5* promoter was lower in satellite cells of Dnmt3a-KO mice than in WT mice, while in whole skeletal muscles, *Gdf5* promoter methylation did not differ between Dnmt3a-KO and WT mice (data not shown). Indeed, in skeletal muscles, expression of Gdf5 was very low in both WT and Dnmt3a-KO mice; Gdf5 expression was not significantly increased in skeletal muscles of Dnmt3a-KO mice, which is consistent with the unchanged DNA methylation level (data not shown).

A global search of methylation differences was analyzed using a methylation-sensitive enzyme (*Hpa*II, recognizing the CCGG sequence) (22). We observed 23 probes (genes) for skeletal muscles (data not shown) and 155 probes (genes) for satellite cells (data not shown) that were markedly less methylated in Dnmt3a-KO mice than in WT mice. Thus,

Dnmt3a deletion in skeletal muscles as well as satellite cells is functional. Among the 155 genes in satellite cells, most were not markedly less methylated in skeletal muscles (data not shown). Namely, Dnmt3a-target genes appear different between skeletal muscles and satellite cells.

Expression of receptors for Gdf5

The known receptors of Gdf5 are Acvr2a, Acvr2b, Bmpr1b, and Bmpr2 (29). Bmpr1b has a high affinity for Gdf5 (29). According to the BioGPS database, containing information on tissue/cell expression patterns of specific mRNAs (http://biogps.org/), Acvr2a, Acvr2b, Bmpr1b, and Bmpr2 are expressed in skeletal muscles. Indeed, we observed expression of these receptors in satellite cells as well as in skeletal muscles (data not shown). Moreover, expression levels of all Gdf5 receptors did not differ between Dnmt3a-KO and WT mice. Thus, Gdf5 is likely to act as an autocrine signal for satellite cells via these receptors to suppress differentiation.

Regulation of endogenous Dnmt3a expression

In the present study, we observed a marked reduction in Dnmt3a expression in skeletal muscles in the atrophy model used. One question that remains unanswered is the molecular mechanism underlying the down-regulation of Dnmt3a expression in the atrophy mouse model. It has been reported that Dnmt3a is reduced in the brain (hippocampus and cortex) of aged mice (30). Moreover, Dnmt3a expression is activated by neuronal activity, and partially through the nuclear calcium signaling-dependent

pathway (30). In the case of skeletal muscles, calcium ions enter the muscle cells during muscle contraction, which is caused by motor neuron stimulation (31). Stimulation of motor neurons may be important for maintaining Dnmt3a expression in skeletal muscles. Indeed, in our preliminary experiment, treatment with a calcium ionophore significantly increased the expression of Dnmt3a mRNA in C2C12 myoblast cells (data not shown); thus, during muscle atrophy, such as denervation and aging (there is a decline in the number of neuromuscular junctions) (32), Dnmt3a expression may decrease as a result of decreased calcium signaling. Elucidation of the regulation of Dnmt3a expression is an interesting area of research and the focus of our future studies.

Comparison with other studies concerning the role of Dnmt3a in skeletal muscles

A few previous studies have examined the role of Dnmt3a in skeletal muscles and satellite cells. Tajrishi et al. reported that overexpression of Dnmt3a in skeletal muscles suppressed FGF-inducible 14 (*Fn14*) gene expression and increased the DNA methylation level at the *Fn14* promoter (8). They also reported that denervation of WT mice decreased Dnmt3a expression and increased Fn14 mRNA expression (8). In our Dnmt3a-KO mice, we did not observe increased Fn14 mRNA expression either in skeletal muscles or satellite cells (data not shown). Thus, KO of Dnmt3a in this study and overexpression of Dnmt3a in skeletal muscles show different effects on the *Fn14* gene (8). Satellite cell-specific KO of Dnmt3a using the *Pax7* promoter to drive a Cre-estrogen receptor fusion protein resulted in decreased DNA methylation at the *p57/Kip2* (*Cdkn1c*) gene, a negative regulator of cell proliferation, and increased its

expression (33). These results, showing a reduced skeletal muscle regeneration capacity (33), are consistent with our study. While we observed decreased methylation levels of the *p57/Kip2* promoter region in the global search of methylation differences (data not shown), we did not observe increased p57/Kip2 mRNA expression in the satellite cells of our Dnmt3a-KO mice (data not shown). There was no difference in the satellite cell proliferation rate between WT and Dnmt3a-KO mice as accessed by an EdU assay (Figure 5B). This difference could result from the subtle culture conditions or the use of different promoters for Cre expression, as this would impact the timing and location of expression.

Conclusion

We summarize our results and conclusions in Figure 8. Based on the Dnmt3a-KO data, in satellite cells, decreased Dnmt3a lead to decreased DNA methylation of the *Gdf5* promoter. Loss of Dnmt3a causes de-suppression of the *Gdf5* promoter, resulting in increased Gdf5 expression and enhanced secretion. This released Gdf5 binds to its receptors on satellite cells and suppresses their differentiation. Decreased Dnmt3a and increased Gdf5 can explain, at least in part, the delayed or impaired regeneration and recovery of skeletal muscle mass following injury during atrophy including aging.

References

1. Guasconi, V., and Puri, P. L. (2008) Epigenetic drugs in the treatment of skeletal muscle atrophy. *Current opinion in clinical nutrition and metabolic care* **11**, 233-241
2. Maunakea, A. K., Nagarajan, R. P., Bilenky, M., Ballinger, T. J., D'Souza, C., Fouse, S. D., Johnson, B. E., Hong, C., Nielsen, C., Zhao, Y., Turecki, G., Delaney, A., Varhol, R., Thiessen, N., Shchors, K., Heine, V. M., Rowitch, D. H., Xing, X., Fiore, C., Schillebeeckx, M., Jones, S. J., Haussler, D., Marra, M. A., Hirst, M., Wang, T., and Costello, J. F. (2010) Conserved role of intragenic DNA methylation in regulating alternative promoters. *Nature* **466**, 253-257
3. Wu, H., Coskun, V., Tao, J., Xie, W., Ge, W., Yoshikawa, K., Li, E., Zhang, Y., and Sun, Y. E. (2010) Dnmt3a-dependent nonpromoter DNA methylation facilitates transcription of neurogenic genes. *Science (New York, N.Y.)* **329**, 444-448
4. Okano, M., Bell, D. W., Haber, D. A., and Li, E. (1999) DNA methyltransferases Dnmt3a and Dnmt3b are essential for de novo methylation and mammalian development. *Cell* **99**, 247-257
5. Taylor, S. M., and Jones, P. A. (1979) Multiple new phenotypes induced in 10T1/2 and 3T3 cells treated with 5-azacytidine. *Cell* **17**, 771-779
6. Liu, R., Kim, K. Y., Jung, Y. W., and Park, I. H. (2016) Dnmt1 regulates the myogenic lineage specification of muscle stem cells. *Scientific reports* **6**, 35355
7. Xie, S., Wang, Z., Okano, M., Nogami, M., Li, Y., He, W. W., Okumura, K., and Li, E. (1999) Cloning, expression and chromosome locations of the human DNMT3 gene family. *Gene* **236**, 87-95
8. Tajrishi, M. M., Shin, J., Hetman, M., and Kumar, A. (2014) DNA methyltransferase 3a and mitogen-activated protein kinase signaling regulate the expression of fibroblast growth factor-inducible 14 (Fn14) during denervation-induced skeletal muscle atrophy. *The Journal of biological chemistry* **289**, 19985-19999
9. Ehrhardt, J., and Morgan, J. (2005) Regenerative capacity of skeletal muscle. *Current opinion in neurology* **18**, 548-553
10. D'Souza, D. M., Zhou, S., Rebalka, I. A., MacDonald, B., Moradi, J., Krause, M.

P., Al-Sajee, D., Punthakee, Z., Tarnopolsky, M. A., and Hawke, T. J. (2016) Decreased Satellite Cell Number and Function in Humans and Mice With Type 1 Diabetes Is the Result of Altered Notch Signaling. *Diabetes* **65**, 3053-3061

11. Mozdziak, P. E., Truong, Q., Macius, A., and Schultz, E. (1998) Hindlimb suspension reduces muscle regeneration. *European journal of applied physiology and occupational physiology* **78**, 136-140
12. Ono, Y., Calhabeu, F., Morgan, J. E., Katagiri, T., Amthor, H., and Zammit, P. S. (2011) BMP signalling permits population expansion by preventing premature myogenic differentiation in muscle satellite cells. *Cell Death Differ* **18**, 222-234
13. Rider, C. C., and Mulloy, B. (2010) Bone morphogenetic protein and growth differentiation factor cytokine families and their protein antagonists. *Biochem J* **429**, 1-12
14. Reynard, L. N., Bui, C., Canty-Laird, E. G., Young, D. A., and Loughlin, J. (2011) Expression of the osteoarthritis-associated gene GDF5 is modulated epigenetically by DNA methylation. *Human molecular genetics* **20**, 3450-3460
15. Kamei, Y., Miura, S., Suzuki, M., Kai, Y., Mizukami, J., Taniguchi, T., Mochida, K., Hata, T., Matsuda, J., Aburatani, H., Nishino, I., and Ezaki, O. (2004) Skeletal muscle FOXO1 (FKHR) transgenic mice have less skeletal muscle mass, down-regulated Type I (slow twitch/red muscle) fiber genes, and impaired glycemic control. *The Journal of biological chemistry* **279**, 41114-41123
16. Kaneda, M., Okano, M., Hata, K., Sado, T., Tsujimoto, N., Li, E., and Sasaki, H. (2004) Essential role for de novo DNA methyltransferase Dnmt3a in paternal and maternal imprinting. *Nature* **429**, 900-903
17. Brennan, K. J., and Hardeman, E. C. (1993) Quantitative analysis of the human alpha-skeletal actin gene in transgenic mice. *The Journal of biological chemistry* **268**, 719-725
18. Miura, S., Tomitsuka, E., Kamei, Y., Yamazaki, T., Kai, Y., Tamura, M., Kita, K., Nishino, I., and Ezaki, O. (2006) Overexpression of peroxisome proliferator-activated receptor gamma co-activator-1alpha leads to muscle atrophy with depletion of ATP. *The American journal of pathology* **169**, 1129-1139
19. Ono, Y., Urata, Y., Goto, S., Nakagawa, S., Humbert, P. O., Li, T. S., and Zammit, P. S. (2015) Muscle stem cell fate is controlled by the cell-polarity

protein Scrib. *Cell reports* **10**, 1135-1148

20. Srinivas, S., Watanabe, T., Lin, C. S., William, C. M., Tanabe, Y., Jessell, T. M., and Costantini, F. (2001) Cre reporter strains produced by targeted insertion of EYFP and ECFP into the ROSA26 locus. *BMC developmental biology* **1**, 4
21. Hatazawa, Y., Tadaishi, M., Nagaike, Y., Morita, A., Ogawa, Y., Ezaki, O., Takai-Igarashi, T., Kitaura, Y., Shimomura, Y., Kamei, Y., and Miura, S. (2014) PGC-1alpha-mediated branched-chain amino acid metabolism in the skeletal muscle. *PloS one* **9**, e91006
22. Ehara, T., Kamei, Y., Yuan, X., Takahashi, M., Kanai, S., Tamura, E., Tsujimoto, K., Tamiya, T., Nakagawa, Y., Shimano, H., Takai-Igarashi, T., Hatada, I., Suganami, T., Hashimoto, K., and Ogawa, Y. (2015) Ligand-activated PPARalpha-dependent DNA demethylation regulates the fatty acid beta-oxidation genes in the postnatal liver. *Diabetes* **64**, 775-784
23. Kumaki, Y., Oda, M., and Okano, M. (2008) QUMA: quantification tool for methylation analysis. *Nucleic acids research* **36**, W170-175
24. Egerman, M. A., Cadena, S. M., Gilbert, J. A., Meyer, A., Nelson, H. N., Swalley, S. E., Mallozzi, C., Jacobi, C., Jennings, L. L., Clay, I., Laurent, G., Ma, S., Brachat, S., Lach-Trifilieff, E., Shavlakadze, T., Trendelenburg, A. U., Brack, A. S., and Glass, D. J. (2015) GDF11 Increases with Age and Inhibits Skeletal Muscle Regeneration. *Cell metabolism* **22**, 164-174
25. Zammit, P. S., Relaix, F., Nagata, Y., Ruiz, A. P., Collins, C. A., Partridge, T. A., and Beauchamp, J. R. (2006) Pax7 and myogenic progression in skeletal muscle satellite cells. *Journal of cell science* **119**, 1824-1832
26. Suchak, A., Hunt, N. P., Shah, R., Sinanan, A. C., Lloyd, T., and Lewis, M. P. (2009) Myosin proteins identified from masseter muscle using quantitative reverse transcriptase-polymerase chain reaction--a pilot study of the relevance to orthodontics. *European journal of orthodontics* **31**, 196-201
27. Zhao, P., Caretti, G., Mitchell, S., McKeehan, W. L., Boskey, A. L., Pachman, L. M., Sartorelli, V., and Hoffman, E. P. (2006) Fgfr4 is required for effective muscle regeneration in vivo. Delineation of a MyoD-Tead2-Fgfr4 transcriptional pathway. *The Journal of biological chemistry* **281**, 429-438
28. Grounds, M. D. (1998) Age-associated changes in the response of skeletal muscle cells to exercise and regeneration. *Annals of the New York Academy of*

Sciences **854**, 78-91

29. Nishitoh, H., Ichijo, H., Kimura, M., Matsumoto, T., Makishima, F., Yamaguchi, A., Yamashita, H., Enomoto, S., and Miyazono, K. (1996) Identification of type I and type II serine/threonine kinase receptors for growth/differentiation factor-5. *The Journal of biological chemistry* **271**, 21345-21352
30. Oliveira, A. M., Hemstedt, T. J., and Bading, H. (2012) Rescue of aging-associated decline in Dnmt3a2 expression restores cognitive abilities. *Nature neuroscience* **15**, 1111-1113
31. Salanova, M., Volpe, P., and Blottner, D. (2013) Homer protein family regulation in skeletal muscle and neuromuscular adaptation. *IUBMB life* **65**, 769-776
32. Rudolf, R., Khan, M. M., Labeit, S., and Deschenes, M. R. (2014) Degeneration of neuromuscular junction in age and dystrophy. *Frontiers in aging neuroscience* **6**, 99
33. Naito, M., Mori, M., Inagawa, M., Miyata, K., Hashimoto, N., Tanaka, S., and Asahara, H. (2016) Dnmt3a Regulates Proliferation of Muscle Satellite Cells via p57Kip2. *PLoS genetics* **12**, e1006167

Legends

Figure 1

Decreased Dnmt3a expression in mouse skeletal muscles atrophied by denervation, plaster cast immobilization, or aging

A-C) mRNA expression in mouse skeletal muscles atrophied by A) denervation, N = 6 each group, B) plaster cast immobilization, N = 6 each group, or C) aging; young (13 weeks old): N = 4, old (25 months old): N = 5. Data are presented as the mean ± SEM. Student's two-tailed unpaired t-test, ***P < 0.001, *P < 0.05.

Figure 2

Expression of Dnmt3a in skeletal muscles of Dnmt3a-KO mice

A) Genotyping of Dnmt3a-KO mice. PCR analysis with tail genomic DNA from WT or Dnmt3a-KO. B) Expression of Dnmt3a mRNA in various tissues from Dnmt3a-KO mice and WT littermates by RT-qPCR. N = 3 each group. C) Protein levels of Dnmt3a and control Gapdh in skeletal muscles and the liver of Dnmt3a-KO and WT mice by Western blotting. Typical blots are shown. N = 2 each group. D) Expression of Dnmt1 and Dnmt3b mRNA in skeletal muscles of Dnmt3a-KO mice assessed by RT-qPCR. Same tissue samples as in (B). Data are presented as the mean ± SEM. Student's two-tailed unpaired t-test, **P < 0.01.

Figure 3

Skeletal muscle-related phenotype of Dnmt3a-KO mice

A) Dnmt3a-KO (16-18 weeks old, males) and age- and sex-matched WT littermates were allowed ad libitum access to food. Whole body weight and weights of liver, WAT, and skeletal muscles (gastrocnemius, quadriceps) are shown. N = 3 each group. B-D) Histological analysis of skeletal muscles of WT and Dnmt3a-KO mice. The structure of muscle cross-sections was analyzed by histological staining. B) HE staining. C) Modified Gomori trichrome staining. D) NADH staining. There were no marked structural differences between Dnmt3a-KO and WT mice skeletal muscles. E) glucose tolerance test, and F) insulin tolerance test showed similar glucose metabolism between WT and Dnmt3a-KO mice. G) Skeletal muscles of WT and Dnmt3a-KO mice were injured by injection of CTX. After 2 weeks, skeletal muscles were stained with HE. Representative images of stained muscles cross-sections are shown. N = 6 each group. H) Skeletal muscles were stained for collagen type I (red), laminin (red), and MyHC (green). Nuclei were counterstained using DAPI (blue). A separate cohort of animals (N = 8) from those used in (G) was used. Cross sectional area (CSA) of representative muscle fibers with centralized nuclei (a feature of nascent myofibers) from each group, obtained after laminin/DAPI staining, is shown in the graph. N = 3. I) Muscle weight (2 weeks after CTX injection) was measured. Same samples as used in (H). N = 5 each group. Data represent the mean ± SEM. Student's two-tailed unpaired t-test, *P < 0.05.

Figure 4

Decreased expression of Dnmt3a in satellite cells from Dnmt3a-KO mice

Satellite cells were isolated from the extensor digitorum longus (EDL) muscle of

Dnmt3a-KO mice and WT littermates. Satellite cells were then cultured in growth medium for 6 days and differentiation medium for 2 days. A) mRNA expression profiles of satellite cells from Dnmt3a-KO mice by RT-qPCR. N = 3-4 each group. B) Protein levels of Dnmt3a and control Gapdh in satellite cells derived from Dnmt3a-KO and WT mice. N = 2 each group. C) Upper panel: schematic diagram of the fluorescent reporter mice (Rosa26-stop-YFP) system. In the absence of Cre expression (non-muscle cells), YFP does not emit fluorescence signals because of a stop codon in front of the gene. In the presence of Cre expression (muscle cells), the stop codon is removed and YFP can emit fluorescence signals. Lower panel: Pax7-positive quiescent satellite cells in myofibers freshly isolated from the EDL muscle of α-actin-Cre mice crossed with fluorescent reporter mice (Rosa26-stop-YFP mice) emitted strong YFP signals. Data represent the mean ± SEM. Student's two-tailed unpaired t-test, ***P < 0.001.

Figure 5

Morphology and immunohistochemistry in satellite cells from Dnmt3a-KO mice

A) Microscopic bright field view. Satellite cells isolated from the EDL of Dnmt3a-KO mice and WT littermates. The cells were cultured in growth medium for 6 days and in differentiation medium for 3 days, and the morphology was observed microscopically. Typical pictures are shown; N = 3 per group. B) Satellite cells were cultured in growth medium for 3 days. Immunostaining of Pax7 (red) in Dnmt3a-KO and WT satellite cells, and Edu (green) incorporation per Pax7-positive cell during cell proliferation are shown. Nuclei were stained using DAPI (blue). C, D) Satellite cells were cultured in growth

medium for 6 days, replated with cell number matching, and in differentiation medium for 2 days. C) Immunostaining of myogenin (red) in myotubes from Dnmt3a-KO and WT satellite cells. The ratio of myogenin-positive cells per nucleus is shown in the graph. D) Immunostaining of MyHC (red) in myotubes from Dnmt3a-KO and WT satellite cells. E) The nucleus number of myotube (myonuclei), myotube length and ratio of MyHC-positive area per microscopic field are shown in the graph. More than 100 myotubes per well were counted in random fields. N = 6 (six individual wells). Data represent the mean ± SEM. Student's two-tailed unpaired t-test, ***P < 0.001, **P < 0.01.

Figure 6

Increased expression of Gdf5 and decreased DNA methylation level of *Gdf5* promoter in satellite cells from Dnmt3a-KO mice

A) Expression of Gdf5 mRNA in satellite cells from Dnmt3a-KO mice, analyzed by RT-qPCR. N = 3-4 each group. B) Protein level of Gdf5 in culture medium of satellite cells from Dnmt3a-KO mice, measured by ELISA. N = 3 each group. C) Bisulfite analysis of the *Gdf5* promoter and the IAP region in satellite cells from Dnmt3a-KO or WT mice. D, E) Quantification of the bisulfite data shown in (C). D) Gdf5, E) IAP. N = 3 each group. F) mRNA expression of Gdf5, 36B4, and pyruvate kinase muscle (PKM) in satellite cells from WT mice in the presence of DNA methylation inhibitor 5-azacytidine. G) Differential expression of representative genes identified by microarrays was confirmed by RT-qPCR. Samples are the same as those used for the

results presented in Table 1. N = 3 each group. Data represent the mean ± SEM. Student's two-tailed unpaired t-test, ***P < 0.001, **P < 0.01, *P < 0.05.

Figure 7

Effect of recombinant Gdf5 in satellite cells from WT mice

A) Satellite cells isolated from WT mice were cultured in differentiation medium containing 100 ng/ml Gdf5 recombinant protein for 2 days; photos are representative of bright field images. B) Satellite cells were cultured in growth medium for 2 days, and then cultured in the same medium containing 10 ng/ml Gdf5 recombinant protein for 24 h. Immunostaining of Pax7 (red) in Gdf5-treated WT satellite cells, and Edu (green) incorporation during proliferation of cells are shown. Nuclei were stained using DAPI (blue). Ratio of Edu incorporation per Pax7 positive cells are shown in the graph. C, D) Satellite cells isolated from WT mice were cultured in differentiation medium containing 10 ng/ml Gdf5 recombinant protein for 2 days. C) Immunostaining of myogenin (red) in myotubes from Gdf5-treated WT satellite cells. The ratio of myogenin-positive cells is shown in the graph. D) Immunostaining of MyHC (red) in myotubes from Gdf5-treated WT satellite cells. E) The nucleus number of myotube (myonuclei), myotube length, and ratio of MyHC-positive area per microscopic field are shown in the graph. More than 100 myotubes per well were counted in random fields; N = 3 (three individual wells). F) mRNA expression was analyzed by RT-qPCR. Cell samples were as used in A); N = 3 per group. Data represent the mean ± SEM. Student's two-tailed unpaired t-test, ***P < 0.001, *P < 0.05.

Figure 8

Schematic diagram of summary

In satellite cells, decreased Dnmt3a lead to decreased DNA methylation of the *Gdf5* promoter, and increased *Gdf5* expression. This released Gdf5 suppresses differentiation of satellite cells. As a result, muscle regeneration, caused by injury, is suppressed in Dnmt3a-KO mice.

Table 1

Microarray analysis of satellite cells derived from Dnmt3a-KO and WT mice

Satellite cells were isolated from the EDL of Dnmt3a-KO mice and age- and sex-matched WT littermates. After isolation, satellite cells were cultured in growth medium for 5 days, replated with cell number matching, and cultured in differentiation medium for 2, 4, 5, and 6 days. Satellite cells were collected and global gene expression analyzed by microarray. (A) List of up-regulated genes (more than 2-fold compared to WT mice) in all samples. (B) List of down-regulated genes (less than 0.5-fold compared to WT mice) in all samples. Numbers show fold changes in gene expression. Expression of Dnmt3a was reduced in Dnmt3a-KO compared to WT cells in all samples. Moreover, expression of Gdf5 was increased in Dnmt3a-KO compared to WT cells in all samples. C, D) Pathway analysis. Compared with WT cells, C) Up-regulated (more than 1.3-fold) and D) down-regulated (less than 0.7-fold) in Dnmt3a-KO satellite cells by microarray and classified into KEGG pathway analysis, as described in Materials and Methods.

Fig.1

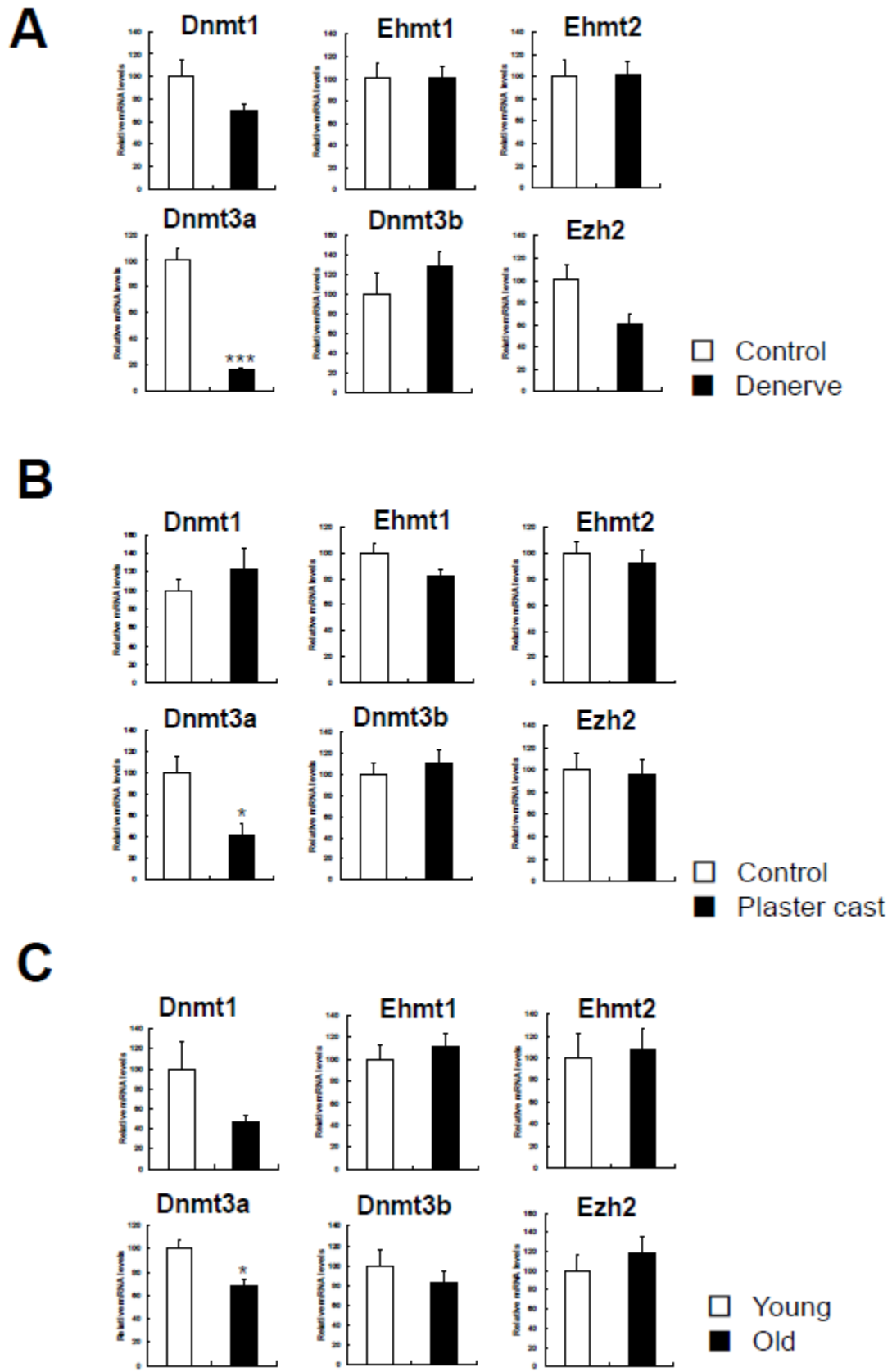
A
Dnmt1
Ehmt1
Ehmt2
Dnmt3a
Dnmt3b
Ezh2
***
Control
Denerve
B
Dnmt1
Ehmt1
Ehmt2
Dnmt3a
Dnmt3b
Ezh2
*
Control
Plaster cast
C
Dnmt1
Ehmt1
Ehmt2
Dnmt3a
Dnmt3b
Ezh2
*
Young
Old

Fig.2

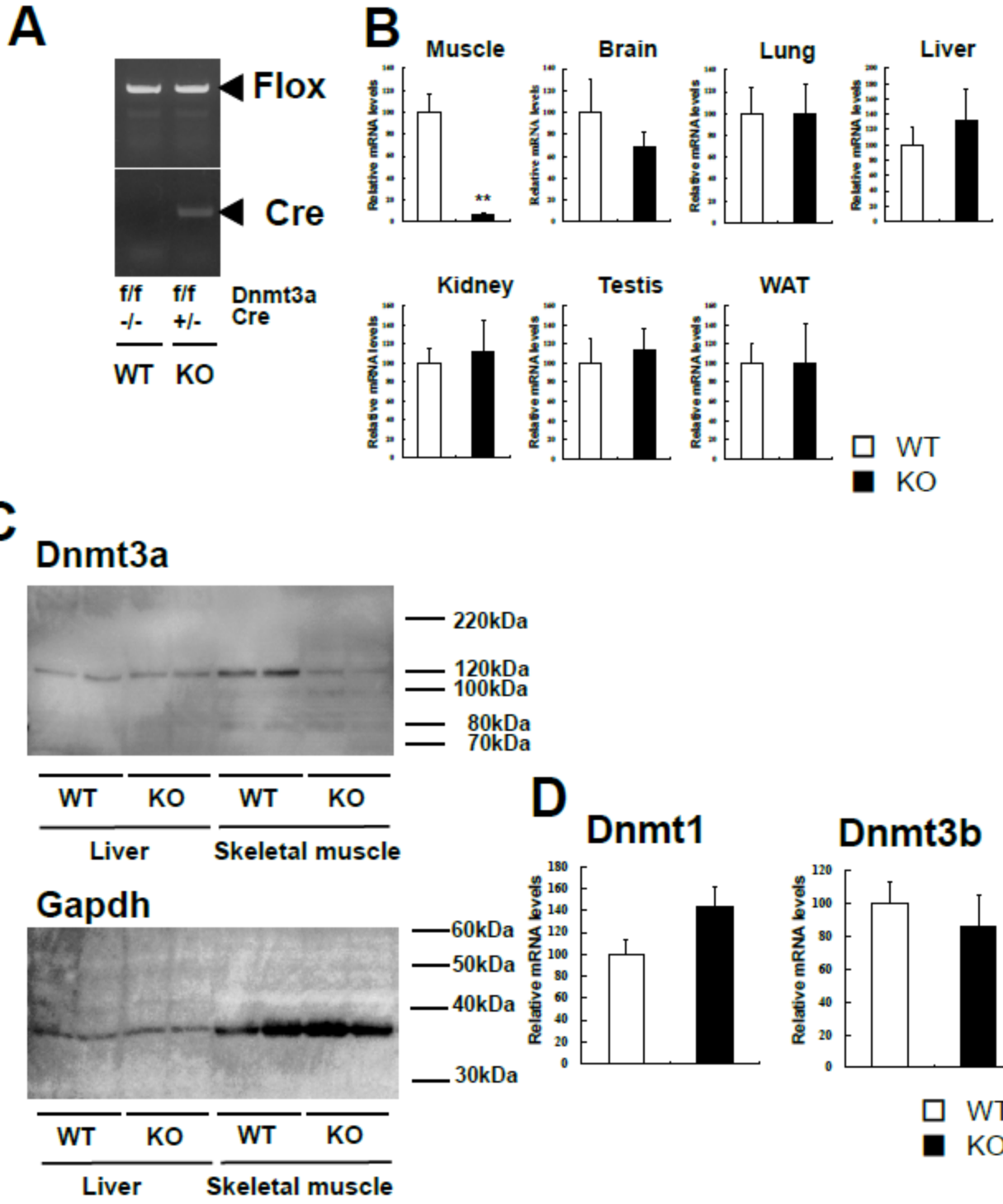
A
Flox
Cre
f/f
-/-
f/f
+/-
Dnmt3a
Cre
WT
KO
B
Muscle
Brain
Lung
Liver
Kidney
Testis
WAT
Relative mRNA levels
**
WT
KO
C
Dnmt3a
220kDa
120kDa
100kDa
80kDa
70kDa
WT
KO
WT
KO
Liver
Skeletal muscle
Gapdh
60kDa
50kDa
40kDa
30kDa
WT
KO
WT
KO
Liver
Skeletal muscle
D
Dnmt1
Dnmt3b
Relative mRNA levels
WT
KO

Fig.3

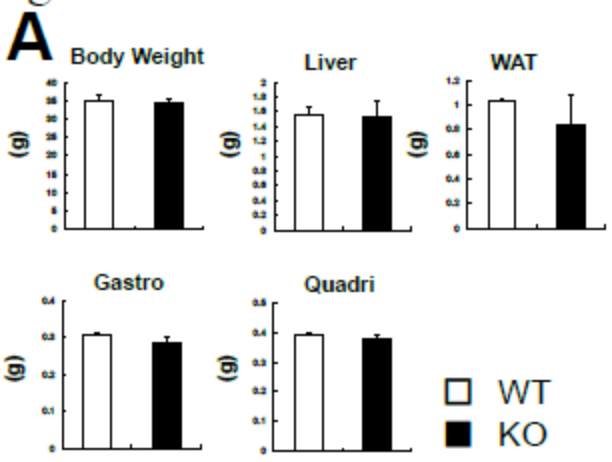
A
Body Weight
Liver
WAT
Gastro
Quadri
(g)
WT
KO

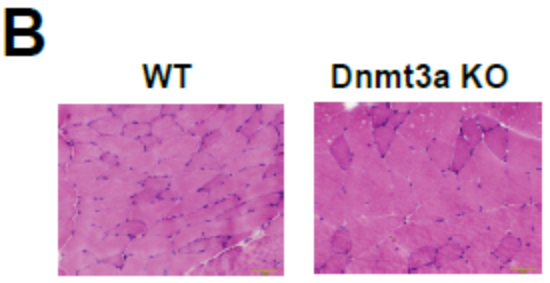
B
WT
Dnmt3a KO

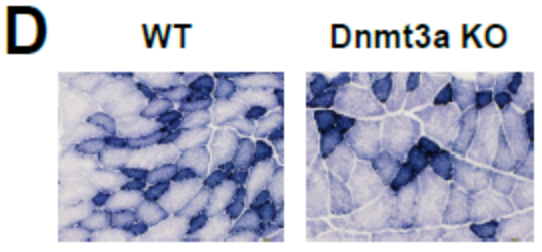
D
WT
Dnmt3a KO

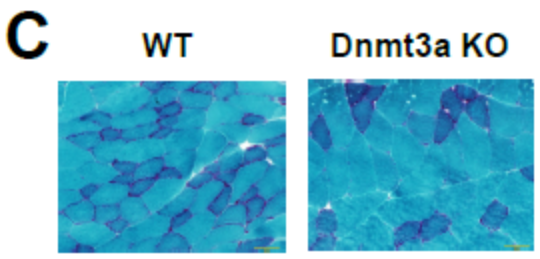
C
WT
Dnmt3a KO

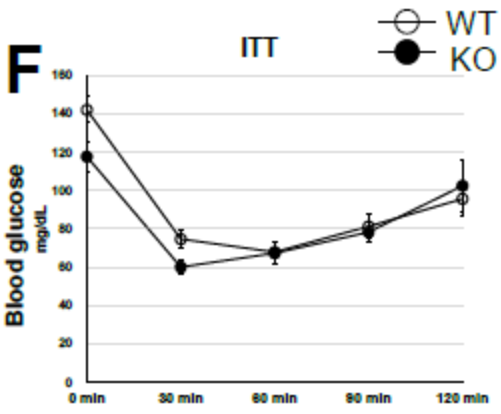
F
ITT
WT
KO
Blood glucose
mg/dL
0 min
30 min
60 min
90 min
120 min

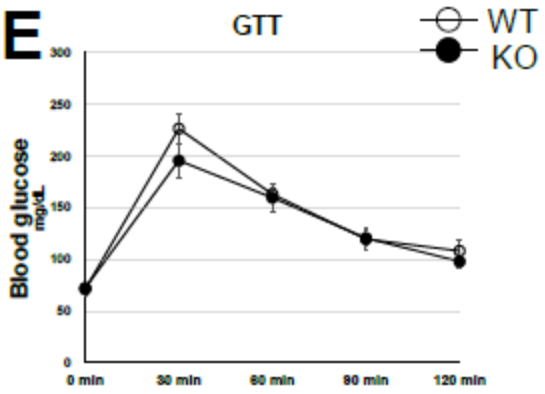
E
GTT
WT
KO
Blood glucose
mg/dL
0 min
30 min
60 min
90 min
120 min

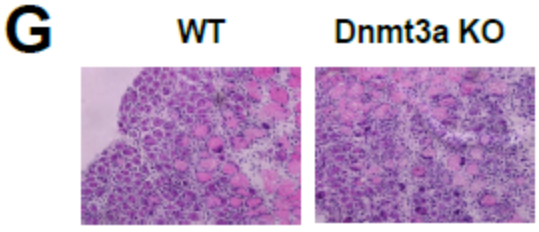
G
WT
Dnmt3a KO

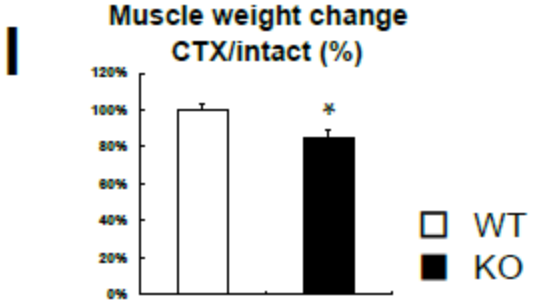
I
Muscle weight change
CTX/intact (%)
WT
KO

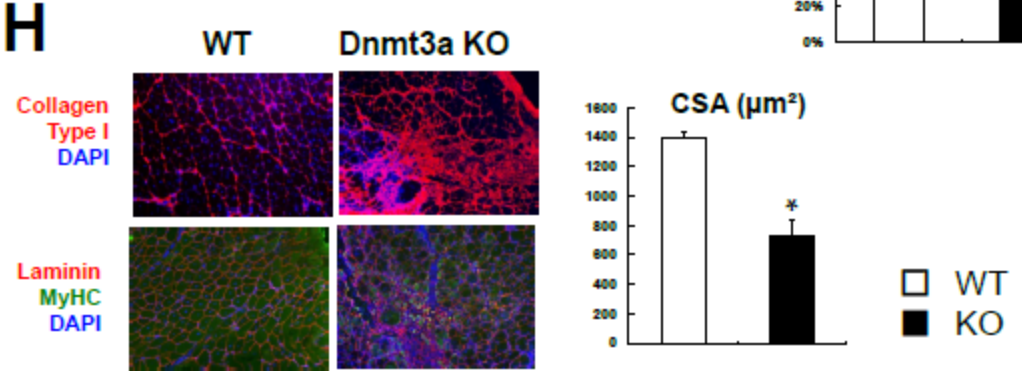
H
WT
Dnmt3a KO
Collagen
Type I
DAPI
Laminin
MyHC
DAPI
CSA (μm²)
WT
KO

Fig.4

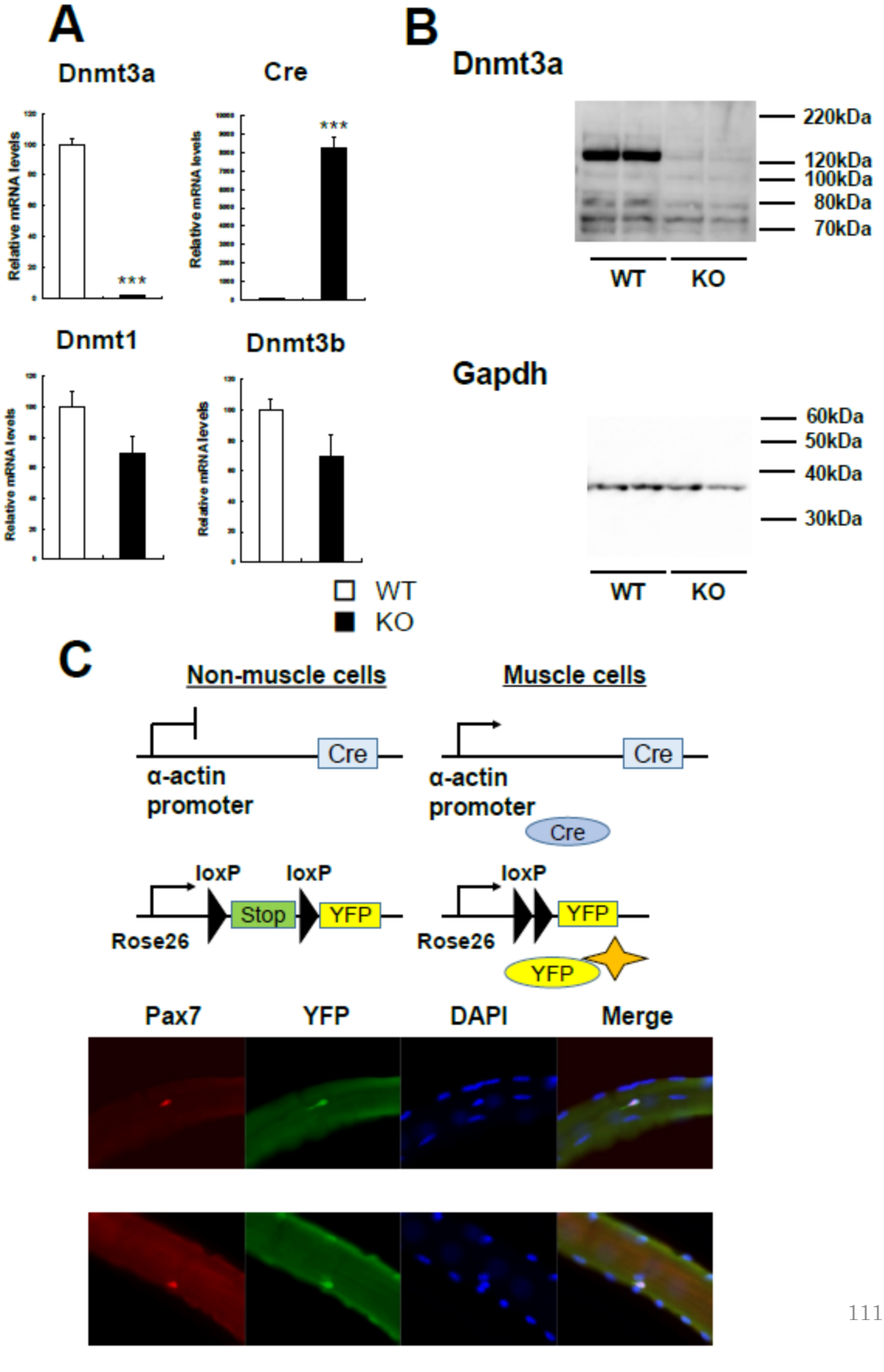
A
Dnmt3a
Cre
Relative mRNA levels
***
***
Dnmt1
Dnmt3b
Relative mRNA levels
WT
KO
B
Dnmt3a
220kDa
120kDa
100kDa
80kDa
70kDa
WT
KO
Gapdh
60kDa
50kDa
40kDa
30kDa
WT
KO
C
Non-muscle cells
Muscle cells
Cre
α-actin promoter
Cre
α-actin promoter
Cre
loxP
loxP
Stop
YFP
Rose26
loxP
YFP
Rose26
YFP
Pax7
YFP
DAPI
Merge

Fig.5

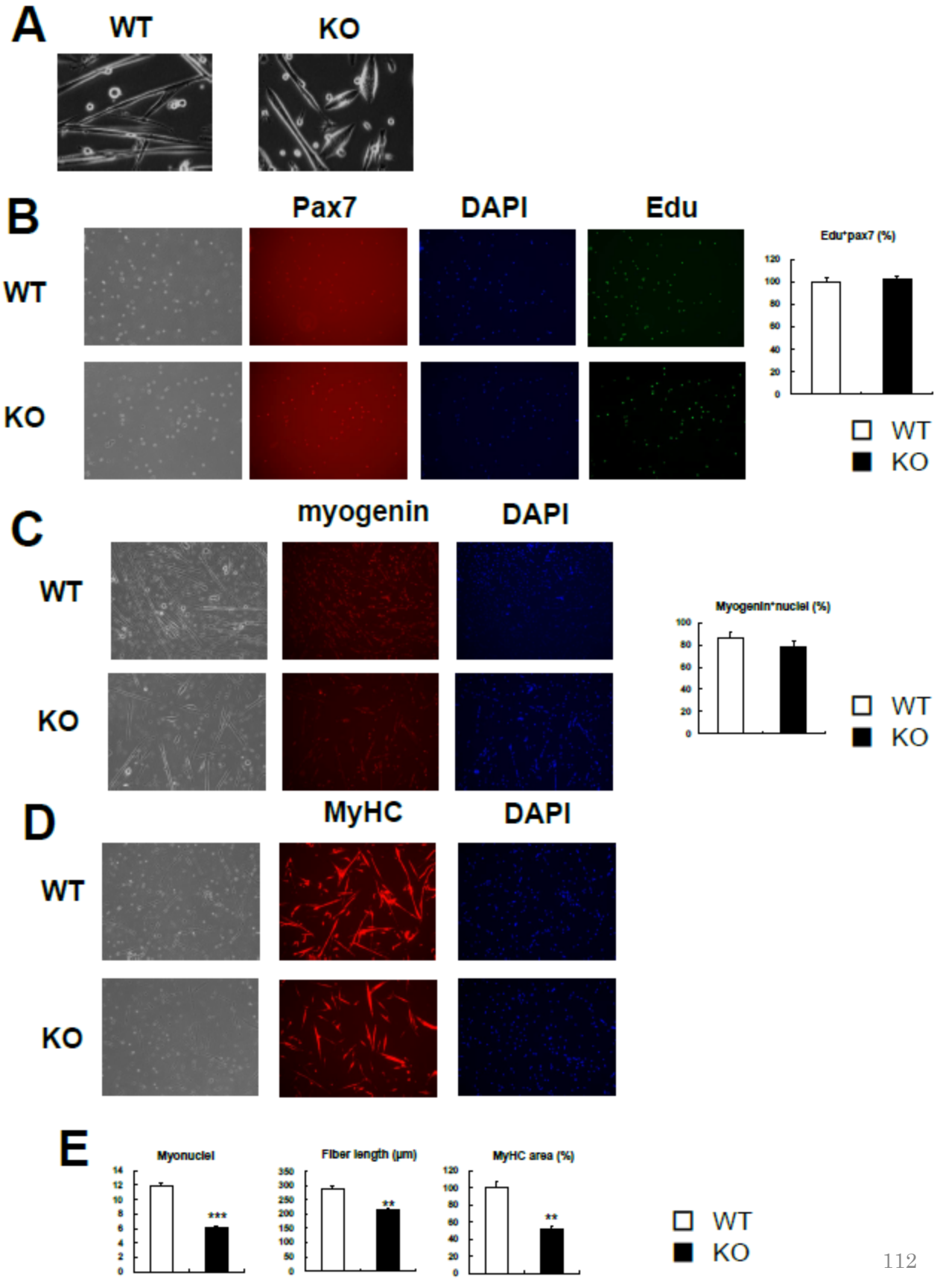
A
WT
KO
B
Pax7
DAPI
Edu
WT
KO
Edu*pax7 (%)
120
100
80
60
40
20
0
WT
KO
C
myogenin
DAPI
WT
KO
Myogenin*nuclei (%)
100
80
60
40
20
0
WT
KO
D
MyHC
DAPI
WT
KO
E
Myonuclei
14
12
10
8
6
4
2
0
***
Fiber length (μm)
350
300
250
200
150
100
50
0
**
MyHC area (%)
120
100
80
60
40
20
0
**
WT
KO

Fig.6

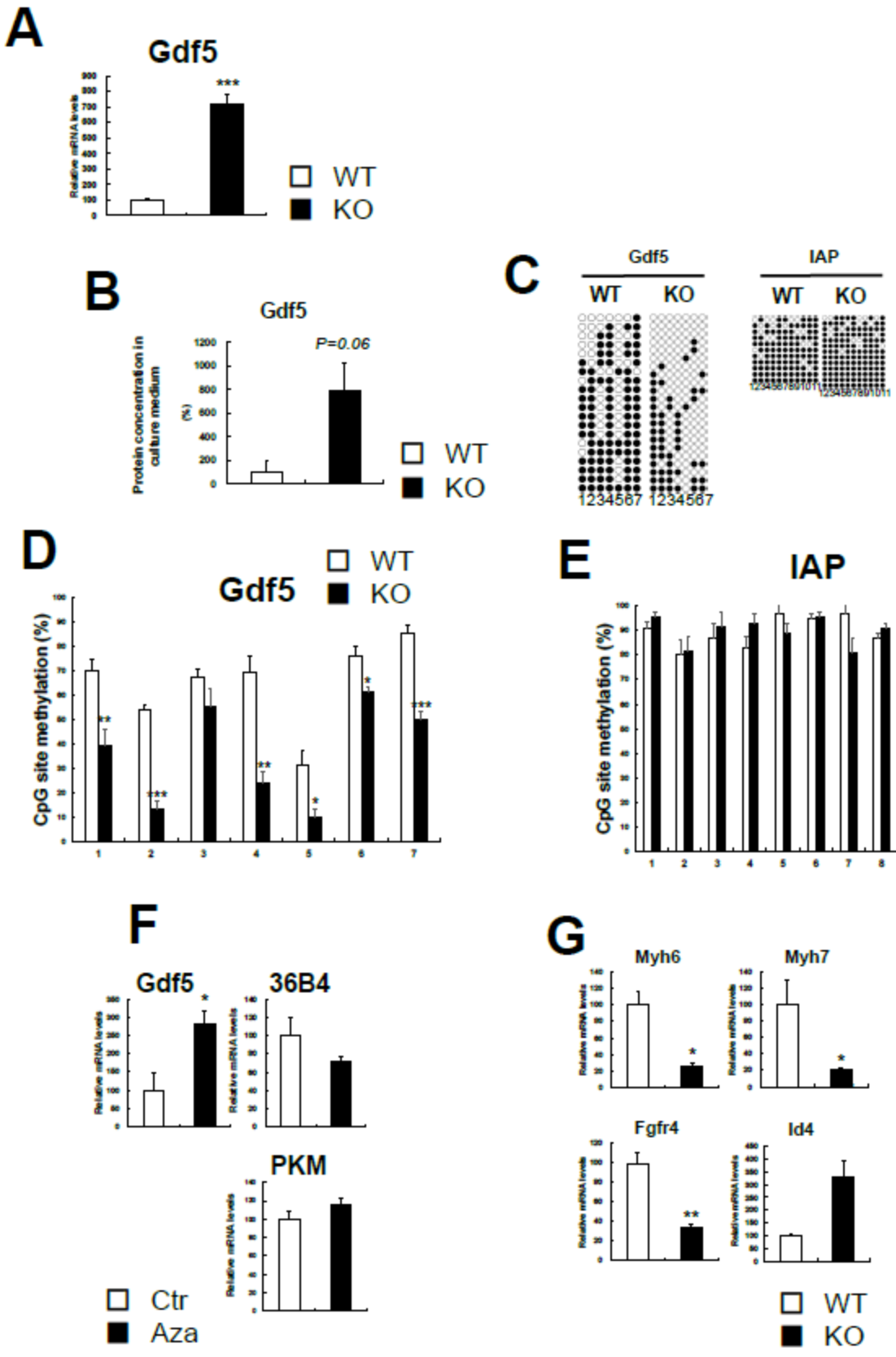
A
Gdf5
Relative mRNA levels
***
WT
KO
B
Gdf5
Protein concentration in culture medium (%)
P=0.06
WT
KO
C
Gdf5
IAP
WT
KO
WT
KO
1234567
1234567
D
Gdf5
WT
KO
CpG site methylation (%)
E
IAP
WT
KO
CpG site methylation (%)
F
Gdf5
36B4
PKM
Relative mRNA levels
Ctr
Aza
G
Myh6
Myh7
Fgfr4
Id4
Relative mRNA levels
WT
KO

Fig.7

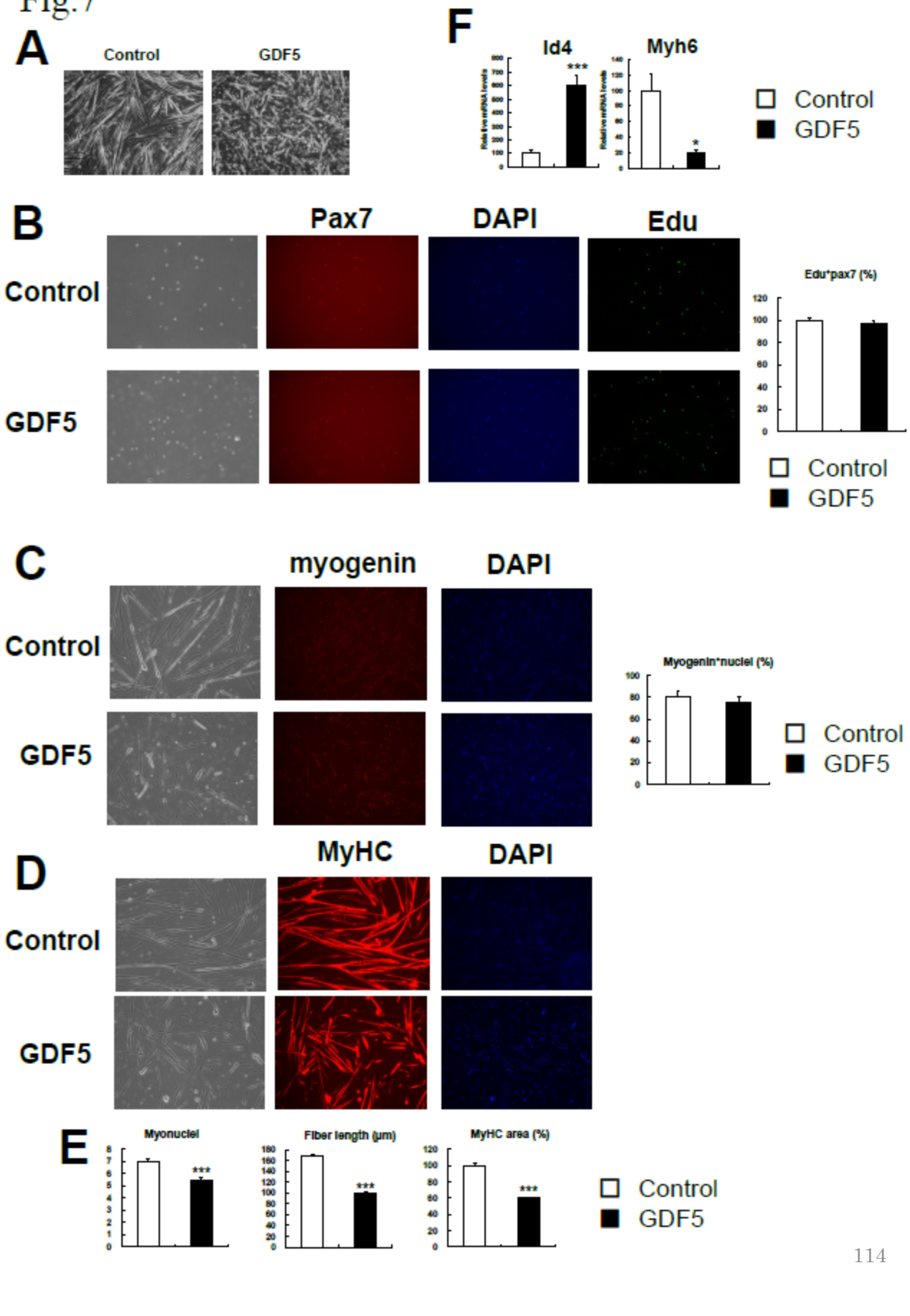
A
Control
GDF5
F
Id4
Myh6
***
*
Control
GDF5
B
Pax7
DAPI
Edu
Control
GDF5
Edu*pax7 (%)
Control
GDF5
C
myogenin
DAPI
Control
GDF5
Myogenin*nuclei (%)
Control
GDF5
D
MyHC
DAPI
Control
GDF5
E
Myonuclei
Fiber length (μm)
MyHC area (%)
***
Control
GDF5

Fig.8

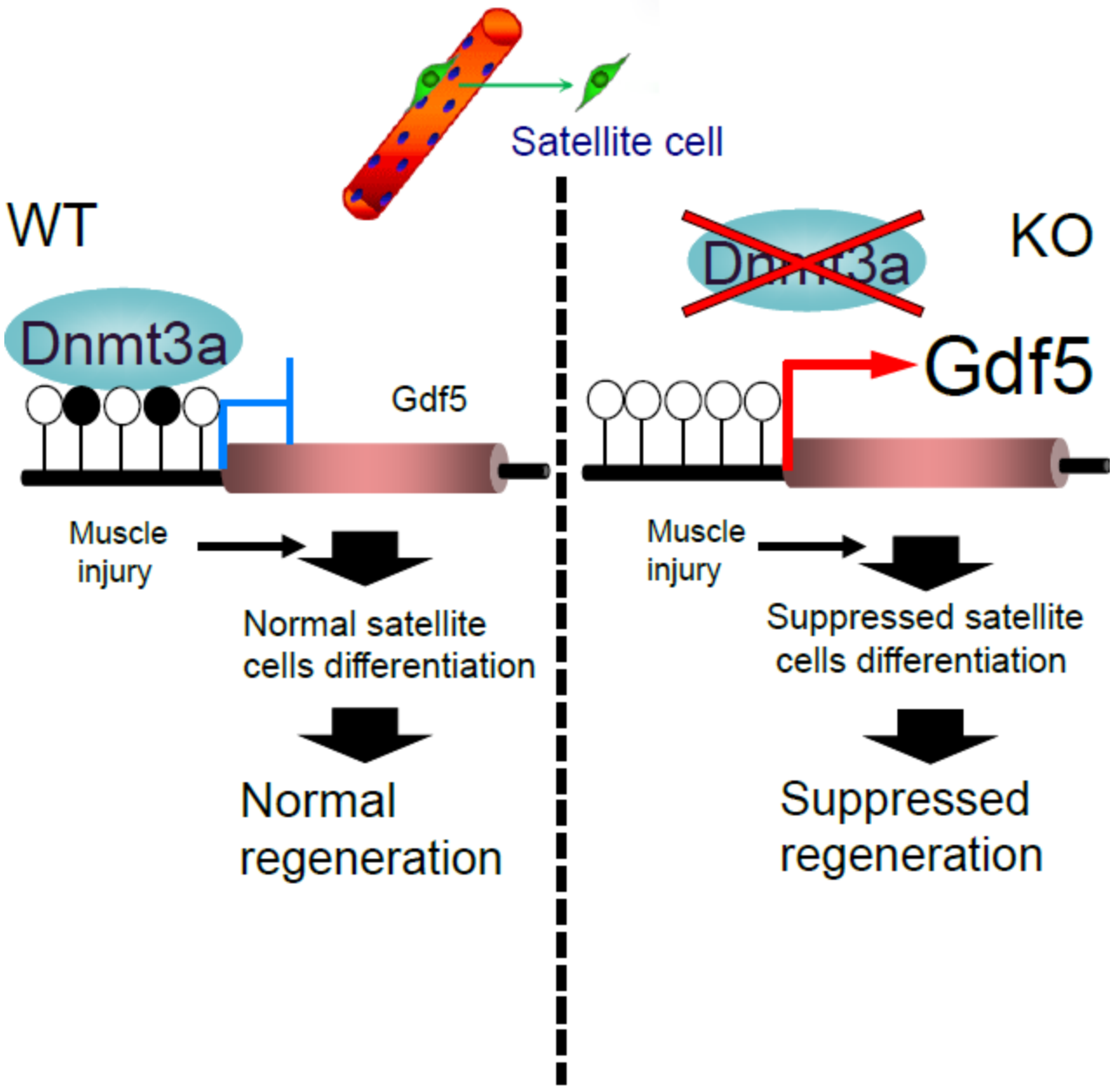
Satellite cell
WT
KO
Dnmt3a
Gdf5
Muscle injury
Normal satellite cells differentiation
Normal regeneration
Muscle injury
Suppressed satellite cells differentiation
Suppressed regeneration

Table 1

A

GeneName	Description	Day2 KO/WT	Day4 KO/WT	Day5 KO/WT	Day6 KO/WT
Gdf5	Growth differentiation factor 5 (Gdf5)	7.1	6.9	6.1	3.9
LOC100045886	Hypothetical protein LOC100045886 (LOC100045886)	4.3	3.0	3.4	2.4
Tchh	Trichohyalin (Tchh)	4.3	3.0	2.3	2.4
Gm3866	Hypothetical protein LOC100042484 (LOC100042484)	3.1	3.8	3.7	4.0
2200002D01Rik	RIKEN cDNA 2200002D01 gene (2200002D01Rik)	2.5	2.2	4.7	2.7
Zmynd17	Zinc finger, MYND domain containing 17 (Zmynd17)	2.3	2.5	2.2	2.2
Svop	SV2 related protein (Svop)	2.2	5.5	2.7	2.4
Ctxn3	Cortexin 3 (Ctxn3)	2.0	2.0	2.2	2.1

B

GeneName	Description	Day2 KO/WT	Day4 KO/WT	Day5 KO/WT	Day6 KO/WT
LOC674761	Similar to beta myosin heavy chain (LOC674761)	0.2	0.3	0.5	0.2
Myh7	Myosin, heavy polypeptide 7, cardiac muscle, beta (Myh7)	0.3	0.3	0.4	0.1
Myh6	Myosin, heavy polypeptide 6, cardiac muscle, alpha (Myh6), transcript variant 1	0.3	0.4	0.4	0.4
Capn6	Calpain 6 (Capn6)	0.3	0.4	0.4	0.5
Dnmt3a	DNA methyltransferase 3A (Dnmt3a), transcript variant 1	0.4	0.2	0.2	0.2
Gm608	Predicted gene 608 (Gm608)	0.4	0.4	0.4	0.2
B3galt5	UDP-Gal:betaGlcNAc beta 1,3-galactosyltransferase, polypeptide 5 (B3galt5), transcript variant 2	0.4	0.3	0.5	0.2
Fgfr4	Fibroblast growth factor receptor 4 (Fgfr4)	0.5	0.3	0.4	0.4
Emid2	EMI domain containing 2 (Emid2)	0.5	0.4	0.4	0.5
ENSMUST00000111103	Collagen alpha-1(XXVI) chain Precursor (EMI domain-containing protein 2)(Emilin and multimerin domain-containing protein 2)(Emu2)	0.5	0.4	0.5	0.4
Gtpbp8	GTP-binding protein 8 (putative) (Gtpbp8), transcript variant 1	0.5	0.5	0.5	0.4

C

Pathways	P-Value	Benjamini
Hippo signaling pathway	0.013	0.26
p53 signaling pathway	0.075	0.61
TGF-beta signaling pathway	0.095	0.55

D

Pathways	P-Value	Benjamini
Tight junction	0.033	0.81

Chapter 5

General discussion and conclusion

Chapters 2 and 3 focused on the transcription coactivator PGC1α in order to examine metabolic changes during exercise in skeletal muscle, and the results obtained showed that PGC1α activated the TCA cycle using substrates such as amino acids including branched-chain amino acids (BCAA), and generated energy for exercise.

The transcriptional coactivator PGC1α is important for muscle metabolism. Its expression is increased in skeletal muscle by exercise. The increased expression of PGC1α prolongs exercise performance (the duration for which running can be continued). In the present study, PGC1α increased the expression of the BCAA metabolism-related enzymes and genes involved in supplying substrates for the TCA cycle. A microarray followed by a bioinformatics analysis showed that the overexpression of PGC1α promoted the pathway of BCAA catabolism as well as other known energy metabolism pathways such as fatty acid oxidation and the TCA cycle. BCAA are an important energy source during exercise and have become common in commercially grown food consumed as supplemental foods. PGC1α-induced BCAA metabolism may play a role in enhancing exercise capacity. A metabolome analysis showed that the metabolites involved in several different pathways, such as the purine-nucleotide and aspartate-malate pathways, which are known to be activated during exercise, were altered in PGC1α-transgenic mice. Therefore, PGC1α appears to play important roles in exercise-mediated metabolic changes in skeletal muscle. Exercise generally affects not only skeletal muscle, but the whole body. PGC1α may mediate its beneficial effects such as improving metabolic diseases.

Chapter 4 focused on the DNA methyltransferase Dnmt3a in order to elucidate the mechanisms responsible for a decreased muscle regeneration capacity during aging, and proposed a new hypothesis in which muscle regeneration is decreased by aging via

changes in DNA methylation.

Aging and unloading cause muscle atrophy and delay the formation of muscle fibers. However, the molecular mechanisms underlying these phenomena remain unclear. The present study examined the possible involvement of DNA methylation, a form of epigenetic regulation that does not involve genomic sequence changes, in the assessment of muscle regeneration. The phenotype of skeletal muscle-specific Dnmt3a (a DNA methyltransferase) knockout mice, focusing on muscle satellite cells, was analyzed, and its physiological and pathophysiological significance was investigated. Based on Dnmt3a-KO data, reductions in Dnmt3a levels in satellite cells inhibited the DNA methylation of the Gdf5 (growth differentiation factor 5) promoter. Decreased Dnmt3a and increased Gdf5 may explain, at least in part, the delayed or impaired regeneration and recovery of the skeletal muscle mass following injury during muscle atrophy including aging.

Chapter 6

List of publications

1 Hatazawa Y, Tadaishi M, Nagaike Y, Morita A, Ogawa Y, Ezaki O, Takai-Igarashi T, Kitaura Y, Shimomura Y, Kamei Y, Miura S. PGC-1alpha-mediated branched-chain amino acid metabolism in the skeletal muscle. PloS one 9, e91006, doi:10.1371/journal.pone.0091006 (2014).

2 Hatazawa Y, Senoo N, Tadaishi M, Ogawa Y, Ezaki O, Kamei Y, Miura S. Metabolomic Analysis of the skeletal muscle of mice overexpressing PGC-1alpha. PloS one 10, e0129084, doi:10.1371/journal.pone.0129084 (2015).

3 Hatazawa Y, Minami K, Yoshimura R, Onishi T, Manio M C, Inoue K, Sawada N, Suzuki O, Miura S, Kamei Y. Deletion of the transcriptional coactivator PGC1alpha in skeletal muscles is associated with reduced expression of genes related to oxidative muscle function. Biochemical and biophysical research communications 481, 251-258, doi:10.1016/j.bbrc.2016.10.133 (2016).

4 Hatazawa Y, Ono Y, Hirose Y, Kanai S, Fujii N L, Machida S, Nishino I, Shimizu T, Okano M, Kamei Y, Ogawa Y. Reduced Dnmt3a increases Gdf5 expression with suppressed satellite cell differentiation and impaired skeletal muscle regeneration. FASEB journal : official publication of the Federation of American Societies for Experimental Biology, doi:10.1096/fj.201700573R (2017).

Chapter 7

Acknowledgements

The author wishes to express her sincerest gratitude to Dr. Yasutomi Kamei, professor of Kyoto Prefectural University, for his useful guidance, valuable discussions, and cordial encouragement throughout the course of this study.
Finally, the author is grateful to the members of Laboratory of Molecular Nutrition, Graduate School of Life and Environmental Sciences, Kyoto Prefectural University, for their encouragement and helpful suggestions.